HIGH SPECIFIC IMPULSE THERMAL ARC JET
THRUSTOR TECHNOLOGY

Technical Report

February 1967

3

BLANK PAGES
IN THIS
DOCUMENT
WERE NOT
FILMED

HIGH SPECIFIC IMPULSE THERMAL ARC JET
THRUSTOR TECHNOLOGY

Technical Report
February 1967

FOREWORD

ABSTRACT

The MPD arcjet program at EOS is aimed at developing the technology of electric thrustors capable of performing efficiently (40-60% conversion of electrical power to beam power) for extended periods of time (up to 100 hours) in the specific impulse range of 1500-5000 seconds, at power levels of 10-100 kilowatts. This program is based upon the optimization of an axisymmetric Hall current accelerator using a low molecular weight alkali metal for propellant. Out of the analytical and experimental studies during the reporting period has arisen the concept for a particular mode of operation of a thrustor of this type, designated ALPHA (ALkali Plasma Hall Accelerator), one of the principal features of which is that most of the beam current is carried by ions rather than electrons. Although the theory of such devices is still incomplete, much progress has been made in gaining a deeper understanding of the interrelated processes which occur in the thrustor. The analytical results are presented for each of the significant mechanisms. Progress in the experimental portion of the program has included the following:

1. The thrustor has been operated continuously for 100 hours with no significant electrode erosion.

2. A novel gas-actuated feed system which had been designed during the previous reporting period was fabricated, tested and calibrated. Because of difficulties which were encountered (especially leakage at the anode-vaporizer joint), several refinements in the design were required. This involved a painstaking process which accounted for a substantial portion of the experimental effort.

3. Test runs were made using ammonia as propellant. Results were inconclusive, but the poor performance obtained appears to indicate that the ALPHA works better with lithium (for which it is specifically designed).

4. Tests with a three-magnet configuration resulted in performance inferior to that obtained with the two-magnet thrustor.

LIST OF SYMBOLS

A	Area
A_θ	Vector potential (azimuthal component)
B	Magnetic field
b	$8\pi\gamma\mu L/\dot{m}(\gamma+1)$
C	Coefficient defined in Eq. 26, Section 3
E	Electric field
e	Ionic charge
F_o	Axial momentum
H	Pseudo potential
H_e	Total effective potential
h	Specific enthalpy
I	Current
I_{sp}	Specific impulse
L	Length
M	Mach number
m	Ion mass
$\dot{m}$	Mass flow rate
n	Particle density
P	Power
P_θ	Azimuthal angular momentum
p	Pressure
Q	Ionization cross section
R	Gas constant
R_A	Anode radius
R_1	Channel radius
r	Radial coordinate
$\bar{r}$	Position vector
T	Thrust
T	Temperature
V	Thermal speed
V_I	Ionization potential

LIST OF SYMBOLS (contd)

W	w_1/w^*
w	Velocity
X	Body force
z	Axial coordinate
γ	Ratio of specific heats
$\eta_{thermal}$, η_{th}	$1 - (P_{anode} + P_{buffer} + P_{cathode})/P_{arc}$
η_{thrust} η_F	$T^2/2\,\dot{m}\,P_{arc}$
η_o	$T^2/2\dot{m}\,(P_{arc} + P_{magnet})$
θ	h_1^o/h^{*o}
θ	Azimuthal coordinate
λ	Mean free path
μ	Viscosity
ζ	$8\,\dot{m}\,\phi_o/e\,R_A^2\,B^2(0)$
ρ	Density
ϕ	Scalar potential
ϕ_o	Total voltage drop
Υ	$(\Sigma\,\dot{m}/m_a)/(I/e)$

Subscripts and Superscripts

a	Atomic species
e	Electron
f	Friction
i	Isentropic
1	Channel inlet
o	Stagnation
wf	Work function
$\overline{x}$	Mean value of x
*	Sonic condition
Δ	Increment

CONTENTS

ILLUSTRATIONS

ILLUSTRATIONS (contd)

ILLUSTRATIONS (contd)

1. INTRODUCTION

An exploratory research program into steady-state plasma thrustor technology has been in progress at EOS over the past 32 months. The aim of the research is to build an accelerator capable of performing efficiently (40-60% conversion of electrical power to beam power) for extended periods of time (up to 100 hours) in the specific impulse range of 1500 to 5000 sec, at power levels of 10-100 kilowatts.

The two main features of the program are:

1. The use of a low molecular weight alkali metal for propellant.
2. The development and optimization of an axisymmetric Hall current accelerator.

Lithium has been used in the majority of the studies conducted to date and considerable progress has been made in developing the necessary technology for carrying out laboratory experiments. Similarly, by a combination of theory and experiment a reliable and efficient plasma accelerator has been developed. Information concerning these investigations can be found in Refs. 1-4. A reasonable amount of detailed diagnostics has also been conducted on the plasma in the exhaust beam. This work was supported by NASA-Lewis Research Center under Contract NAS3-8902. The results of these tests are reported in Refs. 5 and 6.

During the investigation into techniques for improving engine performance many configurations of electrode- and magnet-assemblies were tested. In most instances, due to analytical complexities introduced by geometric requirements as well as the concurrence of inter-related physical processes, it was not possible to base the design of particular components on any but the most elementary calculations.

Inevitably, this resulted in a step-wise approach to optimum design
punctuated by structural failures under repeated testing. This occurred
especially in the anode-vaporizer system (see Sections 3 and 4). Hav-
ing now found a configuration that shows substantial promise, the task
of increasing performance and lifetime has assumed some urgency. Much
of the technical effort discussed in the present report concerns this
problem.

The bellows feed system which was used in most of the tests con-
ducted during the first two-year period has been found unsatisfactory
for testing over extended periods. The development of a vapor feed
system which will allow uninterrupted testing for hundreds of hours
has been another major concern during the period covered by this report.

2. SUMMARY

During the reporting period the experimental and analytical effort included the following:

1. The operating lifetime of the thrustor was successfully extended to 100 hours of continuous operation with no significant electrode erosion. Several test runs were made before this major milestone was achieved, each test leading to further refinements of the thrustor design. The measured data for each test are presented in the form of histograms and performance plots.

2. The gas-actuated feed system, which had been designed in the previous reporting period to replace the bellows-type system then in use, was fabricated, tested and calibrated. Several difficulties were encountered, the most serious being that of obtaining a leak-tight seal between the tungsten anode and the molybdenum vaporizer. Other problems included the tendency for radial cracks to develop in the anode each time a new one was brought up to operating temperature for the first time and inability to maintain sufficiently high temperatures in the vaporizer, resulting in a severe limitation upon the maximum lithium mass flow rate. This third problem has not yet been completely solved. However, a modified anode-vaporizer designed specifically to produce higher temperatures in the vaporizer is presently in fabrication and is scheduled for testing in the near future. The other problems have been effectively overcome. The process of refining the design and fabrication technique for the anode-vaporizer so as to insure a leak-tight joint was so recalcitrant that much of the experimental effort and most of the delays experienced during the reporting period were due to this problem.

3. Two tests were made in which ammonia was used, both as the primary propellant and as the buffering gas. This necessitated the development of a separate gettering system in order to maintain a sufficiently low vacuum chamber pressure. The system consisted of two small lithium boilers situated on the floor of the vacuum chamber during ammonia runs. The thrustor performance obtained with ammonia was very poor. The minimum P/T was about 1000 kW/lb, the maximum thermal efficiency was 34%, and the maximum thrust and overall efficiencies were 4.5% and 3.5%, respectively. Although these results are inconclusive, they do indicate that the thrustor operates better with lithium propellant (for which it was specifically designed) than with ammonia. It is therefore perhaps not surprising that the relatively high performance achieved with lithium has not been duplicated by thrustors whose design differs markedly from the configuration painstakingly developed for this purpose.

4. Tests of a thrustor using three magnets were performed in an attempt to verify a prediction that by adding a third magnet downstream of the two existing coils, a higher voltage could be supported and the currents would extend further downstream, thereby giving better efficiency. However, no significant increase in performance was observed.

5. Analysis of the thrust-producing mechanisms was extended to the case of electrostatic acceleration of ions through the agency of electrons trapped in the magnetic field. This particular mechanism occurs in the less dense volumes and the analysis must be combined with the heating and expansion through a magnetic nozzle to give a complete picture of the acceleration process over a wide range of operating conditions. Analysis of the ionization process shows that the occurrence of volume ionization near the anode by energetic electrons predicts that the anode power loss must be nearly equal to the product of the ionization potential and the current.

3. FEED SYSTEM DESIGN, FABRICATION AND CALIBRATION

3.1 Design and Fabrication

Initial tests to evaluate the gas-actuated feed system (GAF) utilized a large stainless steel propellant reservoir (see Fig. 1). This can was suspended from the balance and piped into the lower vaporizer joint, using an expandable bellows to accommodate thermal expansion. The entire assembly was covered with high-temperature insulating cement to afford thermal and electrical insulation. A small, lightweight feed reservoir (shown in Fig. 2) was designed and fabricated for the GAF feed system calibration tests. Low tare weight is essential for accurate mass flow rate determinations because the amount of lithium expended during a test of reasonable duration is necessarily small. Insulating material and cement were not used to cover the reservoir since some unknown quantity of these materials would be lost during handling and testing.

The final reservoir design, illustrated in Fig. 3, is a thin-walled can of 304 stainless steel, with external sheathed heaters, a flanged and heated top plate, and direct-insertion thermocouple for propellant temperature measurement. The disconnectable joints have specially designed hollow metal O-ring seals at the large joints, and stainless steel "Swageloks" for gas and filling lines. Only the former is satisfactory for the high temperatures encountered near the vaporizer joint.

3.2 Calibration

Run 727 (Figs. 4-9) constituted the second successful test of the gas pressure-type feed system. Near the start of this run relatively low thrust and poor performance were obtained. This led to excessive engine heating and the burning of some insulator material.

From visual observations as well as from the voltage and thrust behavior, it was concluded that the actual propellant mass flow rate must be less than half the preset value of 14 mg/sec. The argon driver pressure corresponding to this flow rate was calculated from isentropic theory assuming $\gamma = 1.67$ and a value for the discharge coefficient of the metering orifice which was independently measured by a cold gas calibration using argon (see Fig. 10). The discrepancy between the isentropic prediction and the actual flow rate obtained during the run (as indicated by correlation with past experience in operating thrustors at various feed rates) pointed up the need for a separate series of calibration runs. In addition to actually measuring mass flow rate as a function of driver gas pressure, an attempt was made to improve the correlation between theory and experiment by refining the simple analysis. By taking into account three hitherto neglected effects, viz., friction, heat addition and variation of γ with temperature and pressure, a much closer, although still imperfect, agreement was obtained.

In order to calibrate the lithium feed system in a manner which simulates as closely as possible the actual conditions during a typical thrustor test, it was decided to heat the vaporizer by conduction from a hot anode. Three methods of heating the anode were considered, viz., electrical resistance, rf induction, and arc-heating. The first method would have necessitated fabrication and mounting of carefully designed graphite blocks in which the anode would be embedded. This would have required a separate engineering program of its own in order to insure proper current distribution in these blocks and at the same time to allow for thermal expansion at the graphite-tungsten interface. Hence this approach was considered impractical. On the other hand, rf induction heating was discarded because the only equipment at EOS capable of doing the job was not portable, the available vacuum facility was marginal, and scheduling problems were anticipated. It was therefore decided to do the feed system calibration tests with an

actual thrustor, but without its second (downstream) magnet. The three-foot diameter vacuum chamber was used so as not to interfere with work which was in progress involving modification of the lid of the 6 foot x 14 foot chamber.

A small (400-gram capacity) stainless steel lithium reservoir was fabricated for the calibration runs. This was done to permit before-and-after weighing of the _entire_ feed system on a balance of sufficient accuracy. Of the seven runs made, four yielded reliable data (points A, B, F and E in Fig. 10). During Run C there was sufficient deposition of lithium between the graphite radiator and the magnet housing to bridge the gap. The heat conduction path thus created resulted in rapid cooling of the anode so that flooding occurred and it was impossible to obtain an accurate measurement of the lithium consumption. The anode was badly cracked during this run and several attempts to braze a new anode to the old vaporizer proved unsuccessful due to leakage at the joint. These difficulties necessitated several design changes in the anode-vaporizer assembly (see Section 4) and was responsible for most of the delay in completing the calibration run series.

Run D failed to yield useful data because the anode temperature could not be continuously maintained at a sufficiently high value to vaporize all of the lithium flow fed at 350 torr. The final run (G) was an attempt to obtain a point at 600 torr. In order to keep the vaporizer hot enough it was necessary to use very high current (550 amp). Operation at such high temperature apparently deteriorated the braze joint between the anode and vaporizer sufficiently to permit some lithium leakage, particularly at the relatively high feed pressure. Nevertheless, the four good runs provided enough data to plot the curve of measured $\dot{m}$ versus pressure shown in Fig. 10. Excluding those points obtained during runs when the vaporizer was leaky or too cold, it is seen that only the 500 torr point (E) fails to lie on a straight line intersecting the origin. The remarkable absence of

scatter of the three other points (A, B and F) and their consistency
with the point (O, O) probably indicate that the value of $\dot{m}$ measured
at 500 torr was slightly low because of inadequate vaporizer tempera-
ture during one or more short periods in that run, rather than any
real flow rate anomaly.

The next problem was to try to explain the experimental re-
sults analytically, since it was felt that a clear understanding of
the physical processes would be a prerequisite for possible future
design changes in the vaporizer. Apart from replacing the oversimpli-
fied assumption that $\gamma = 5/3$ by a variable $\gamma = \gamma(p, T)$, the only way
in which the following analysis differs from straightforward isentropic
calculations is that it takes into account the fact that the sonic
"orifice" is in reality more like a channel in which friction and heat
addition have great influence on the choked flow. The geometry and
other assumptions of this analysis are shown in Fig. 11.

The energy balance at station 1 is:

$$\frac{w_1^2}{2} + \frac{\gamma}{\gamma-1} \frac{p_1}{\rho_1} = h_1^o \tag{1}$$

and at the sonic condition it is

$$\frac{w^{*2}}{2} + \frac{\gamma}{\gamma-1} \frac{p^*}{\rho^*} = h_1^o + \Delta h \tag{2}$$

Making use of the general relation

$$\frac{1}{\rho} = \frac{wA}{\dot{m}} , \tag{3}$$

we can solve Eq. 1 for p_1 to obtain

$$p_1 = \frac{\gamma-1}{\gamma} \frac{\dot{m}}{A_1} \frac{2h_1^o - w_1^2}{2w_1} \tag{4}$$

Since

$$w^{*2} = \gamma R T^* = \frac{\gamma p^*}{\rho^*} = \frac{\gamma p^* w^* A_1}{\dot{m}} \tag{5}$$

we have

$$p^* = \frac{\dot{m} w^*}{\gamma A_1} \tag{6}$$

and we can solve Eq. 2 for w^{*2}:

$$w^{*2} = 2 \frac{\gamma - 1}{\gamma + 1} (h_1^o + \Delta h) \tag{7}$$

Assuming that the velocity distribution between stations 1 and * is parabolic, we can write

$$\left(\frac{\partial w}{\partial R}\right)_{wall} = \frac{2 w_{max}}{R_1} \tag{8}$$

where w_{max} is the velocity on the axis of symmetry. Letting

$$\bar{w} = \frac{w_1 + w^*}{2} \tag{9}$$

and

$$\overline{w_{max}} = 2\bar{w} \tag{10}$$

we have

$$\left(\frac{\partial w}{\partial R}\right)_{wall} = \frac{2\overline{w_{max}}}{R_1} = \frac{4\bar{w}}{R_1} = \frac{2}{R_1} (w_1 + w^*) \tag{11}$$

Hence the pressure drop due to wall friction may be written as

$$(\Delta p)_f = \frac{(2\pi R_1 L)\mu \overline{\left(\frac{\partial w}{\partial R}\right)}_{wall}}{\pi R_1^2} = \frac{4\mu L}{R_1^2} (w_1 + w^*) \tag{12}$$

$$= \frac{4\pi \mu L}{A_1} (w_1 + w^*)$$

Thus we can write a momentum equation in the form:

$$p^* + \frac{\dot{m}}{A_1} v^* = P_1 + \frac{\dot{m}}{A_1} v_1 - \frac{4\eta_\mu L}{A_1} (v_1 + v^*) \tag{13}$$

Substituting Eqs. 4 and 6 into Eq. 13 we obtain, after multiplying both sides by w_1/v^{*2} and rearranging:

$$\left(\frac{\gamma+1}{2\gamma} - \frac{4\eta_\mu L}{\dot{m}}\right) \frac{w_1^2}{v^{*2}} - \left(\frac{\gamma+1}{\gamma} + \frac{4\eta_\mu L}{\dot{m}}\right) \frac{w_1}{v^*} + \frac{\gamma-1}{\gamma} \frac{h_1^0}{v^{*2}} = 0 \tag{14}$$

Substituting Eq. 7 into Eq. 14, rearranging the coefficients and multiplying both sides by $2\gamma/(\gamma + 1)$ gives

$$(1-b)W^2 - (2+b)W + \theta = 0 \tag{15}$$

where

$$W = \frac{w_1}{v^*} \tag{16}$$

$$b = \frac{8\pi\eta_\mu L}{\dot{m}(\gamma+1)} \tag{17}$$

and

$$\theta = \frac{h_1^0}{h_1^0 + \Delta h} = \frac{h_1^0}{h^{*0}} \tag{18}$$

Since $v^* > w_1$, the only root of Eq. 15 which is physically meaningful is

$$W = \frac{2+b - \sqrt{(2+b)^2 - 4(1-b)\theta}}{2(1-b)} \tag{19}$$

For isentropic flow,

$$P_1 = P_o \left(\frac{h_1}{h_1^0}\right)^{\frac{\gamma}{\gamma-1}} = P_o \left(1 - \frac{v_1^2}{2h_1^0}\right)^{\frac{\gamma}{\gamma-1}} \tag{20}$$

10

Eliminating p_1 between Eqs. 4 and 20 gives

$$P_0 \left(1 - \frac{w_1^2}{2h_1^o}\right)^{\frac{\gamma}{\gamma-1}} = \frac{\gamma-1}{\gamma} \frac{\dot{m}}{A_1} \left(\frac{2h_1^o - w_1^2}{2w_1}\right) \tag{21}$$

Solving for $\dot{m}$ we obtain

$$\dot{m} = \frac{2p_0 A_1 \gamma w_1}{\gamma-1} \frac{(2h_1^o - w_1^2)^{\frac{1}{\gamma-1}}}{(2h_1^o)^{\gamma/(\gamma-1)}} \tag{22}$$

But from Eqs. 16 and 7,

$$w_1 = \sqrt{2 \frac{\gamma-1}{\gamma+1} (h_1^o + \Delta h)} \ W \tag{23}$$

Finally, substituting Eq. 23 into Eq. 22 yields, after some algebraic manipulation:

$$\dot{m} = C \dot{m}_i \tag{24}$$

where $\dot{m}_i$ is the mass flow rate for isentropic flow through a sonic orifice, given by

$$\dot{m}_i = \frac{\gamma p_0 A^*}{\sqrt{(\gamma-1)h_1^o}} \sqrt{\left(\frac{2}{\gamma+1}\right)^{\frac{\gamma+1}{\gamma-1}}} = \frac{\gamma p_0 A_1}{\sqrt{(\gamma-1)h_1^o}} \left(\frac{2}{\gamma+1}\right)^{\frac{\gamma+1}{2(\gamma-1)}} \tag{25}$$

The coefficient C is given by

$$C = \sqrt{\frac{W}{\theta^{\frac{\gamma+1}{\gamma-1}}}} \left[\left(\frac{\gamma+1}{2}\right) \theta - \left(\frac{\gamma-1}{2}\right) w^2\right]^{\frac{1}{\gamma-1}} \tag{26}$$

$$= W \left[\left(\frac{\gamma+1}{2}\right) \theta^{-\frac{\gamma-1}{2}} - \left(\frac{\gamma-1}{2}\right) w^2 \theta^{-\frac{\gamma+1}{2}}\right]^{\frac{1}{\gamma-1}}$$

5090-IR-3

11

The results of calculations based upon the foregoing analysis are plotted in Fig. 10. Values of γ were obtained from Ref. 7. The temperature dependences of other lithium properties were obtained from Ref. 8. It is seen that the analysis with friction and heat transfer is in much better agreement with measurements than is the simple isentropic flow theory. All of the remaining discrepancy can be accounted for by (a) inaccuracies in the best available data on lithium properties, and (b) the pressure drop across the five parallel channels in the vaporizer upstream of the critical orifice. The latter is the larger effect. In fact, it became the dominant one in tests where the "long channel" orifice was replaced by a more conventional one. This was done in anode-vaporizer assemblies 5A and 6 (see Section 4) specifically in order to more closely approximate isentropic flow (as well as for the mechanical reasons discussed in Section 4). Under typical operating conditions, the pressure drop across the entire length of the vaporizer channels (assuming the liquid-gas interfaces to be located near the channel inlets) can amount to as much as 1/10 atm.

4. ANODE-VAPORIZER DESIGN MODIFICATIONS

During the third phase of the program the lithium feed system manifested the following chronic problems:

1. Difficulty was experienced in obtaining a leak-tight joint between the anode and the vaporizer.

2. Radial cracks tended to develop in the anode each time a new one was brought up to operating temperature for the first time.

3. Inability to maintain sufficiently high temperatures in the vaporizer resulted in a severe limitation upon the maximum lithium mass flow rate.

Highest priority was assigned to the solution of problem (1), since no useful data could be obtained until the feed system leaks were eliminated. On the other hand, although problems (2) and (3) were quite serious they did not require immediate attention in order to proceed with the program. Once the excessive thermal stress in an anode had been relieved by cracking, no further cracks would develop and the anode appeared to function without significant performance degradation in subsequent tests. Furthermore, it was possible to temporarily accept the cool-vaporizer limitation and to explore the low mass flow regime. Although flooding sometimes occurred despite precautionary efforts to keep the lithium flow rate low enough, this still did not block further progress, as did problem (1).

The steps taken to achieve a leak-tight seal between the anode and vaporizer are summarized below. Success was achieved only after several months of effort involving design modifications as well as trial-and-error improvements in joining techniques. This process represented a major detour in the program and resulted in delays in meeting some of the forecast milestones.

<u>Anode-Vaporizer No. 1</u> (Figs. 12 and 13, change 1)

This assembly was used from Run 725 through Run 728B, at which time a bad crack developed in the anode.

<u>Anode-Vaporizer No. 2</u> (Figs. 12 and 13, change 2)

The same vaporizer was used, but the anode was slightly modified. The previously flat bottom was changed to a rounded contour in order to provide a greater mass of tungsten in the joint region. This effort, however, was insufficient to prevent further cracking. Moreover, while performing a calibration run (728G) at the relatively high feed pressure of 600 torr, a leak occurred in the anode-vaporizer braze joint. Several unsuccessful attempts were made to seal this leak by rerunning the assembly in the brazing furnace with various temperature cycles.

<u>Anode-Vaporizer No. 3</u> (Figs. 12 and 13, change 3)

The anode on this assembly was of the same design as the previous one, but the vaporizer was modified to provide a larger cross section at the joint in order to enhance the heat conduction. All attempts to seal the joint were unsuccessful, despite the trial of different braze materials as well as different furnace cycles.

<u>Anode-Vaporizer No. 4</u> (Figs. 14 and 13, change 1)

In this assembly the original vaporizer was brazed to a new anode with a modified joint configuration embodying the following features:

1. Deeper insertion of the vaporizer into the anode.
2. Closer tolerances on the fit.
3. Flat bottom on the anode with a chamfer to hold the braze material in place.

Although a leak-tight joint was obtained after the second furnace heating, this joint developed a leak during an attempted test run. A blockage in the feed line caused by the deposition of a small amount of lithium compound impurities prevented lithium operation. This resulted in extraordinarily high temperatures which in turn caused the joint to leak.

Anode-Vaporizer No. 5 (Fig. 15)

The second vaporizer was electron-beam welded to a new anode which was redesigned specifically for this type of welding. However, troubles were encountered during the welding procedure when cracking developed at the joint. This was probably due to boiling out of thoria from the tungsten anode.

Anode-Vaporizer No. 5A (Fig. 16)

It was determined impractical to electron-beam weld the molybdenum vaporizer directly into the thoriated tungsten anode, so both parts were modified. In this version a small molybdenum disc containing the sonic orifice used for metering the propellant flow was electron-beam welded into the top of the molybdenum vaporizer, making a leak-tight seal capable of withstanding high temperatures without deterioration. This subassembly was then brazed into the anode (in which the old metering orifice had been machined out). The essential feature of this design is that the braze joint is no longer subjected to the upstream orifice pressure, and, since metering is accomplished before lithium passes by the anode-vaporizer joint, any slight leakage at this joint cannot degrade the accuracy of the flow rate measurement. This design proved satisfactory during a test run, except that even more heat than usual was required in the vaporizer, which had the effect of limiting the operation to even higher arc currents and lower propellant flow rates than in the past.

Anode-Vaporizer No. 6 (Fig. 17)

Since problem (1) (above) appeared to have been solved, some attention could finally be devoted to problems (2) and (3). A new anode-vaporizer assembly was designed incorporating the features developed in Nos. 5 and 5A as well as the following additional features:

1. Some of the radiation fins at the top of the vaporizer were eliminated in order to achieve higher temperatures in this region.

2. A thicker cross section was provided on the anode in order to help minimize the tendency for radial cracking to occur.

5090-IR-3   15

Anode-vaporizer 6 was successfully used in an endurance test of the engine. This test was voluntarily terminated after 109 hours of operation, 108 of which were on lithium and 100 of which were uninterrupted. At the end of this test the anode-vaporizer assembly was found to have undergone no noticeable erosion and its condition was like new in every respect. Although problems (1) and (2) were solved by this design, the cool-vaporizer difficulty was not appreciably helped by the elimination of the upper fins. Work is currently under way on a modified design aimed at eliminating this final problem. The approach involves increasing the area of contact between the anode and the vaporizer so as to provide a broader path for the conduction of heat down into the vaporizer. This design will be tested in the near future.

5. AMMONIA TESTS

Two tests were made in which ammonia was used, both as the primary propellant and as the buffering gas. The thrustor configuration used for both tests is shown in Fig. 18. A schematic diagram of the ammonia feed system is shown in Fig. 19. Although the problem of feeding gaseous ammonia is certainly more straightforward than that of feeding lithium vapor, there is one significant complication in the use of ammonia: a separate gettering system is required in order to maintain a sufficiently low vacuum chamber pressure. After investigating a number of alternate schemes, it was decided that lithium would be a good choice as the gettering agent since it was known to be effective and the technology for handling it was available. The simplest way of injecting lithium vapor into a vacuum chamber is, of course, a boiler. Two such units, of about 1/4 lb capacity each, were fabricated and placed on the floor of the vacuum chamber as shown in Fig. 20.

Although the gettering system worked well, the tests themselves were disappointing. The results, in the form of histograms and performance plots, are presented in Figs. 21 through 26. The poor performance obtained probably stems more from the fact that the thrustor used in the tests was designed specifically for lithium than from the intrinsic inferiority (from the standpoint of frozen flow efficiency) of ammonia as a propellant. In view of the inconclusive results, it is perhaps not surprising that the relatively high performance achieved with lithium is not easily duplicated without simultaneously duplicating the thrustor configuration which was painstakingly developed for this purpose.

6. TESTS WITH THREE MAGNETS

Tests of an accelerator configuration using three magnets failed to give the increased performance which had been theoretically predicted. Our analysis had predicted that by adding a third magnet downstream of the two existing coils (Fig. 27), a higher voltage could be supported, and the currents would extend further downstream into the acceleration zone, giving better efficiency. Three tests were conducted using this geometry. Two of these were tests using ammonia as an expellant for which we do not have any other data for comparison. The other test (Run 731) was with lithium, and the results (Figs. 28 through 33) show that the voltage was not increased, and that the thrust and efficiency were about the same as in the two-magnet configuration.

In principle, the shape of the magnetic field produced by the three magnet coils could have contributed to the failure of Run 731, which was an attempted life test. The third coil not only lengthened the field, but also increased the relative strength of the field downstream from the cathode, producing a greater mirror ratio, which may have affected particle motions. Also the magnetic field gradient near the cathode was reversed (or made nearly zero) which would affect cathode performance. Since the accelerator ran for more than three hours before the failure occurred (when trying to restart after a momentary shut-down to obtain a zero reading for thrust measurements), it is likely that the third magnet was not the direct cause of the failure. Accelerator performance with three magnet coils was similar to that with two except that more power was required to energize the coils.

Tests with three coils (Runs 729 and 730) using ammonia as an expellant showed that the anode melted at some spots. Since this did not occur with lithium in Run 731, it is believed that this melting was due to ammonia and not the magnet configuration.

7. LIFE TESTS

The main effort over the past several months of this program has been that of increasing the lifetime of the engine. A new feed system (see Sections 3 and 4) has been developed specifically for this purpose. The first test conducted with this feed system was Run 725. Although it was planned primarily as a checkout of the gas-actuated feed system, this run produced some usable performance data (see Figs. 34 through 41).

Three tests have been conducted for the specific purpose of evaluating the lifetime capability of the accelerator and feed system. The first test lasted 30 hours, using the engine configuration shown in Fig. 42. Since the mass flow rate appeared somewhat low during the test, at the end of 30 hours attempts were made to increase the lithium flow rate. These resulted in flooding the engine with liquid lithium and the test was then terminated. The P/T values obtained during this test and the thermal, thrust and overall efficiencies are plotted versus I_{sp} in Figs. 43 through 46. Figure 47 shows the thermal efficiency versus arc power. Histograms of the measured data are presented in Figs. 4 through 9. Several features are worthy of note. First, the performance level is not very high since a maximum thrust level of only about 33 grams was obtained. When this engine had been tested previously under similar conditions, except with a higher mass flow rate (7-8 milligrams/sec instead of 6-7), more than 40 grams of thrust had been obtained. Second, some periodicity in the data can be seen. The low mass flow rate and the periodicity were found, after some investigations, to be due to problems with the new feed system. Tentatively, it was assumed that variation in the level of the vapor-liquid interface was occurring, thus giving rise to fluctuations in the lithium flow rate. Also, it was felt that the

interface was quite low in the vaporizer so that viscous pressure
drops through the various gas passages could seriously reduce the mass
flow rate below what should be obtained for a given applied pressure
at the lithium reservoir.

Extensive calibration tests were carried out on the feed system
to study the relation between mass flow rate and applied pressure. Some
calculations on the magnitude of viscous pressure losses were also
carried out. As indicated at the end of Section 3, this pressure drop
can be significant.

The engine configuration used in the second endurance test is
shown in Fig. 48. This test was terminated after 3-1/2 hours, when
arcing between the buffer and anode was observed. Performance plots
similar to those for the 30-hour test appear in Figs. 31 through 33
and histograms of the data are presented in Figs. 28 through 30. It
is felt that arcing to the buffer may have been related to the reversal
of the magnetic field gradient in the cathode-buffer region due to the
addition of the third magnet. Previous tests have indicated that when
this occurs, arcing to the buffer may result. Another possible reason
for the arcing is that the position of the buffer relative to the anode
changed slightly during the test (a failure in the support structure
was observed). The third magnet was removed in subsequent tests.

The third test was originally scheduled as a 65-hour run. The
thrustor configuration was identical with that of the previous test
(Fig. 48). Note the shortening of the buffer "nose". This was done
in an unsuccessful effort to decrease the power loss to the buffer.
After 7 hours and 44 minutes of operation the run was interrupted in
order to repair the heater on the top plate of the lithium reservoir.
Three hours later the test was resumed, but after another hour and a
half of running, it was necessary to shut down again, this time because
of loss of mercury from the pots to the main reservoir heater. After
a 2 hour and 42 minute delay the trouble was finally corrected and the
arc was turned on. Thereafter, it ran very smoothly and with no

electrode erosion that could be discerned with a telescope mounted out-
side the aft end of the vacuum chamber. Consequently, after having
exceeded 65 hours of operation since the last interruption it was
decided to allow the test to continue. It was shut down after 100
hours of continuous operation. Subsequent examination corroborated
the telescopic observations of the remarkably good condition of the
electrodes. Histograms of the measured data are shown in Figs. 49
through 67 and photographs of the electrode components after the test
are shown in Figs. 68 through 71.

8. THEORY AND MECHANISMS

8.1 Introduction

Attempts to obtain a complete theoretical understanding of the operation of a plasma Hall current accelerator have been unsuccessful. Nevertheless, solutions have been found for simplified portions of the problem which are useful in design and optimization of accelerators.

The Hall current accelerator which is presently being tested is an axially symmetric device, with a pointed cathode along the centerline, a buffer or constrictor through which the cathode arc must pass, an annular anode, a magnet for producing a magnetic field, and an expellant feed system. The expellant is ionized by the discharge, and accelerated along the axis by electromagnetic forces. For the purpose of analysis the problems have been classified into the following categories:

1. Cathode and Cathode Buffer - The pointed, conical cathode has a high current density attachment at the point. This mode of operation appears possible only when relative high pressure is maintained by the buffer and gas feed, and it seems desirable since losses are smaller. Problems which need study are power losses to these components, lifetime limits, and stability of operation.

2. Cathode Jet - The electrons emitted by the cathode and the gas fed around the cathode emerge through the buffer constriction as a current-carrying jet which proceeds downstream. This feature is readily apparent in experimental tests. Problems are ionization, heating, confining, rotation, and acceleration.

5090-IR-3   25

3. __Anode__ - The circular anode with expellant fed through its inner surface has a diffuse current attachment. The amount of power which appears in the anode is dependent upon the mechanisms in the arc (anode sheath) and so for convenience we have included ionization in the anode sheath as an anode problem. Problems which need study are power loss and ionization efficiency.

4. __The Anode Sheath__ - The expellant introduced through the anode is ionized and forms an annular zone which carries the ions and the current axially downstream where it eventually merges with the cathode jet. This annular anode sheath does not appear to be as sharply defined as the cathode jet. The problems include heating, confining, rotation and acceleration.

5. __The Magnetic Nozzle__ - That region of the flow field which is downstream of where the jets meet and which carries no axial or radial currents but may produce acceleration by converting internal and rotational energy into directed kinetic energy, is called the magnetic nozzle.

6. __Magnetic Field__ - A solenoidal magnetic field is supplied by a set of coils. Magnetic field optimization is achieved as a compromise between minimum power requirements for magnets and good acceleration and voltage characteristics of the discharge.

8.2 Acceleration

The analytical effort has been directed toward the study of the mechanisms for adding momentum and energy to the plasma in a plasma accelerator. This analysis has used the two jet model, which was suggested by the experimental evidence. A cathode jet and anode sheath extend downstream from the electrodes, roughly following the lines of the applied magnetic field. These two jets then converge due to diffusion across the applied magnetic field. In this section

results will be shown for (1) the study of the ion trajectories in the anode sheath in a magnetic field which decreases in strength downstream from the anode, and (2) a more detailed look at the conservation of axial momentum in the cathode jet.

In the volume of the anode sheath collisions are rare, so we shall examine the collisionless trajectories of the ions. ∴ vector notation these equations are

$$m\ddot{\bar{r}} = e(\bar{E} + \dot{\bar{r}} \times \bar{B})$$

(27)

Since we have axial symmetry we use cylindrical (r,θ,z) coordinates. B_r and B_z come from the vector potential.

$$B_r = -\frac{\partial A_\theta}{\partial z}; \quad B_z = \frac{1}{r}\frac{\partial}{\partial r}(rA_\theta)$$

(28)

E_r and E_z come from the scalar potential.

$$E_r = -\frac{\partial \varphi}{\partial r}; \quad E_z = -\frac{\partial \varphi}{\partial z}$$

(29)

E_θ is zero, and we shall neglect B_θ. The three component equations of Eq. 27 can be written, and the θ-component equation can be integrated to give

$$mr^2\dot{\theta} + erA_\theta = P_\theta$$

(30)

where P_θ is a constant. As was shown in Ref. 4, Eq. 30 can be used to eliminate θ from the r and z component equations of Eq. 27 to give

$$m\ddot{r} = -e\frac{\partial \varphi}{\partial r} - \frac{\partial H}{\partial r} = -\frac{\partial H_e}{\partial r}$$

$$m\ddot{z} = -e\frac{\partial \varphi}{\partial z} - \frac{\partial H}{\partial z} = -\frac{\partial H_e}{\partial z}$$

(31)

In Eq. 31, H is the pseudo potential, and is given by

$$H = \frac{(P_\theta - erA_\theta)^2}{2mr} \tag{32}$$

The total effective potential H_e for a magnetic field which changes slowly with z will be examined and its effect upon the ion motion will be discussed.

To see how the diverging magnetic field affects the solution, consider some models for the potentials which are similar to those in the accelerator. The vector potential

$$A_\theta(r,z) = \frac{rB(z)}{2} \tag{33}$$

gives

$$B_r(r,z) = -r\frac{\partial B}{\partial z}/z$$

$$B_z(r,z) = B(z) \tag{34}$$

If we take $\theta = 0$ at $z = o$, $r = R_A$ (the anode)

$$P_\theta = R_A^2 B(0)/2 \tag{35}$$

$$H(r,z) = e^2\left[R_A^2 B(0) - r^2 B(z)\right]^{-2}/8 \ mr^2 \tag{36}$$

For the scalar potential, we know that it is ϕ_o (applied voltage) at the anode, zero at the cathode, and approximately constant along the magnetic field lines.
Choose

$$\phi(r,z) = \phi_o B(z) \ r^2/B(0) \ R_A^2 \tag{37}$$

Combining:

$$H_e = \frac{e^2}{8m} \left\{ \frac{\left[R_A^2 \, B(0) - r^2 \, B(z) \right]^2}{r^2} + \zeta \, r^2 \, B(0) \, B(z) \right\} \tag{38}$$

where the dimensionless parameter ζ is given by

$$\zeta \equiv \frac{8m \, \phi_o}{e \, R_A^2 \, B^2(0)} . \tag{39}$$

Roughly ζ is a ratio of electric to magnetic forces, and motions with large ζ are dominated by electric field forces while small ζ indicates that magnetic field Lorentz forces are dominant. In the accelerator ζ is of order one.

Now look at some contour lines of the effective potential $H_e(r,z)$. Consider the case where $B(z)$ is constant, and the case where $B(z)$ is a decreasing function. Such contour plots are shown in Fig. 72. As can be seen the axial force is zero in the constant $B(z)$ case, and positive when $\partial B(z)/\partial z$ is negative. The motion of the ion is confined between the two lines where $H_e = (e^2/8m) \, \zeta \, R_A^2 \, B^2(0)$ and the total effective potential has a valley between these two contours. This can be seen more clearly if we rewrite Eq. 38 as

$$H_e = \frac{e^2}{8m} \left\{ 2 \, R_A^2 \, B(0) \left[\sqrt{B^2(z) + \zeta \, B(0) \, B(z)} - B(z) \right] \right.$$

$$\left. + \left[\frac{R_A^2 \, B(0)}{r} - r \sqrt{B^2(z) + \zeta \, B(0) \, B(z)} \right]^2 \right\} \tag{40}$$

The location of the "valley floor" can be found by finding the value of r which makes the second term zero, and the "height" is given by the first term. The axial acceleration can be found from $d \, H_e \, (r_{valley}, z)/dz$.

29

In conclusion a decreasing magnetic field will produce acceleration, but this acceleration will be greatest when $B(z)$ is much less than $\zeta B(o)$.

Next look at the axial momentum in the cathode jet. Use quasi-one dimensional flow theory. The total momentum convected by the jet can be found by integrating across the jet and is given by

$$\dot{m}w + Ap = F_o \tag{41}$$

Two cases are easy to analyze. In a pure axial magnetic field, F_o is a constant, since there are no axial forces. In the case of a flow in a duct, the surface pressures cause F_o to change by $dF_o/dz = p\, dA/dz$. In the cathode jet in an expanding magnetic field neither of these is correct. We evaluate dF_o/dz by the integral over the cross section of the axial body force. In a neutral plasma, the only forces are JXB, which are perpendicular to the lines of force. Thus

$$X_z = -\frac{\partial B_r}{\partial B_z} X_r \tag{42}$$

Since there is a negative X_r to overcome radial pressure gradients and centrifugal forces, there will be a momentum increase.

Now determine how this momentum change is distributed between Ap and $\dot{m}w$. It is conventional to introduce the Mach number such that the ratio

$$\dot{m}w/Ap = \gamma M^2 \tag{43}$$

Then

$$Ap = F_o/(1 + \gamma M^2) \tag{44}$$

$$\dot{m}w = F_o\, \gamma M^2/(1 + \gamma M^2) \tag{45}$$

Using the continuity equation,

$$\dot{m} = \rho A w \qquad (46)$$

the enthalpy in internal and axial kinetic energy is related to the Mach number by

$$\frac{\gamma}{\gamma-1} \frac{p}{\rho} + \frac{w^2}{2} = \frac{\frac{\gamma}{\gamma-1} (\gamma M^2) + \frac{1}{2} (\gamma M^2)^2}{(1 + \gamma M^2)^2} \frac{F_o^2}{\dot{m}^2} . \qquad (47)$$

Figure 73 comes from eliminating M between Eq. 44 and Eq. 47. Here we see that if F_o is constant (uniform magnetic field) increasing the enthalpy decreases Ap in the subsonic region. If F_o increases (cathode jet in diverging field) with no increase in enthalpy, Ap/F_o decreases, which means that Ap decreases also. Thus adding total axial momentum (F_o) decreases pressure (Ap). Of course this is explained by an increase in $\dot{m}w$. The ratio of enthalpy to the square of F_o is a monotonic function of Mach number, so that the pressure (Ap) may increase or decrease depending upon the relative rates of change of enthalpy and momentum. Finally one can observe that Ap/F_o can only change about a factor of two, so if great precision is not needed, or if derivatives are not needed, $Ap \approx F_o$.

8.3 Ionization

The two types of losses which are related to ionization are expellant losses due to incomplete ionization and power loss due to thermal conduction to electrodes and radiation. Volume ionization occurs in the anode sheath and the cathode jet when electrons of sufficient energy collide with atoms. This ionization may occur to any atoms which are present, for example, background gas in the test facility. If the number density of the background is nearly as large as the number density of supplied expellant, the device can entrain and accelerate enough ambient atoms to invalidate the test results.

The high mass utilization and moderate power loss can be explained in terms of the electron energy.

The electron energy in the volume where ionization occurs is regulated by the ionization process. This is due to the threshold in the ionization cross section (probability of ionization) at low energy. The ionization cross section for lithium by mono-energetic atoms is zero for less than 5.36 eV, climbs rapidly to a peak of about 5×10^{-20} m^2 at 10 to 12 eV, and falls off at higher energy. The electrons in the discharge have a distribution of energy (probably non-Maxwellian due to the strong applied magnetic field and low collision rate). A large fraction of these electrons must have energies above the threshold values in order to produce the ions. In a typical operation, the number of atoms to be ionized per second is of the same order of magnitude as the number of charged particles per second needed to carry the applied current past a given point, hence most of the electrons must produce ions in order to get good mass utilization.

We conclude that, because of the rapid rise of ionization probability at energies greater than the ionization energy threshold, the energy of the electrons will be about the same as the ionization potential. Electrons with energies much larger than this are not required, and are prevented by the heat sink effect of the ionization.

Mass utilization will be great if the mean free path for ionization of an atom is small compared with the path length of the atoms through the anode sheath. Atoms are fed from the inside of the anode, and around the cathode. From either location the atoms must pass through the discharge in order to escape un-ionized. The mean free path length is given by:

$$\lambda = V_a / n_e Q_{ea} V_e$$

where V is the thermal speed, and Q_{ea} is the ionization cross section. Substituting some typical values (MKSA units)

$$\lambda = \frac{(1.3 \times 10^3)}{(6.2 \times 10^{19})(3 \times 10^{-20})(1.3 \times 10^6)} = (5.4 \times 10^{-4})$$

Since this is much less than the thickness of the anode sheath, the chance of ionization is quite good. On the other hand, the mean free path of an electron before it causes an ionization is $1/n_a Q_{ea}$, which is several orders of magnitude larger than λ (of the order of centimeters). The presence of the magnetic field, which can trap electrons in orbits whose guiding center motion is small compared to the electron motion, can make the displacement of an electron much less than the length of the helical path. Thus the physical parameters of the problem are such that high mass utilization is possible, with electrons about as energetic as the ionization potential.

The anode power is largely due to electrons convecting their energy to the surface and then falling through the work function potential as they enter the material. This means that the anode power (not taking into account the regenerative heat used to vaporize the liquid expellant) is equal to the product of the current and the effective potential

$$P_{anode} \approx I \, (V_{ioniz} + V_{wf})$$

If we compare this with the power to ionize

$$P_{ioniz} = (e \, \dot{m}/m_a) \, V_{ioniz}$$

the ratio is

$$\frac{P_{anode}}{P_{ioniz}} = \frac{m_a I}{e \, \dot{m}} \left(1 + \frac{V_{wf}}{V_{ioniz}} \right)$$

The anode losses will be the same order of magnitude as the frozen flow losses unless the current is less than the mass flow rate (converted to equivalent units).

Ionization in the cathode jet is like the anode sheath, in that it is the result of volume ionization of any ambient gas. Because of the higher number density of particles in the cathode jet, the electrons are more thermalized than in the anode sheath. This produces a few electrons at very high energy, which is the reason for the presence of the observed green radiation from the lithium ions.
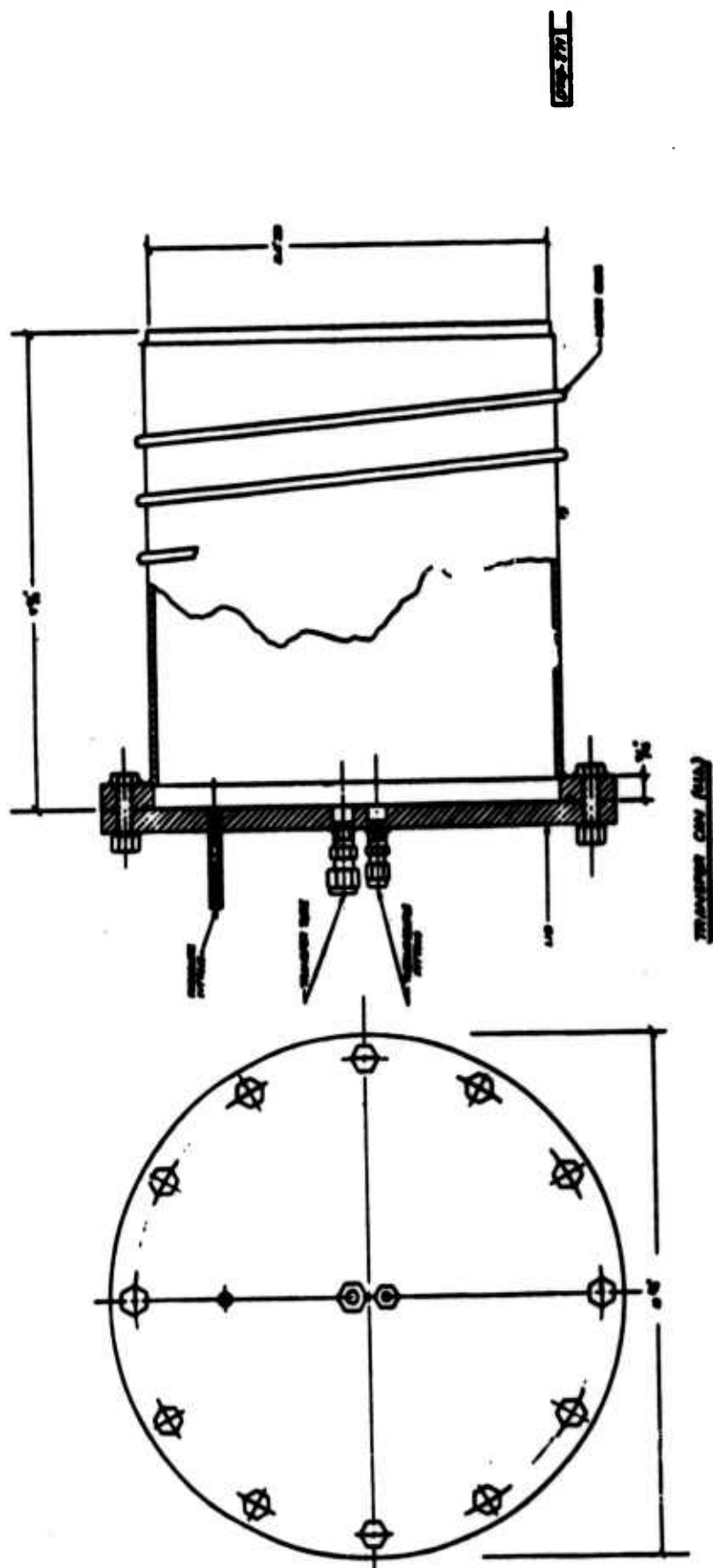
Figure 1 Four-Pound Propellant Reservoir

35
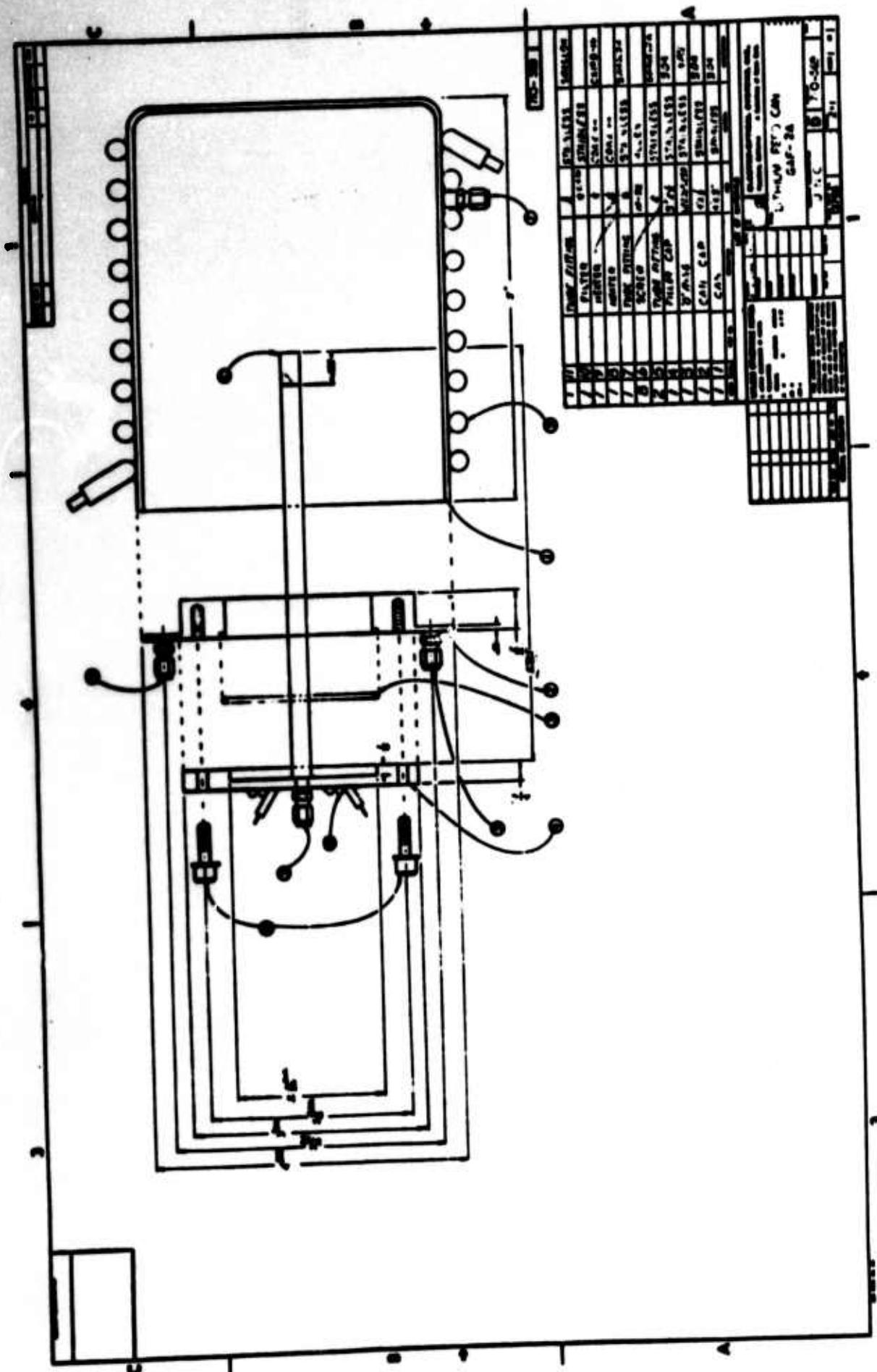
Figure 2 One-Pound Propellant Reservoir

5090-IR-3

36
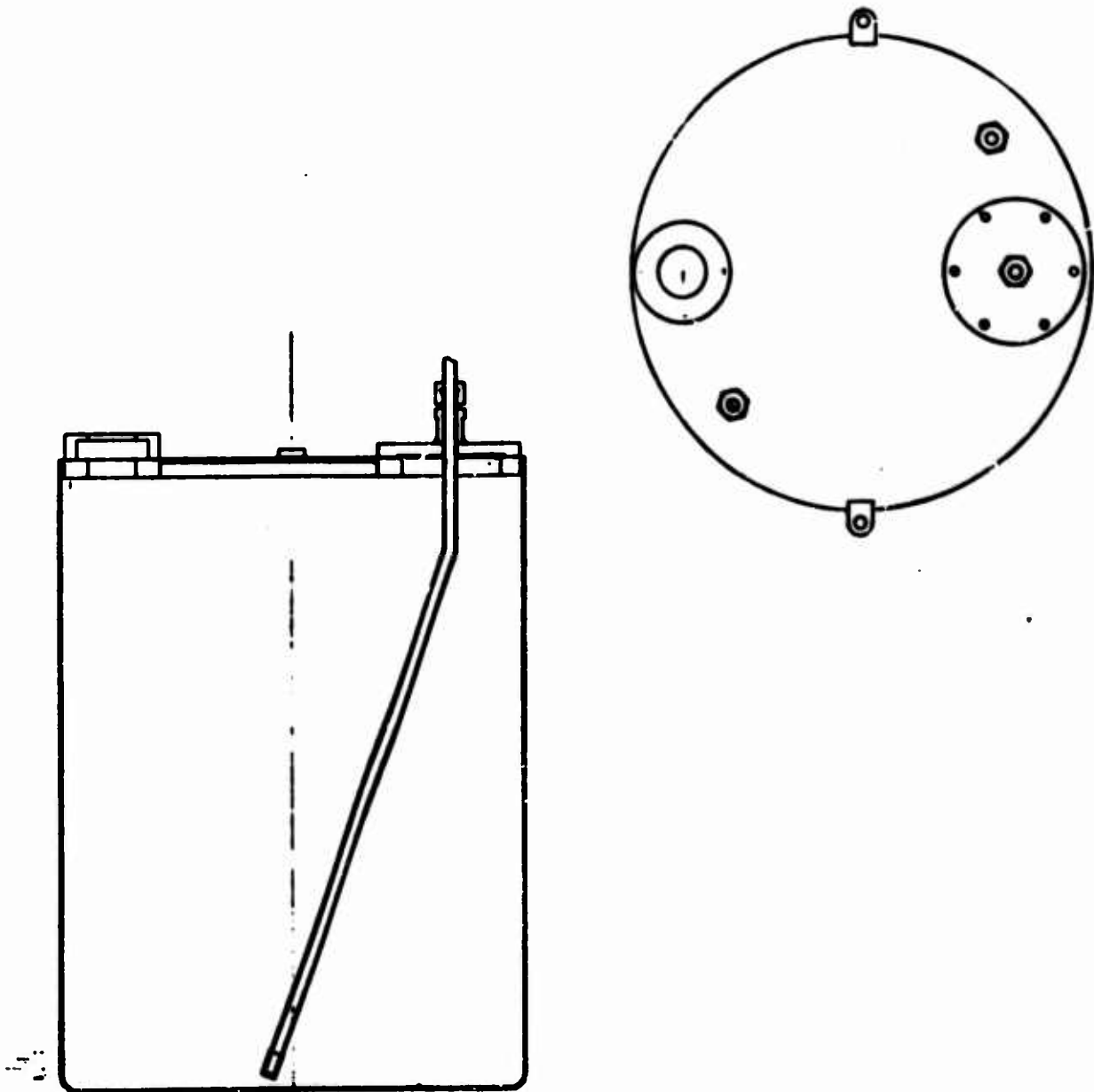
Figure 3   Eight-Pound Propellant Reservoir
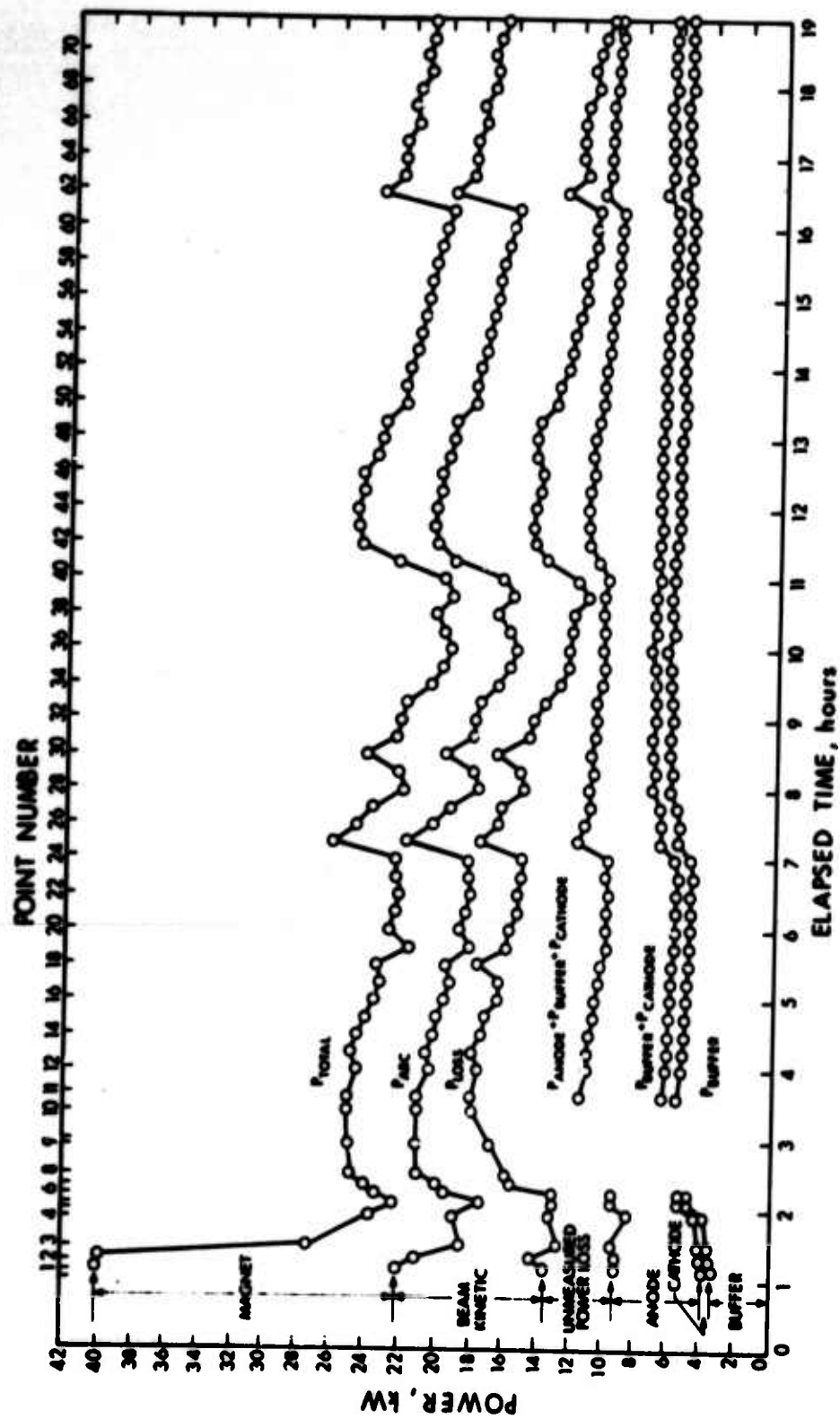
Figure 4 Histogram of Power Distribution for Run 727
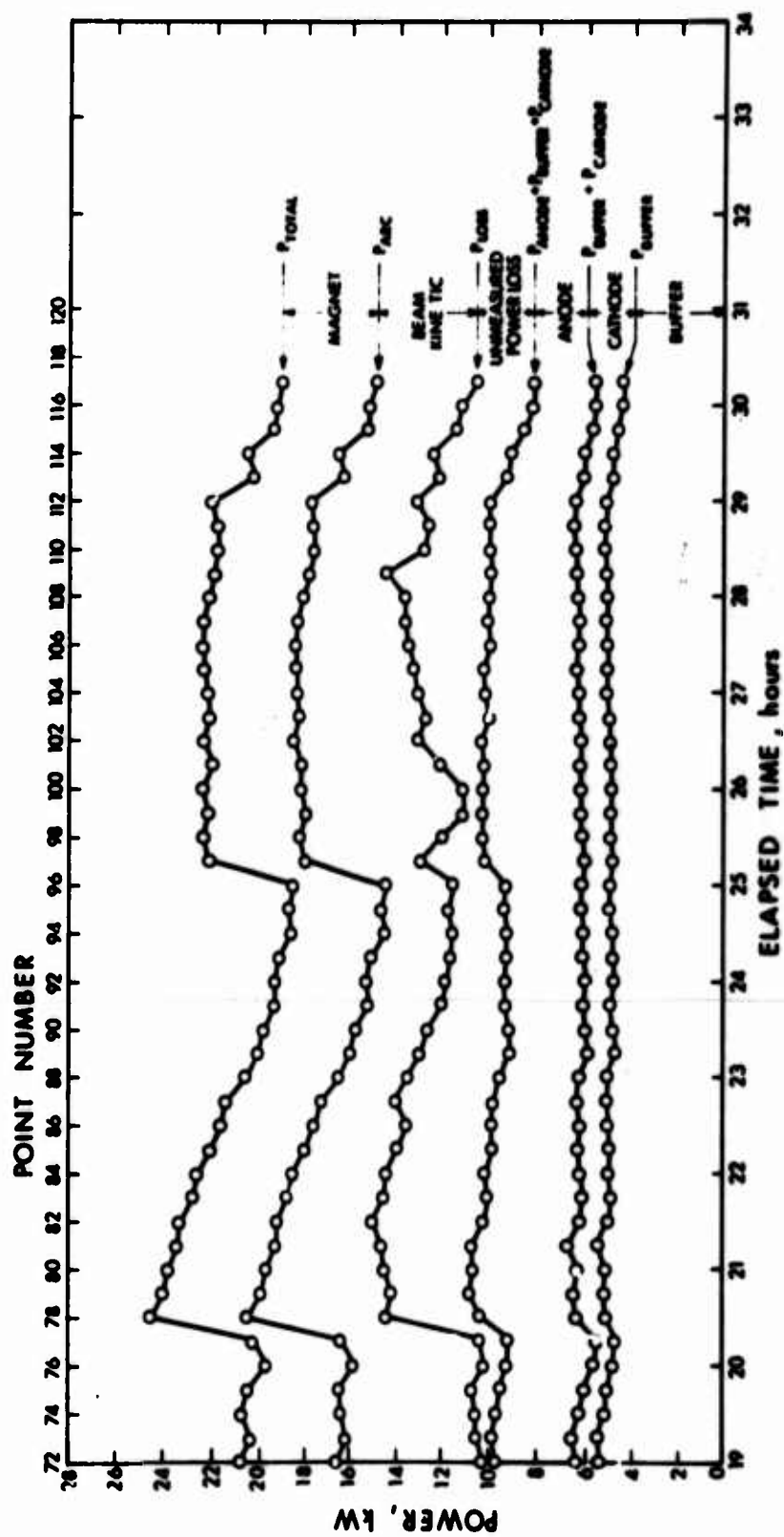
Figure 5 Histogram of Power Distribution for Run 727 (continued)

5090-IR-3

39
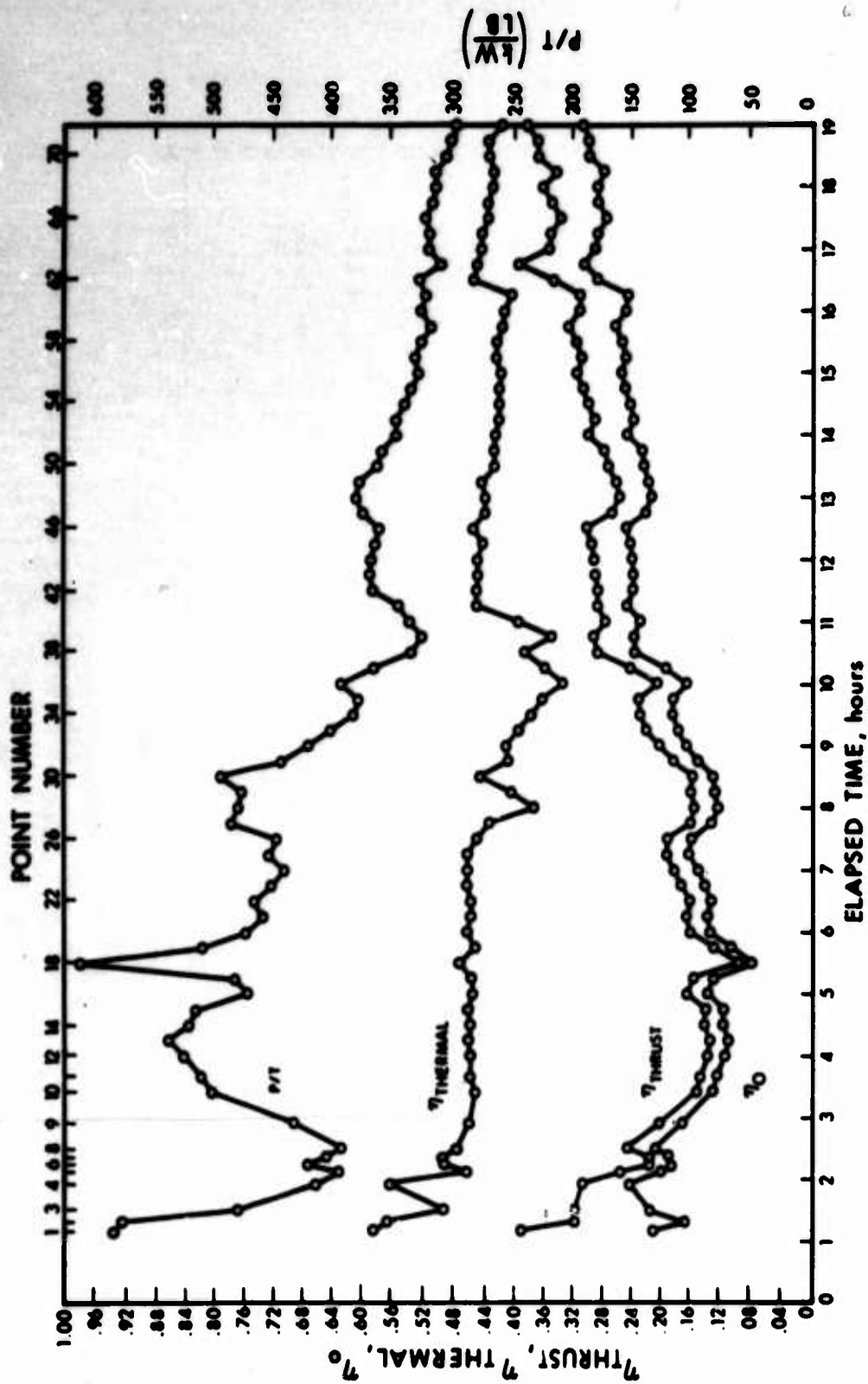
Figure 6 Histogram of Efficiencies and P/T for Run 727
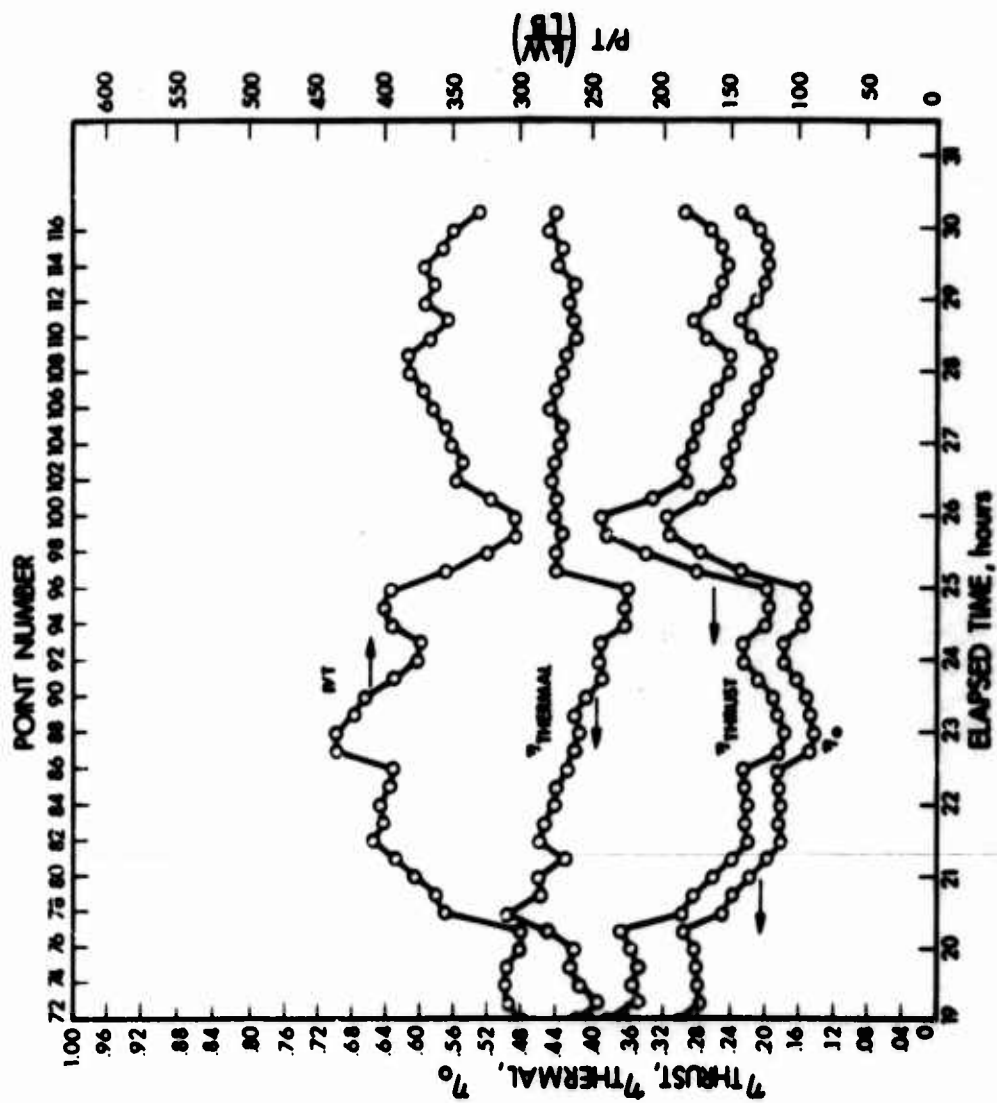
Figure 7 Histogram of Efficiencies and P/T for Run 727 (continued)
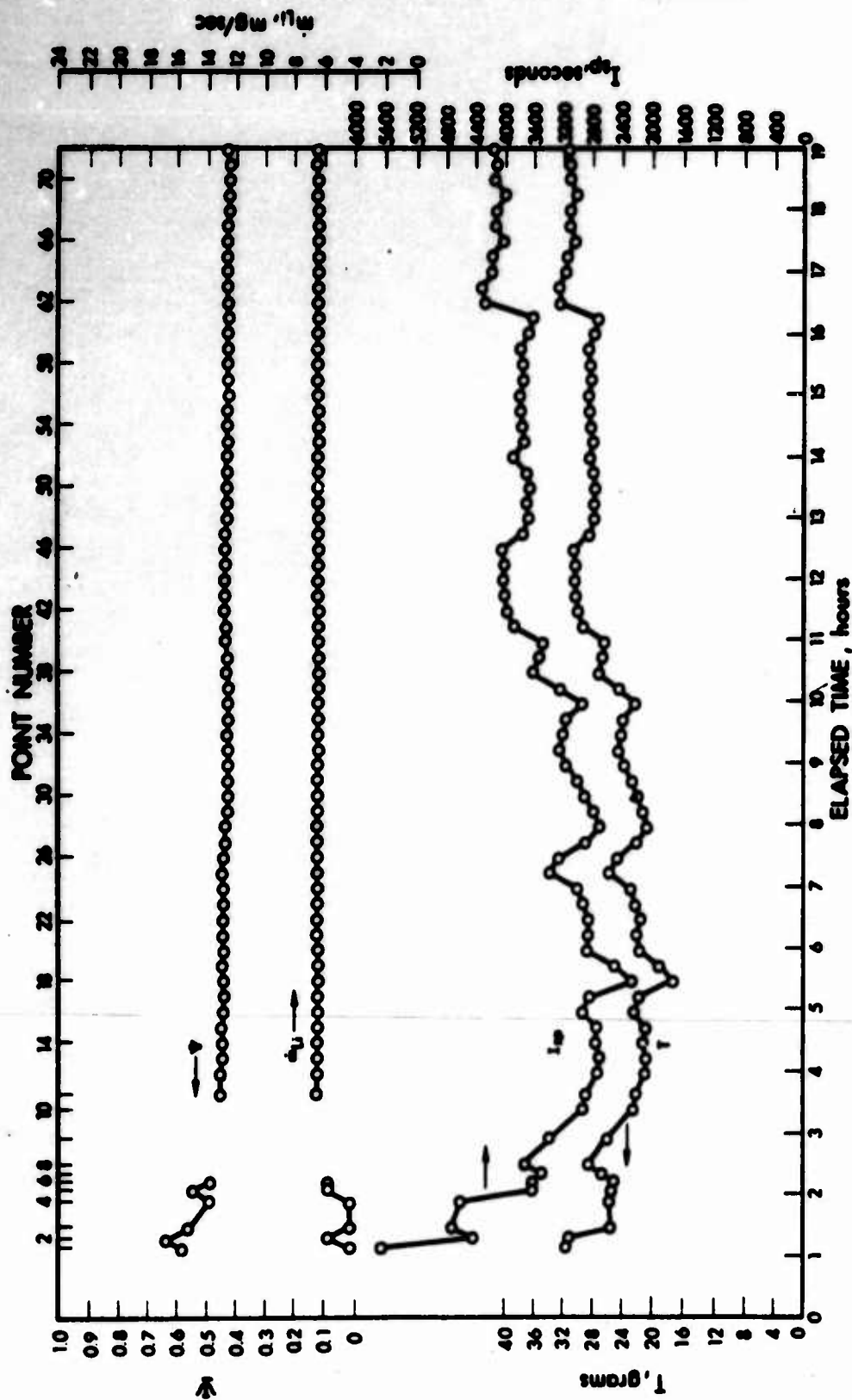
Figure 8 Histogram of T, I_{sp}, $\dot{m}$ and γ for Run 727

Figure 9 Histogram of T, I_{sp}, $\dot{m}$ and Y for Run 727 (continued)
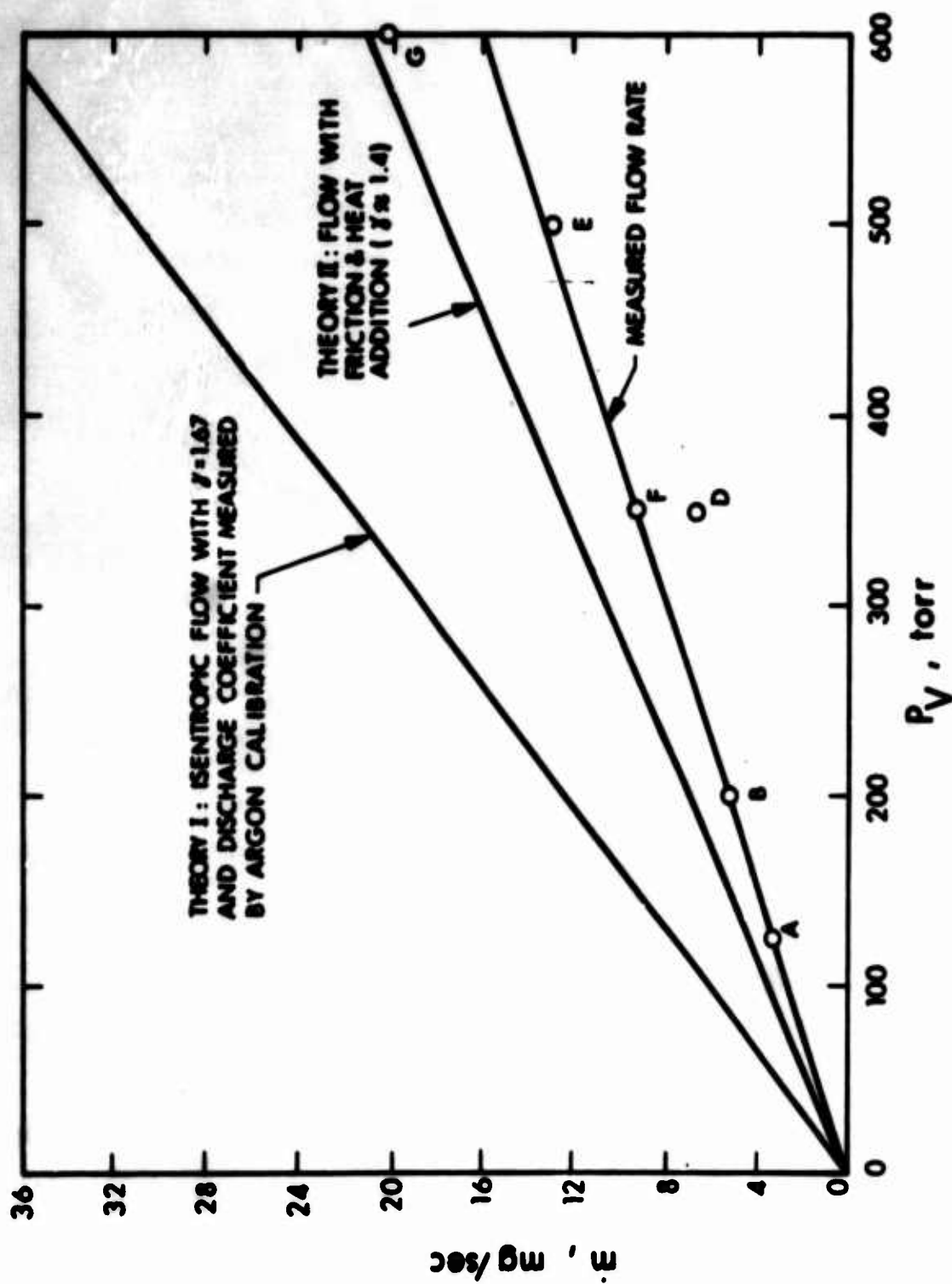
Figure 10 Lithium Mass Flow Rate versus Pressure

THEORY I: ISENTROPIC FLOW WITH $\gamma = 1.67$
AND DISCHARGE COEFFICIENT MEASURED
BY ARGON CALIBRATION

THEORY II: FLOW WITH
FRICTION & HEAT
ADDITION ($\gamma = 1.4$)

MEASURED FLOW RATE

P_V , torr

$\dot{m}$, mg/sec
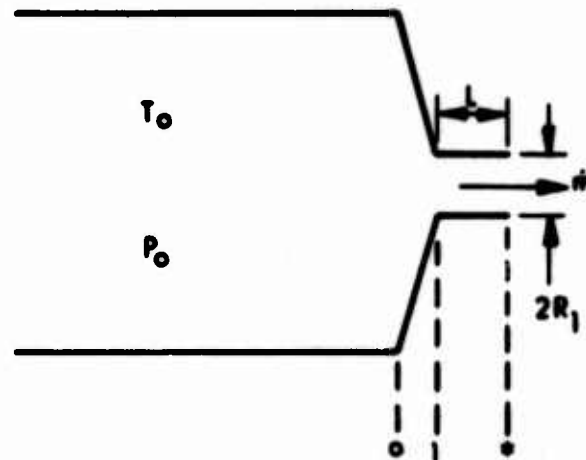
ASSUMPTIONS

1. UPSTREAM OF STATION o THE LITHIUM IS A STAGNANT VAPOR WHOSE TEMPERATURE AND PRESSURE ARE T_o AND P_o RESPECTIVELY.

2. ISENTROPIC EXPANSION OCCURS BETWEEN STATIONS o AND I.

3. HEATING AND FRICTION OCCUR BETWEEN STATIONS I AND *.

4. AT STATION * THE FLOW IS CHOKED AND THE STAGNATION TEMPERATURE IS $T^{o*} = T^o_I + \Delta T$.

5. CONDENSATION DOES NOT OCCUR.

Figure 11   Geometry and Assumptions for Choked Flow Analysis
With Friction and Heating

73625316

Figure 12 Anode Nos. 1, 2 and 3
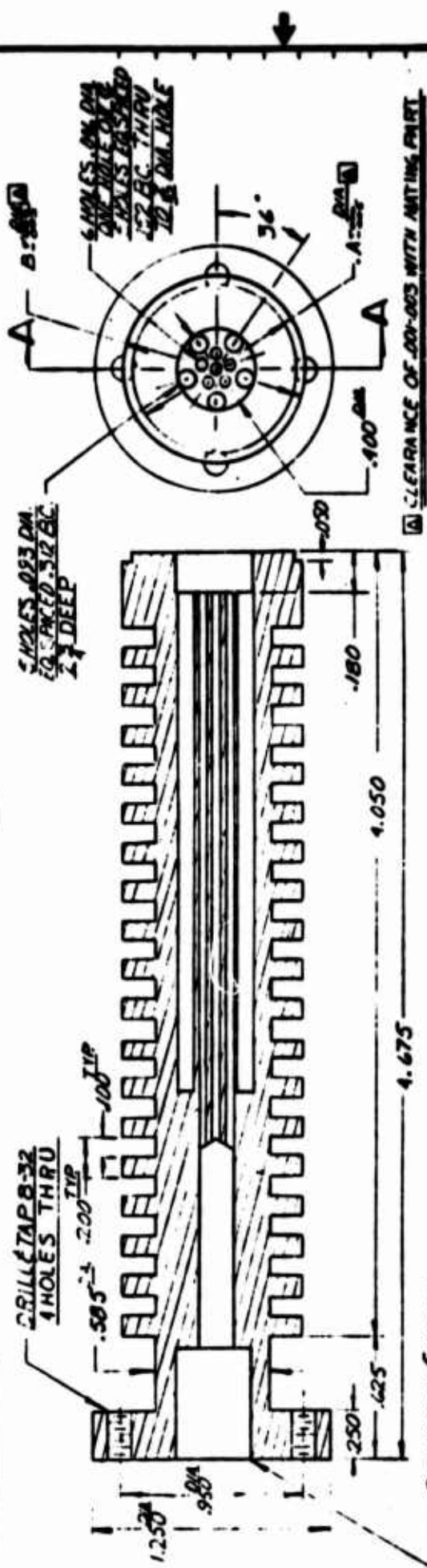
Figure 13 Vaporizer Nos. 1, 2, and 3

3.125 DIA.

30°
45°
1.900 ± .002
1.300
.800
C
.950
.475

VIEW A-A

.0433 DIA

30°
.355
.050 × 45°
CHAM
.400 +.010 -.000
.725

DETAIL C
SCALE 2-1
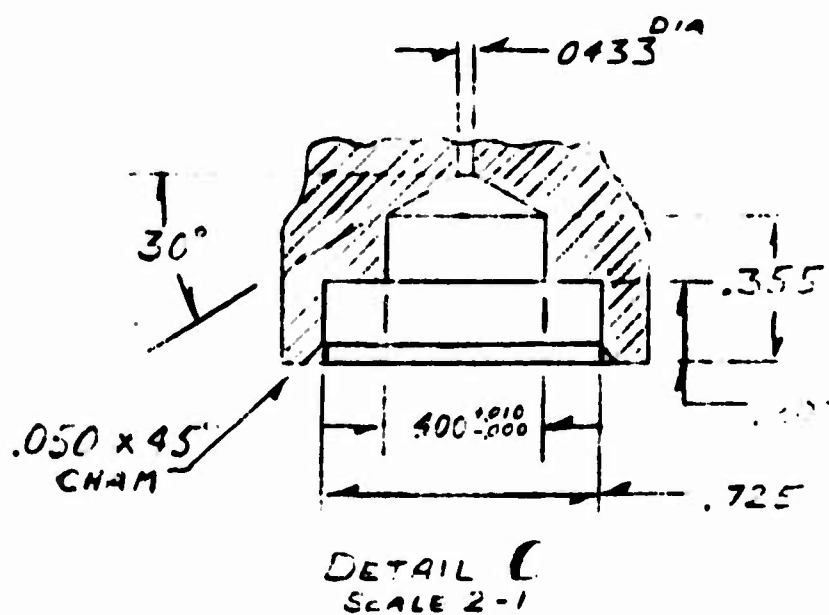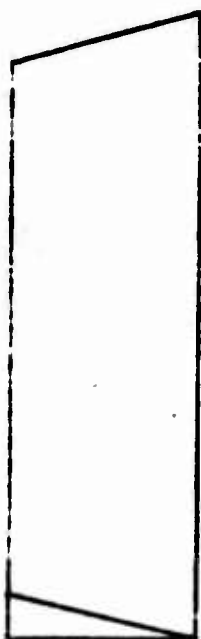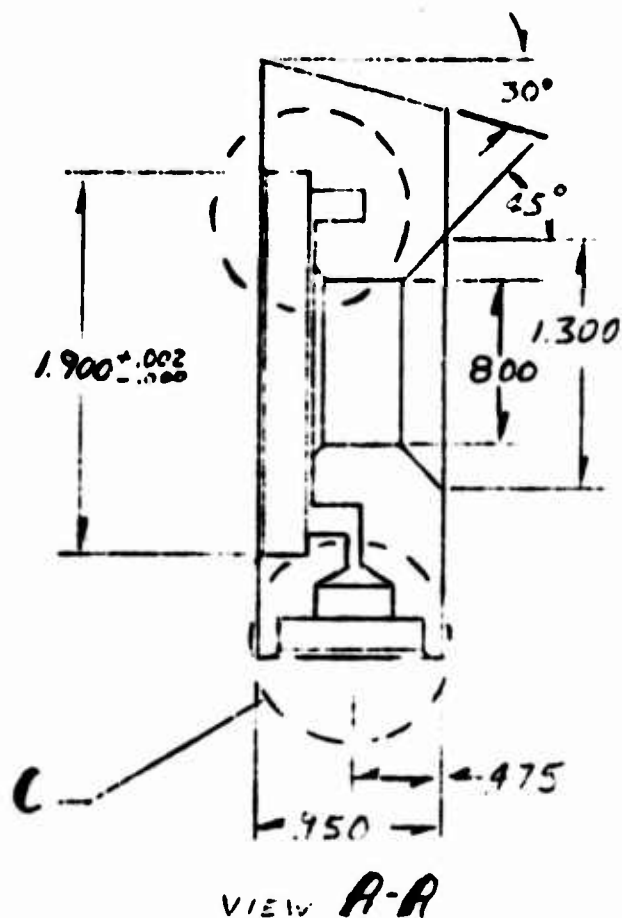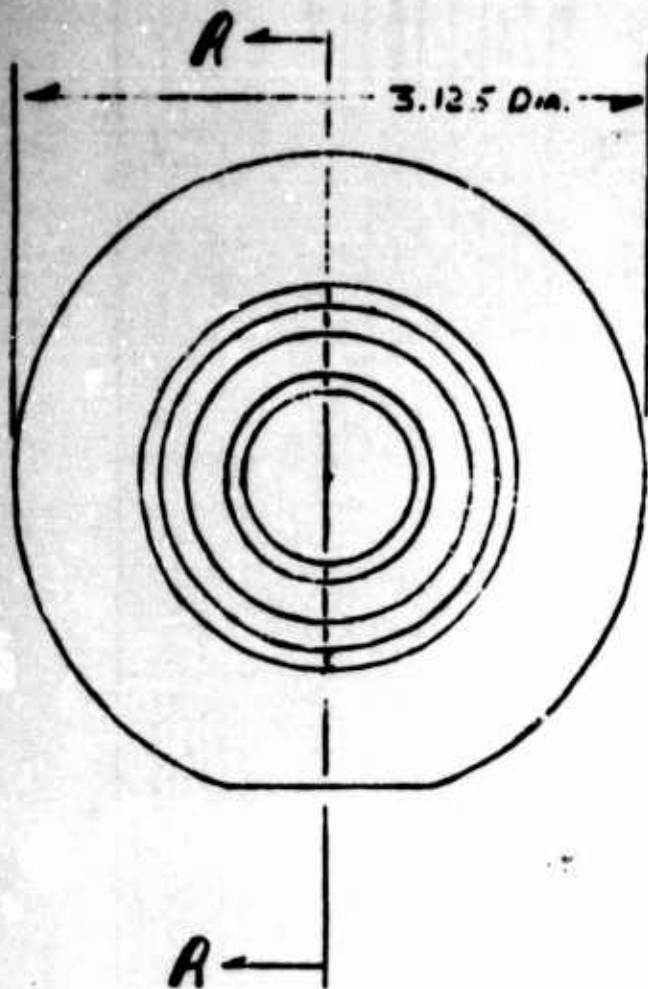
Figure 14   Anode No. 4

VIEW AA
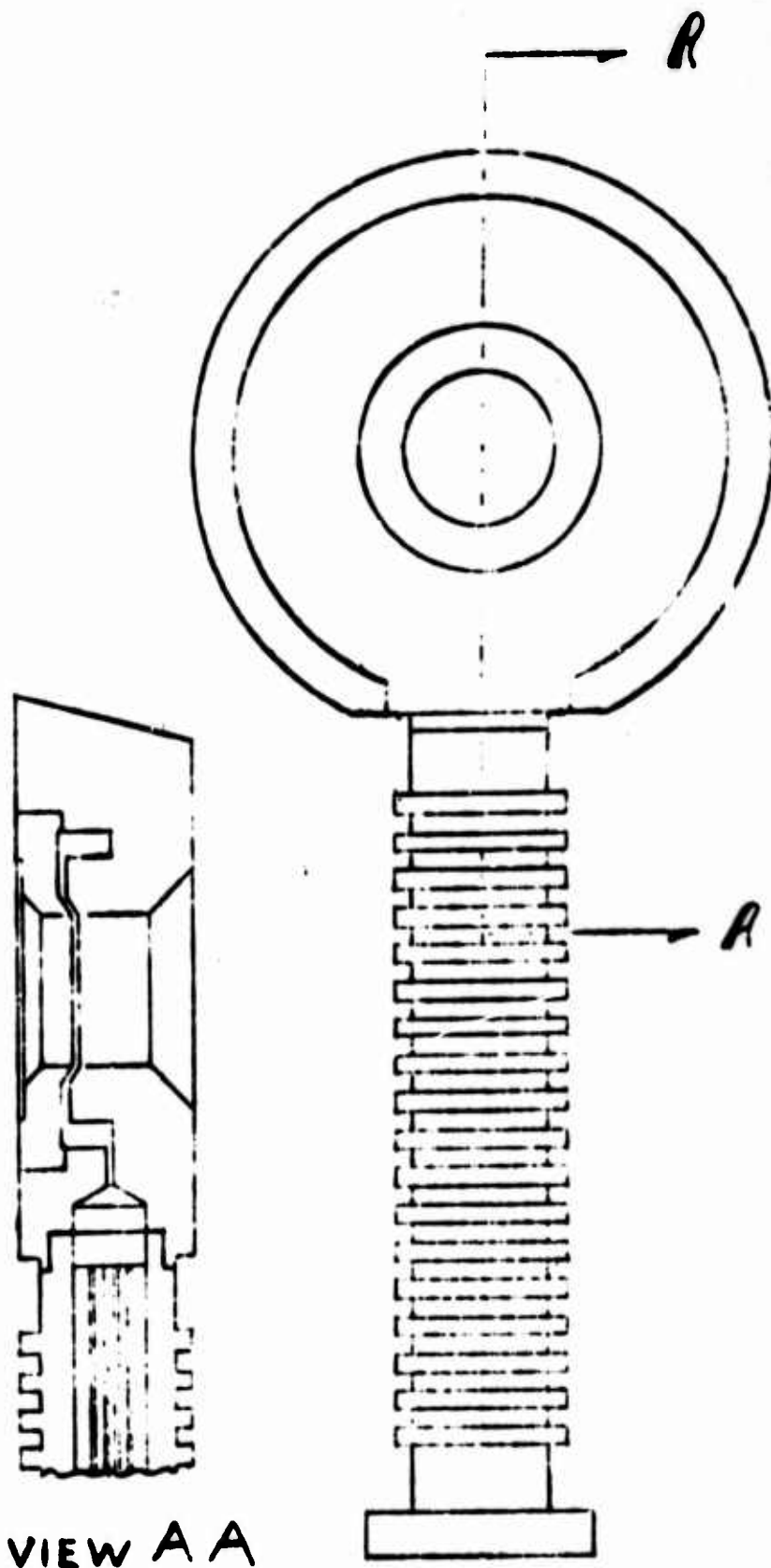
Figure 15   Anode-Vaporizer No. 5

VIEW A A
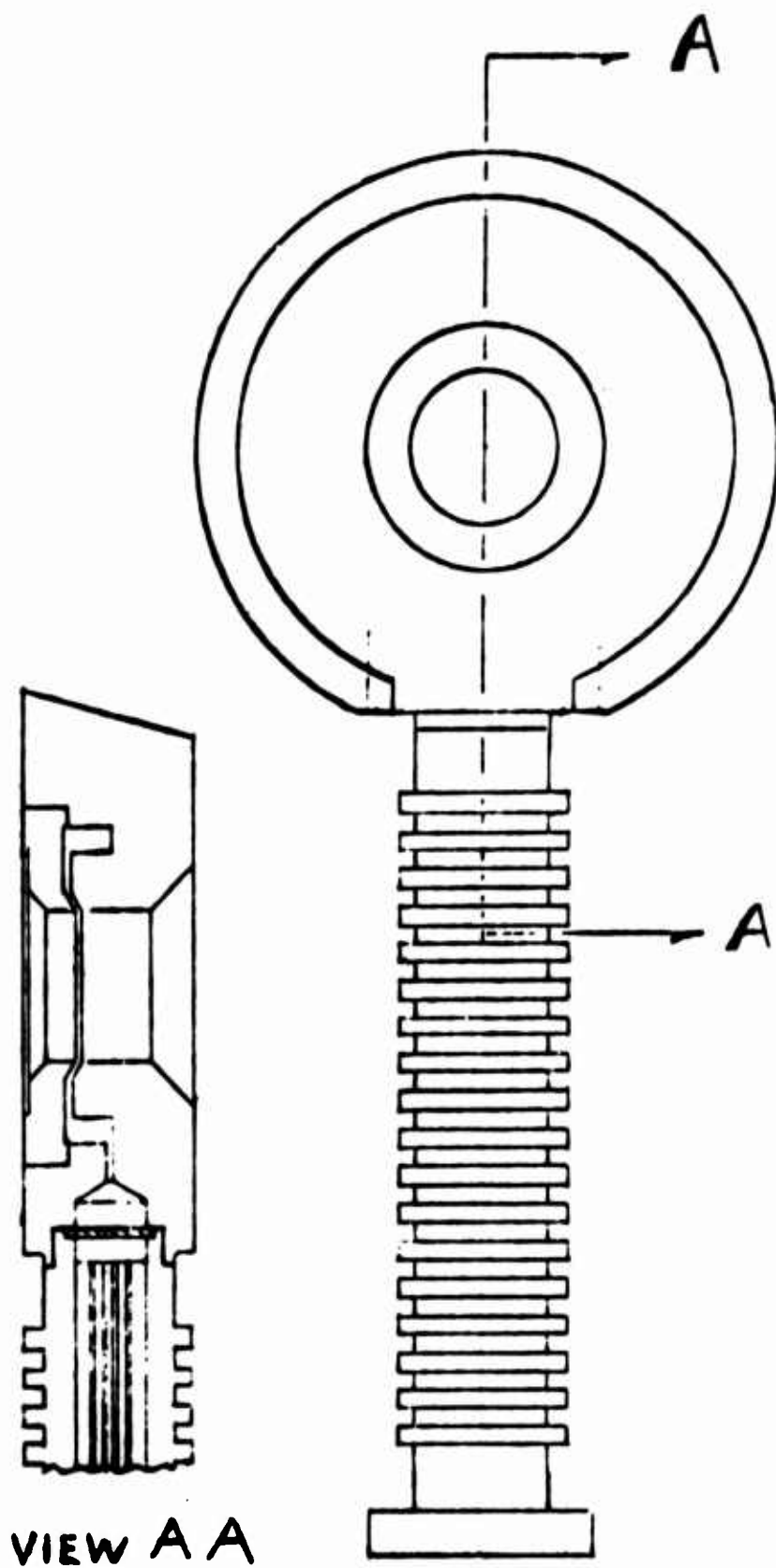
Figure 16   Anode-Vaporizer No. 5A

VIEW. A-A
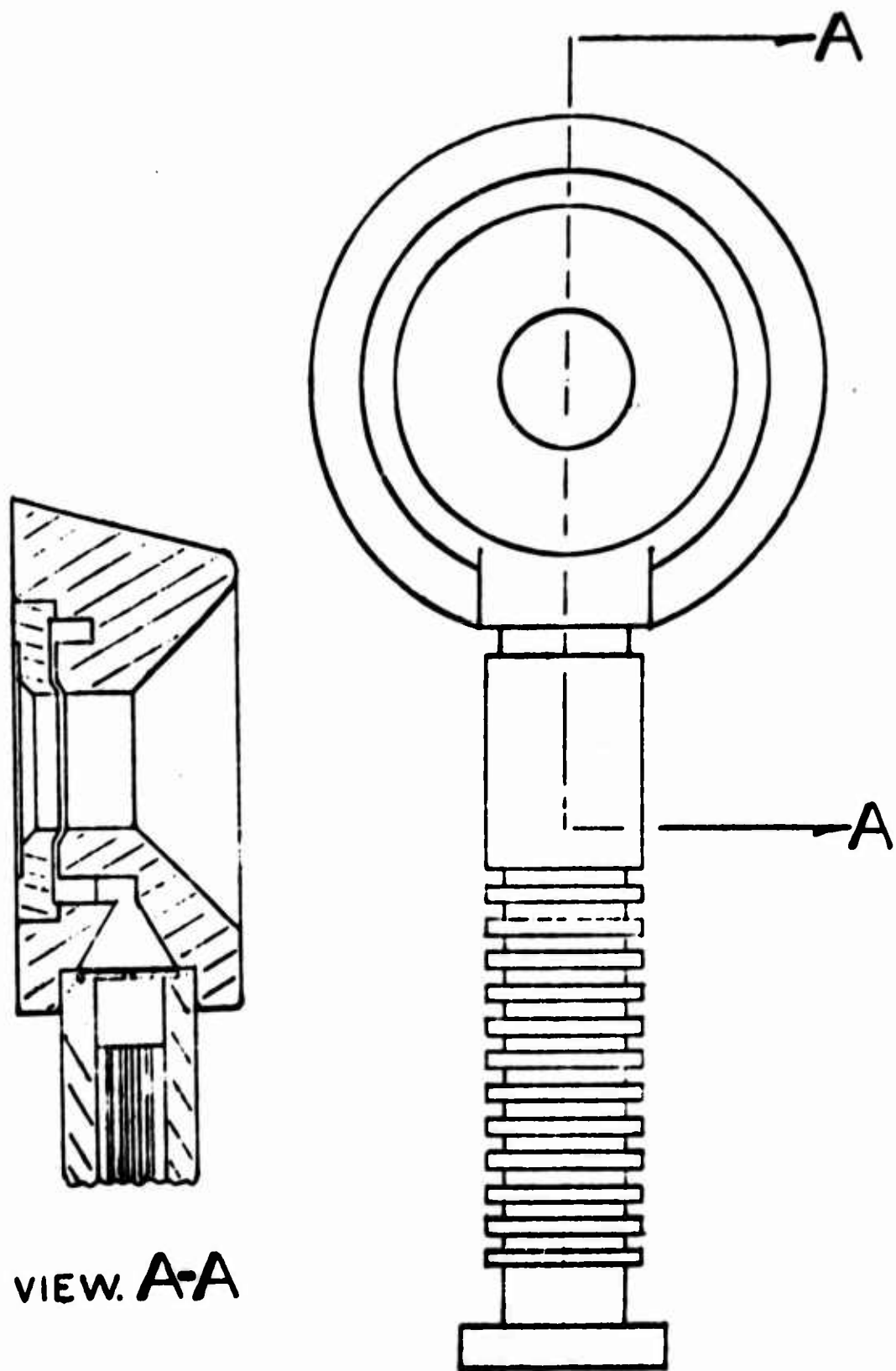
Figure 17   Anode-Vaporizer No. 6
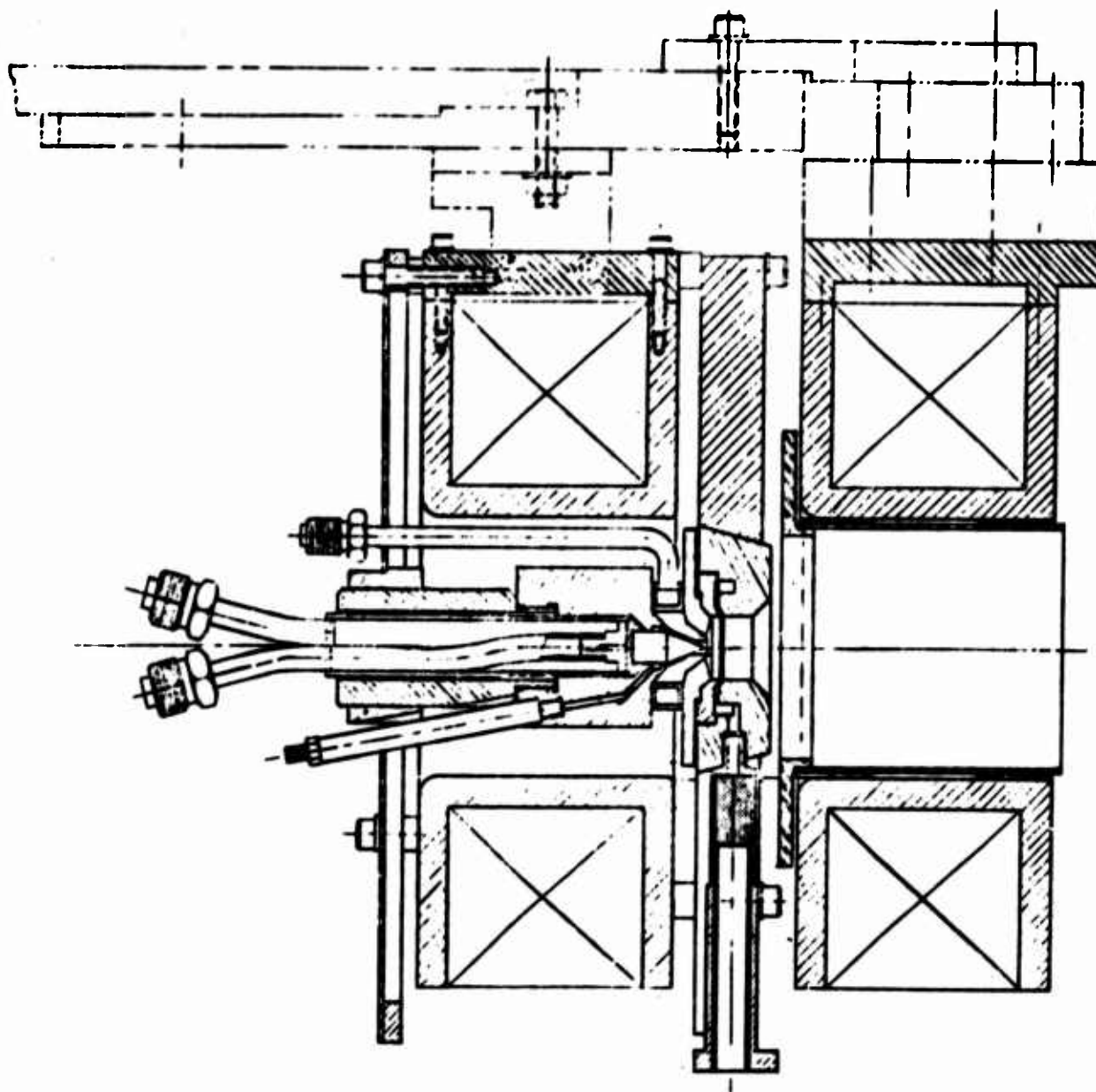
Figure 18 Thrustor Configuration for Ammonia Tests
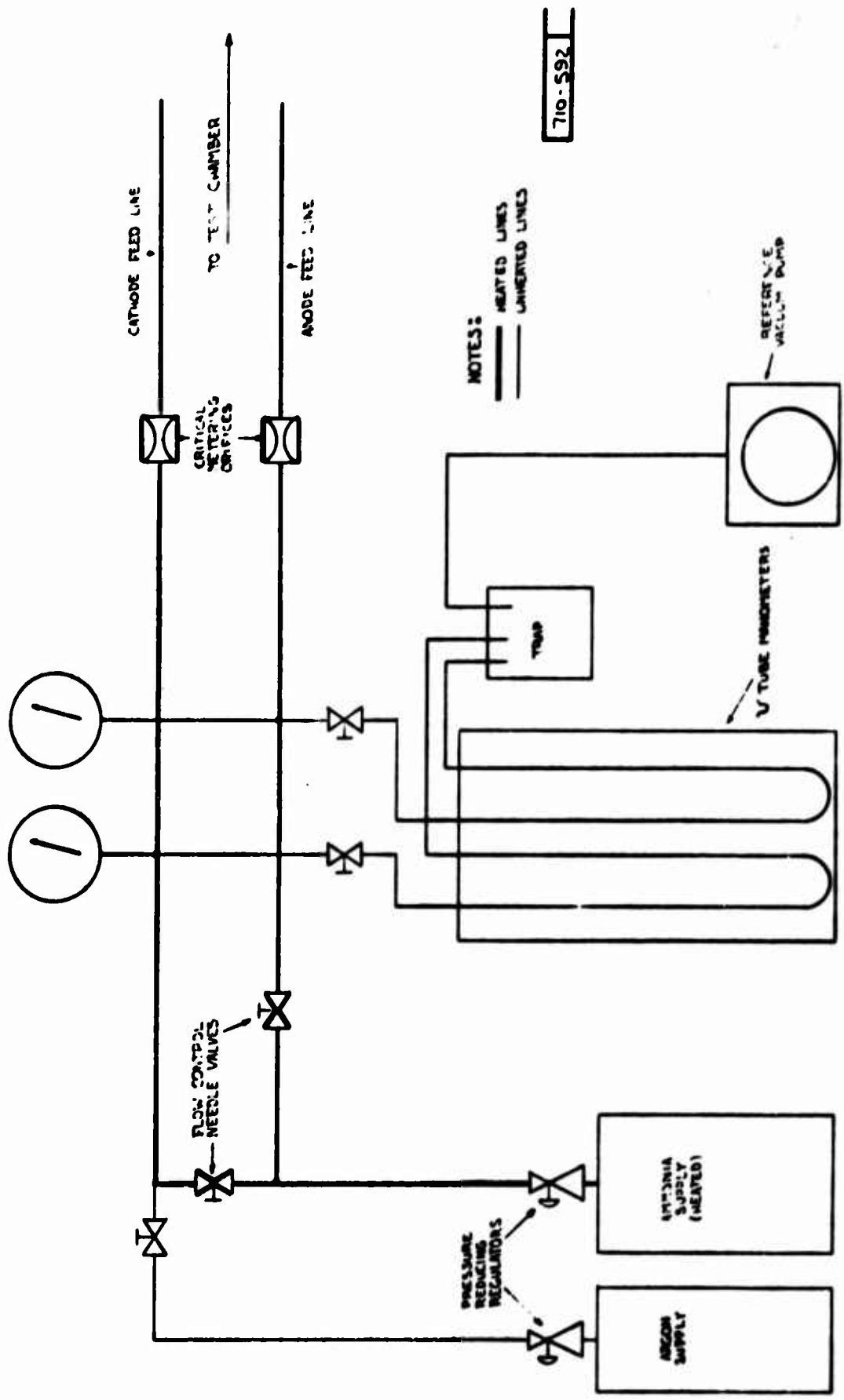
52

Figure 19 Ammonia Feed System

710-592

6' - 14' TEST CHAMBER

THRUST BALANCE

THRUSTOR

LITHIUM BOILERS

TEMP. RECORDERS

HEATER POWER SUPPLIES

CATHODE FEED LINE

ANODE FEED LINE

TO AMMONIA FEED SYS.

TO OIL DIFFUSION PUMPS (3 PLACES)
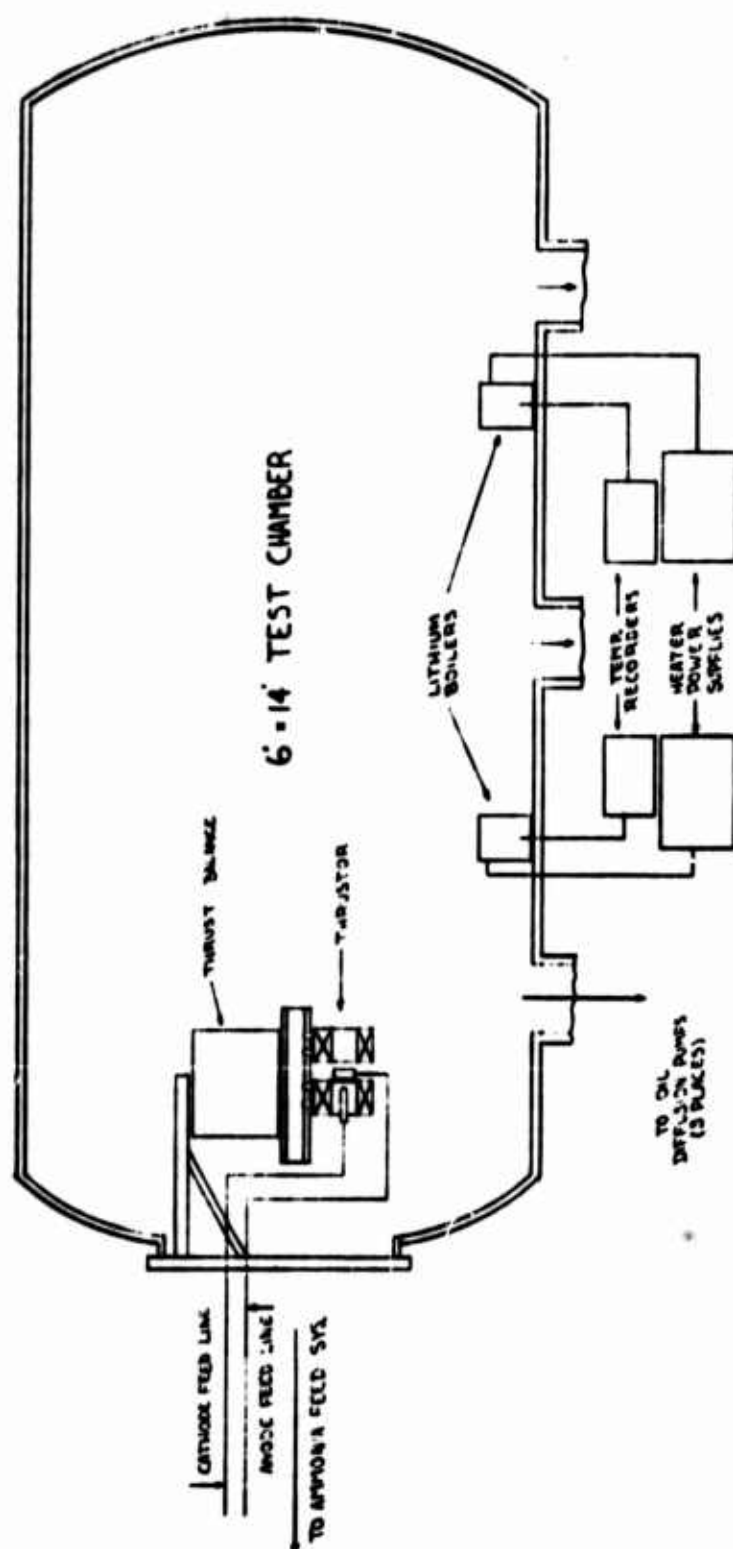
Figure 20   Lithium Gettering System
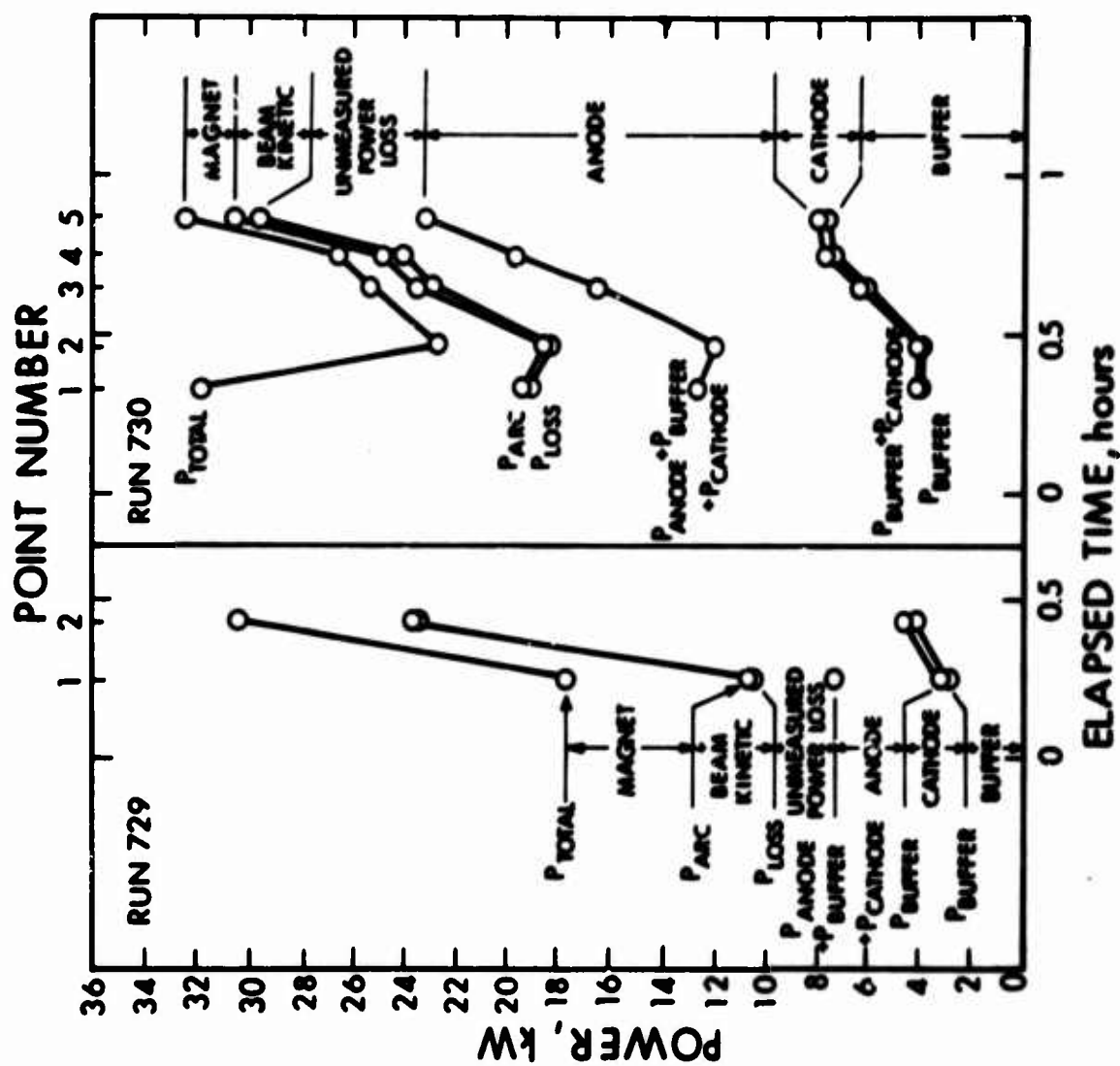
Figure 21 Histogram of Power Distribution for Runs 729 and 730

73625206
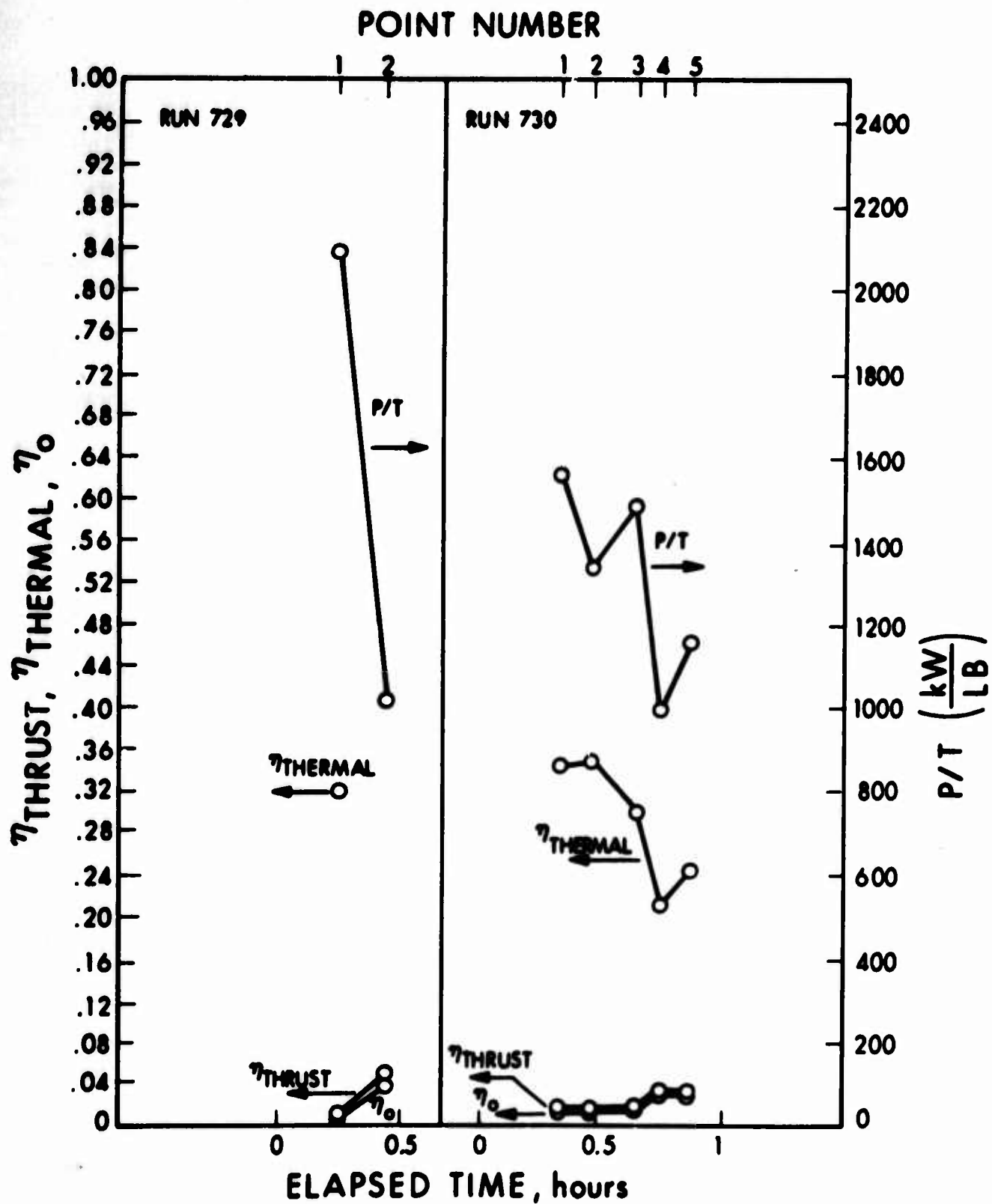
Figure 22   Histogram of Efficiencies and P/T for Runs 729 and 730

73625310
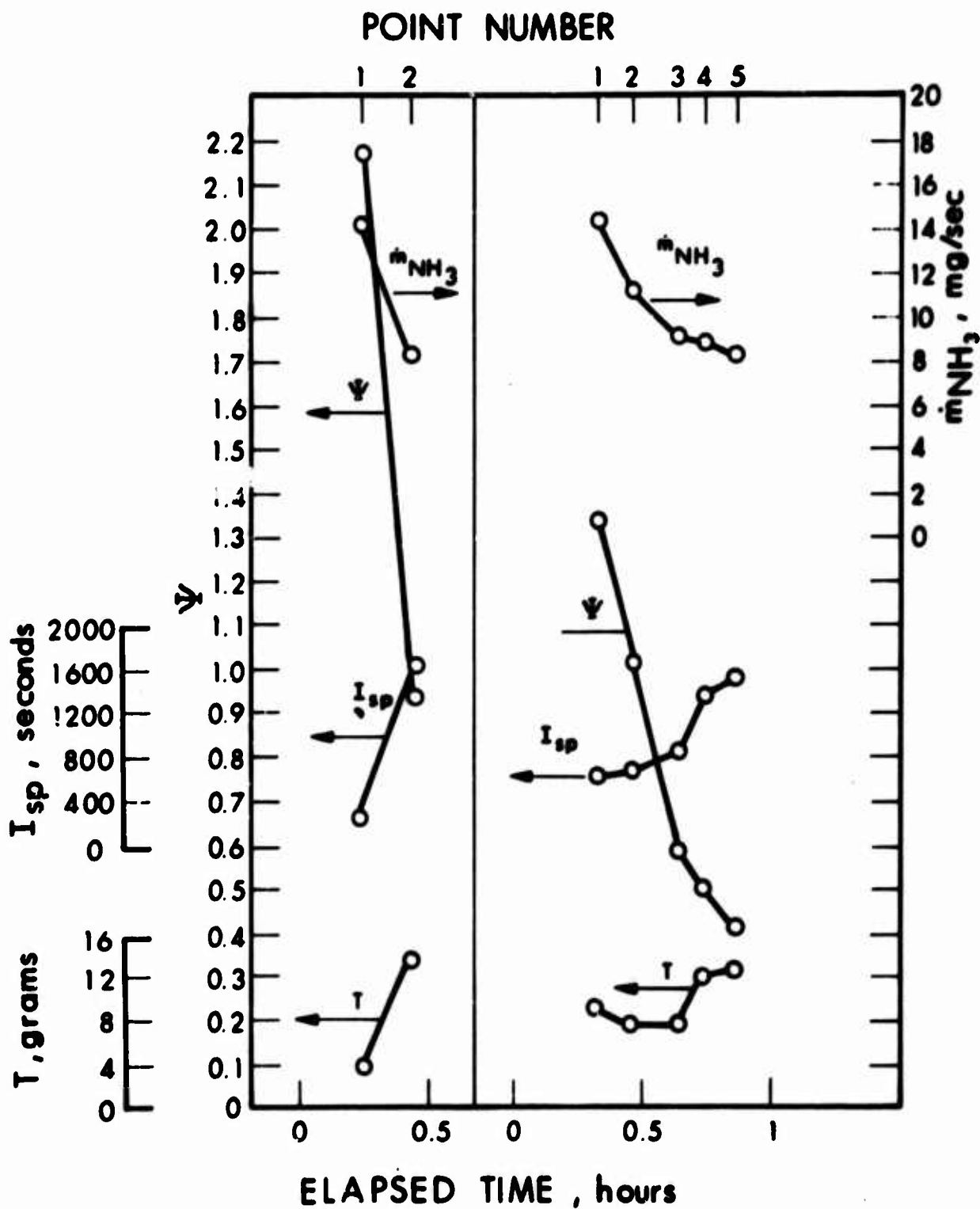
Figure 23 Histogram of T, I_{sp}, $\dot{m}$ and Ψ for Runs 729 and 730
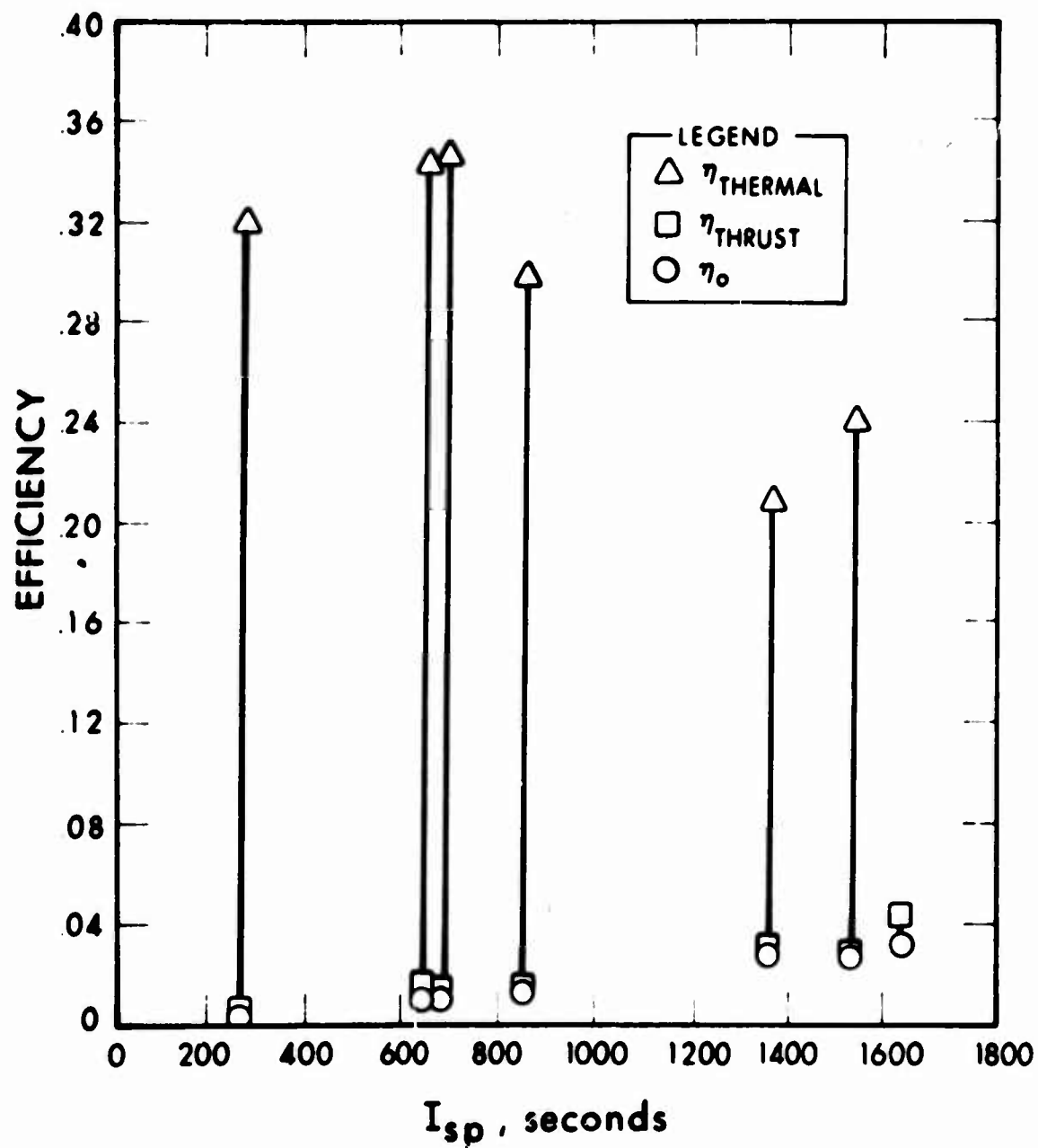
Figure 24   Thermal, Thrust and Overall Efficiencies Versus I_{sp} for Runs 729 and 730

73625390
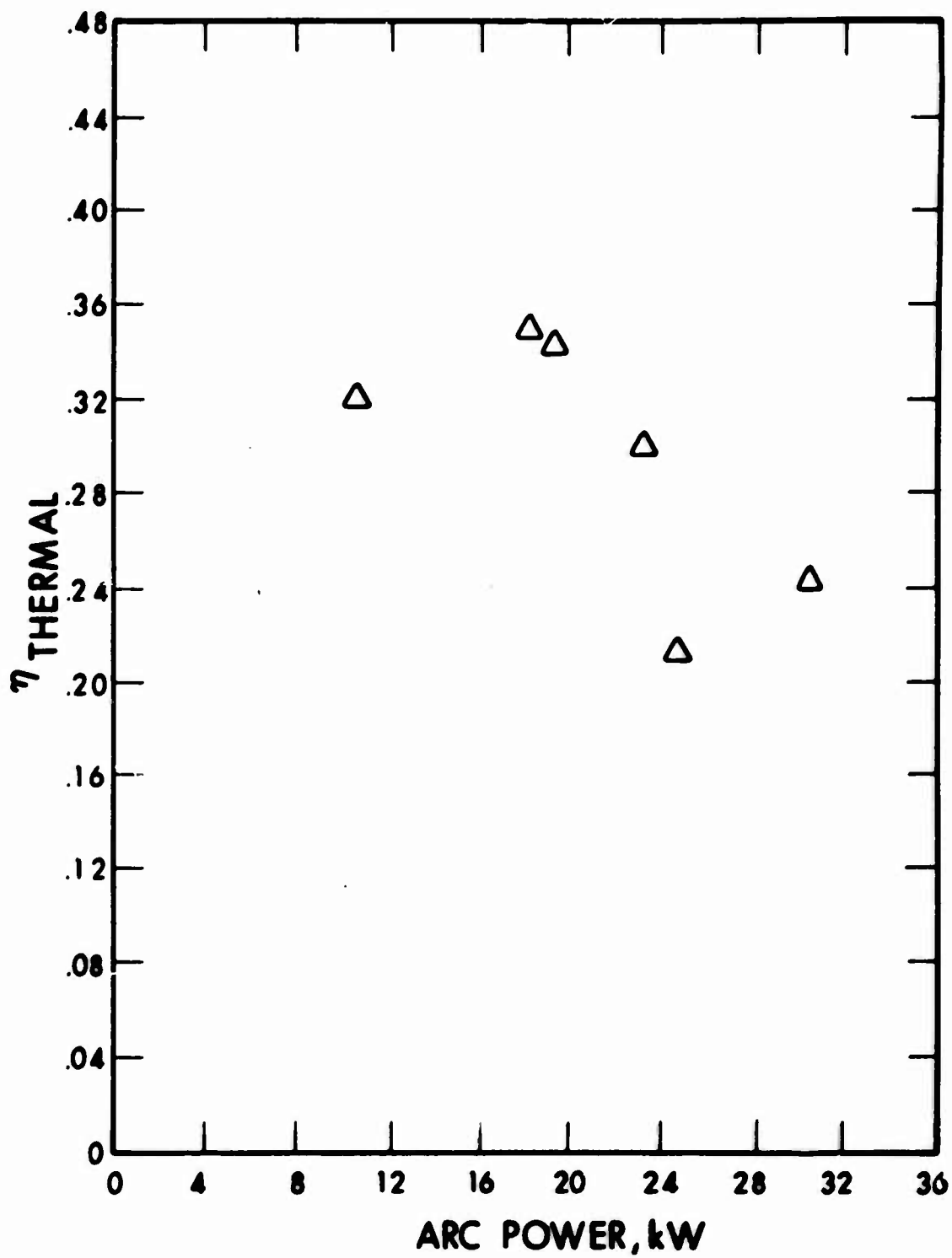
Figure 25   Thermal Efficiency versus Arc Power for Runs 729 and 730

5090-IR-3   59

7362 5391
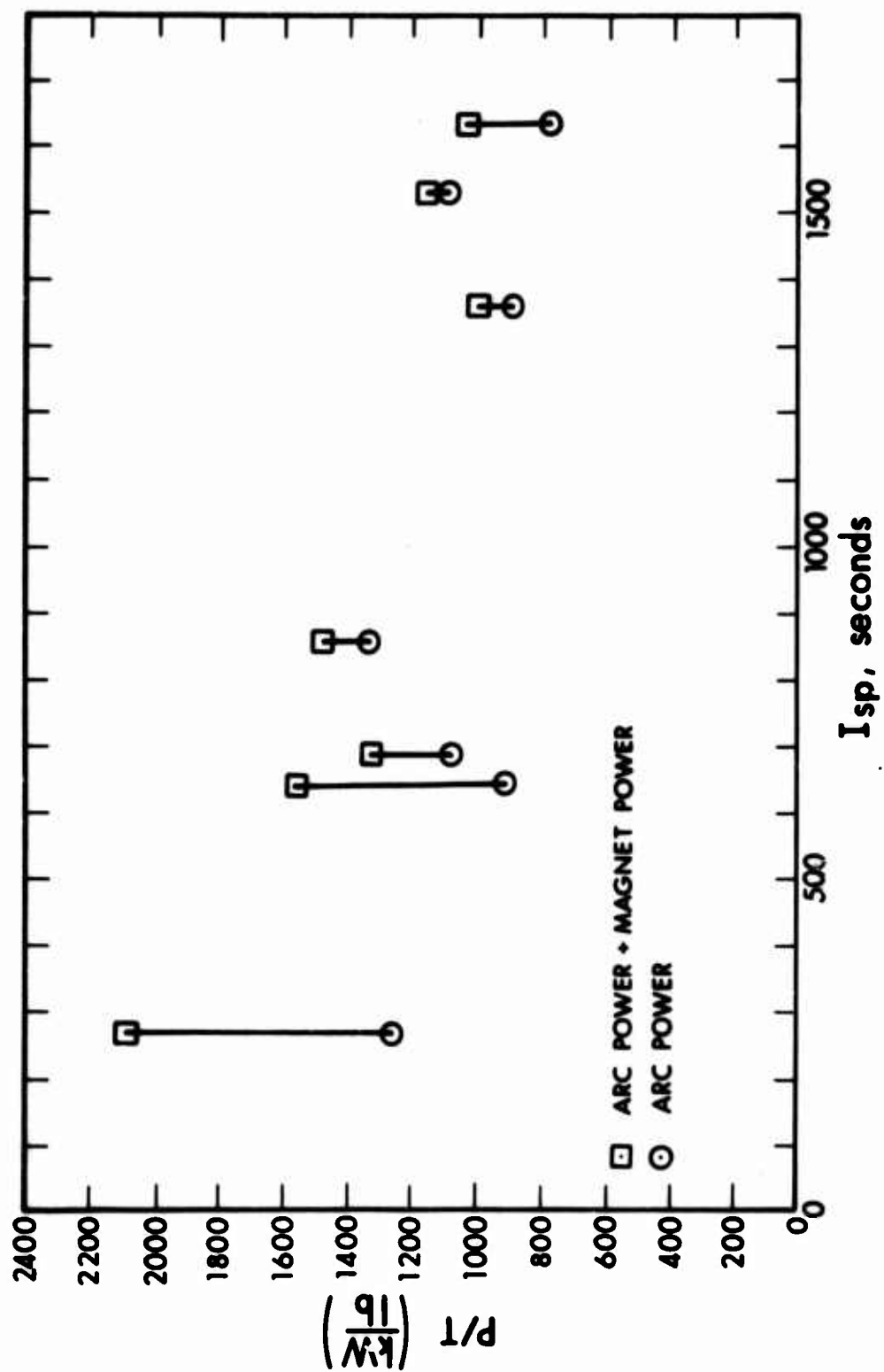
Figure 26 P/T versus I_{sp} for Runs 729 and 730

25281
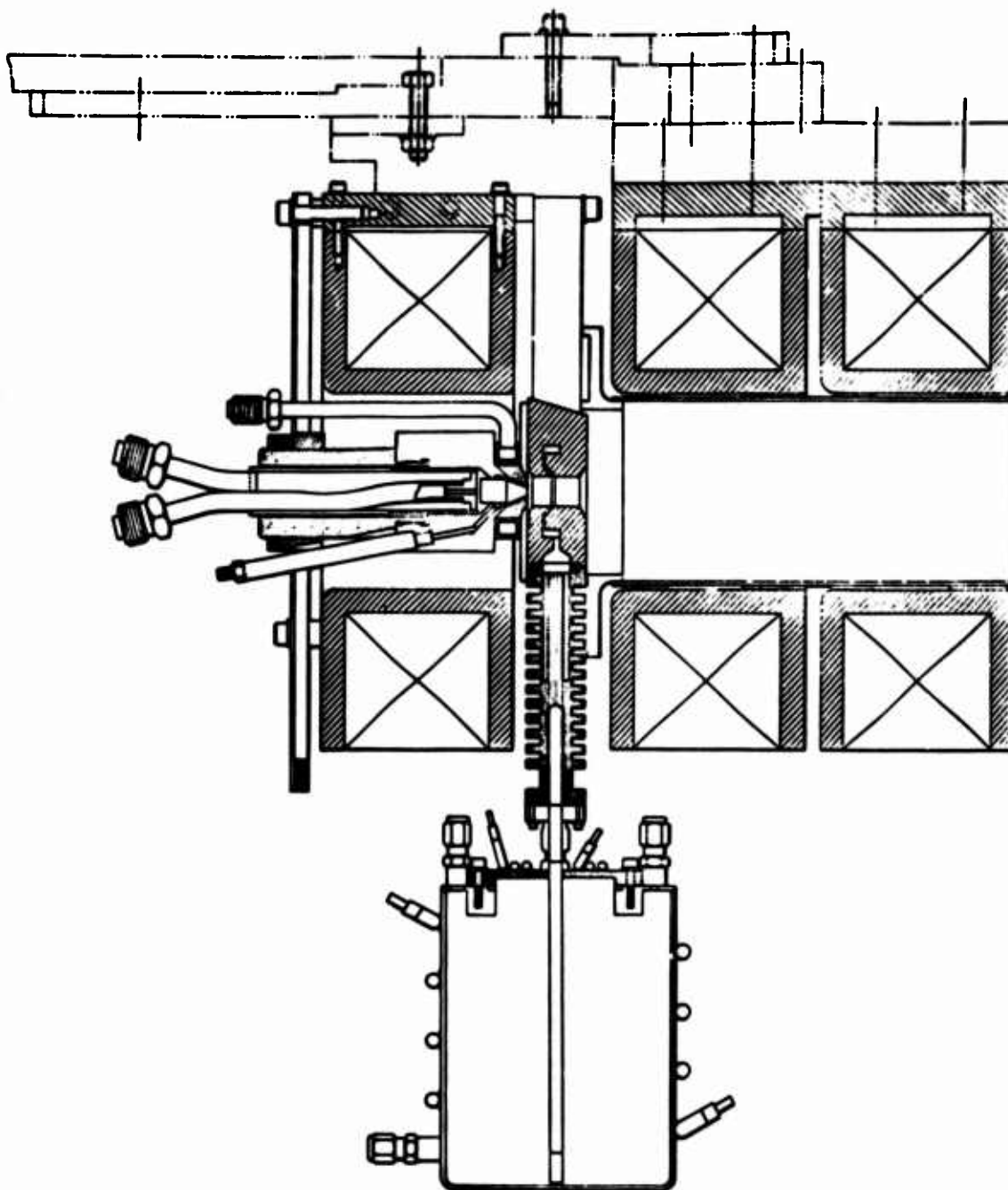
Figure 27   Three-Magnet Configuration for Lithium
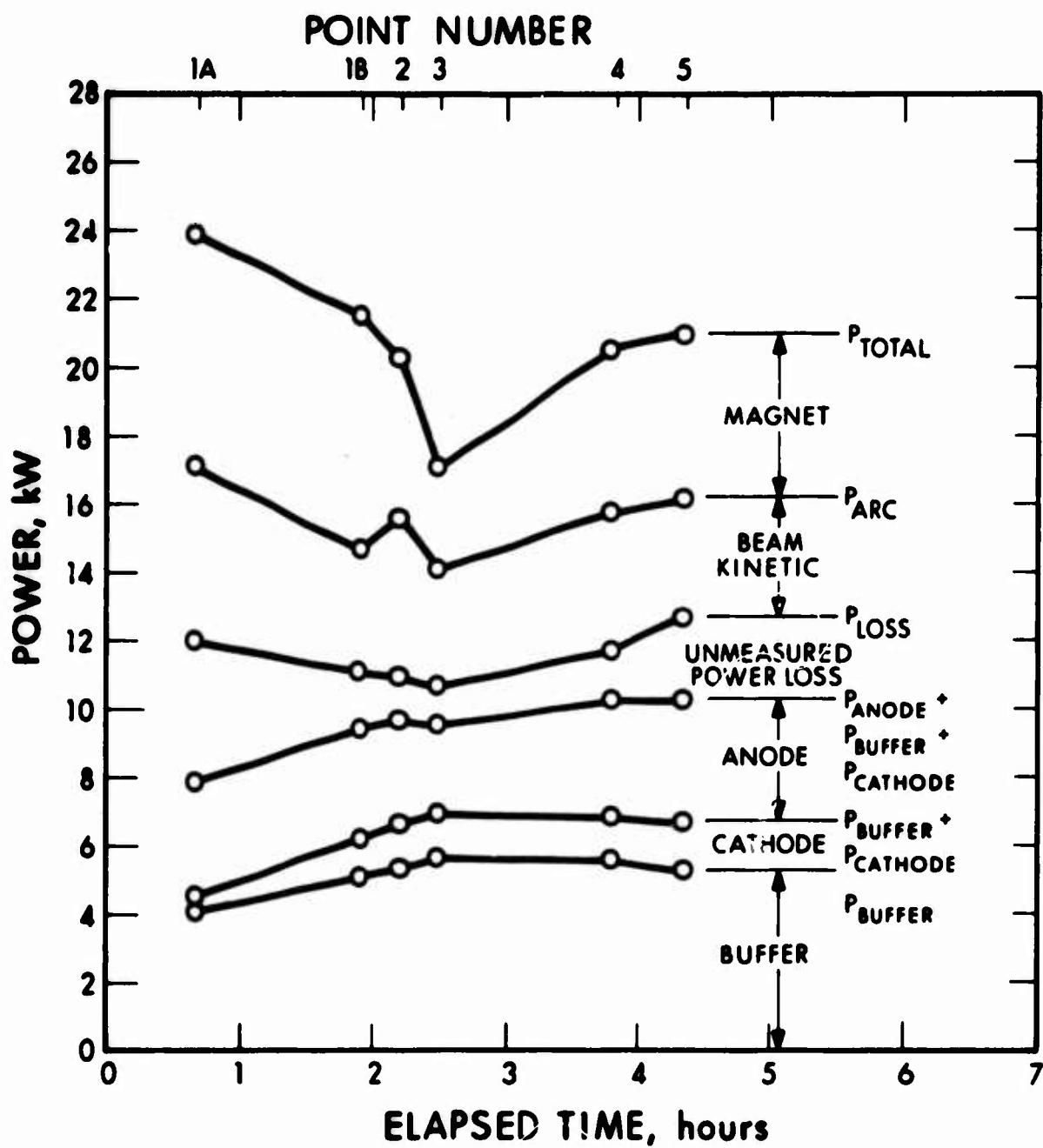
Figure 28   Histogram of Power Distribution for Run 731
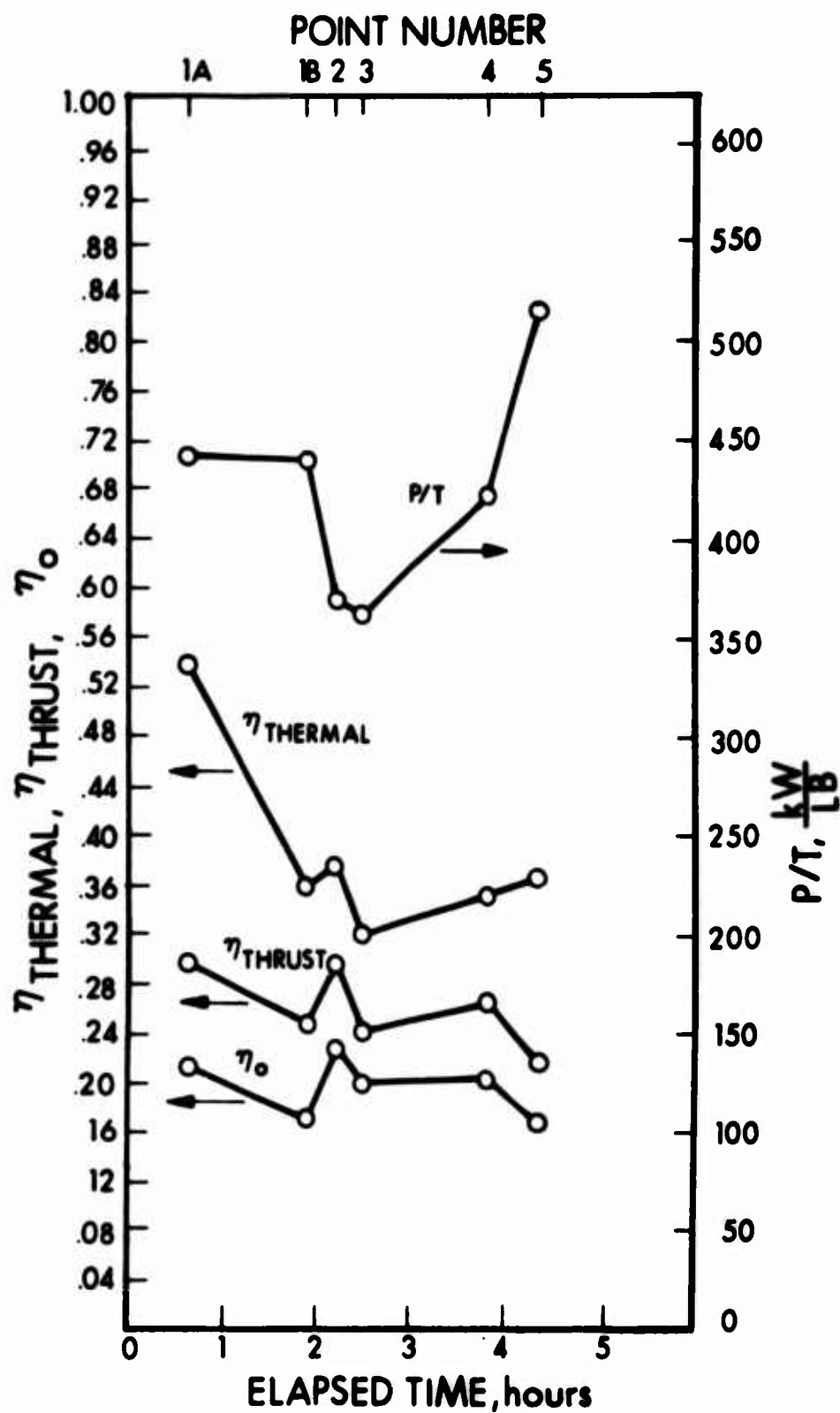
Figure 29 Histogram of Efficiencies and P/T for Run 731

73625311
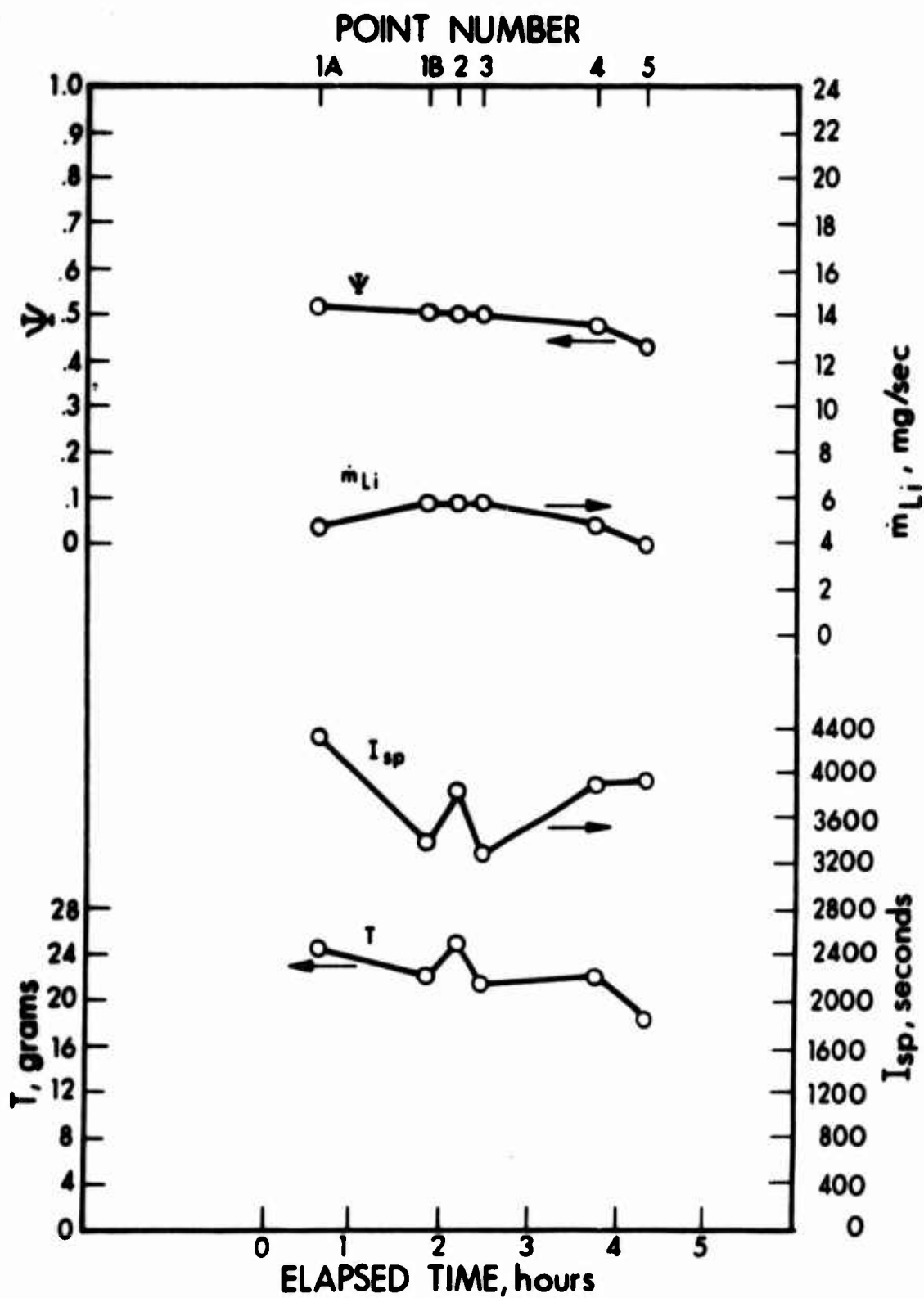
Figure 30 Histogram of T, I_{sp}, $\dot{m}$ and Ψ for Run 731

73625314
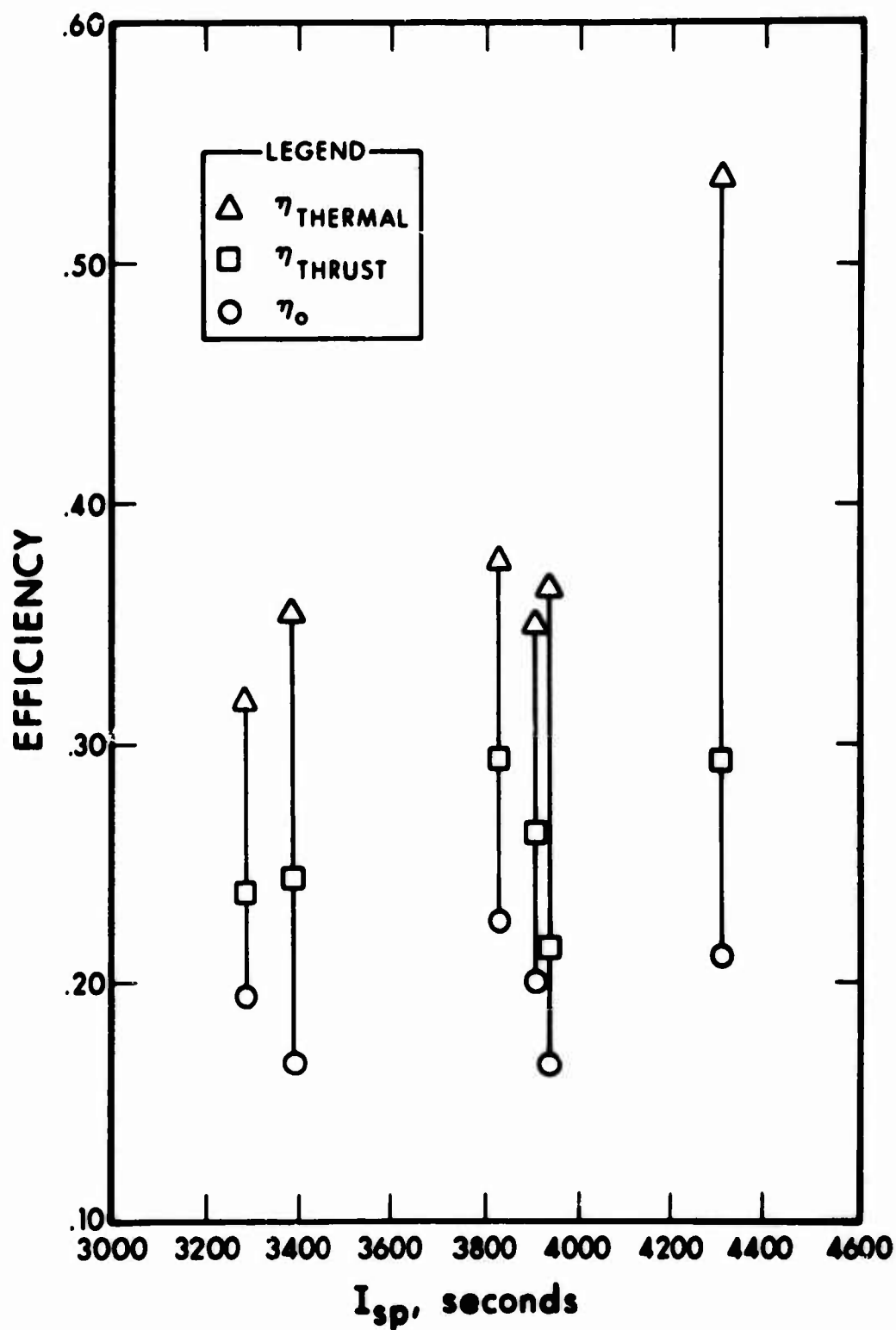
Figure 31   Thermal, Thrust and Overall Efficiencies versus I_{sp} for Run 731
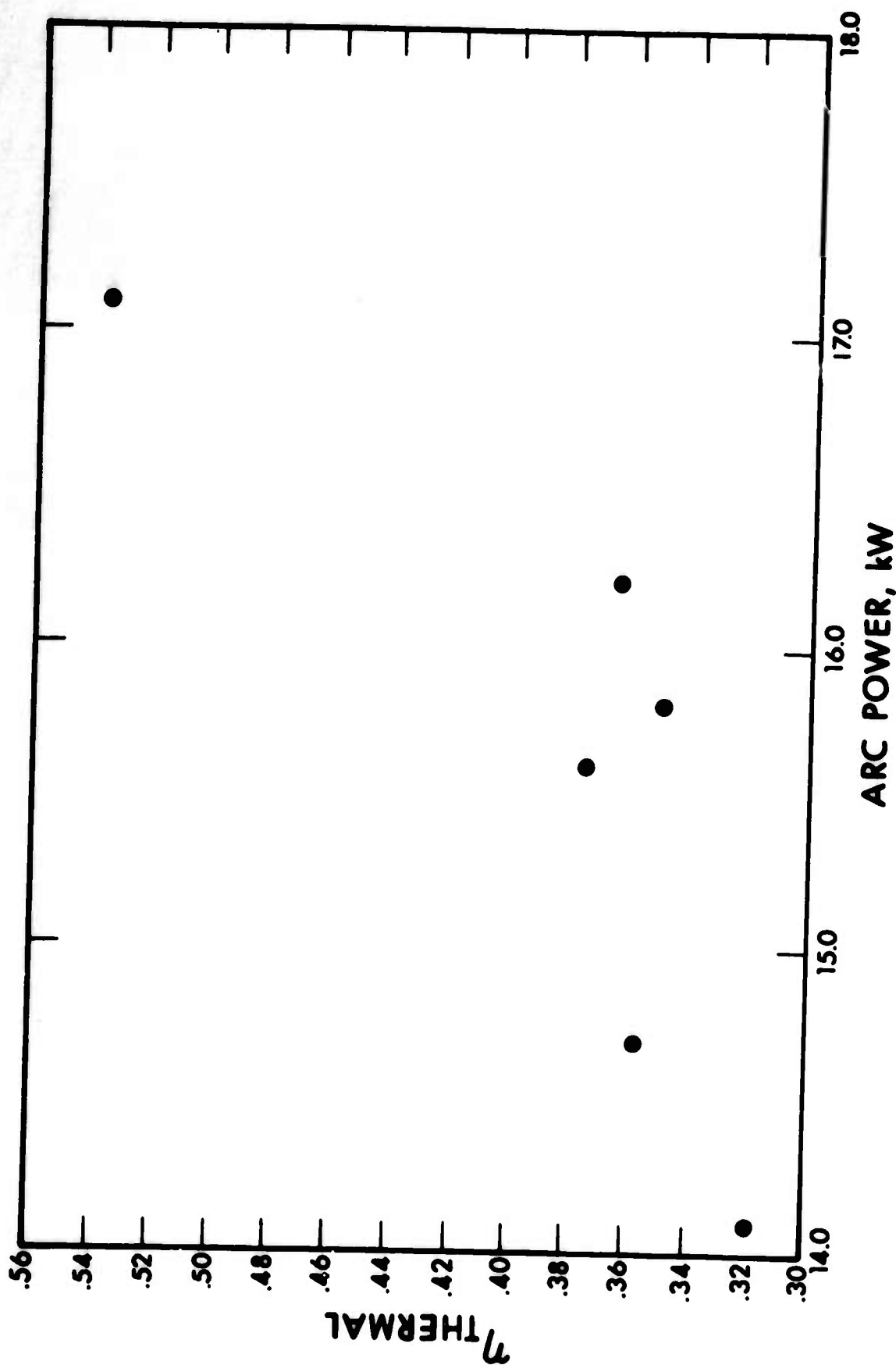
Figure 32 Thermal Efficiency versus Arc Power for Run 731
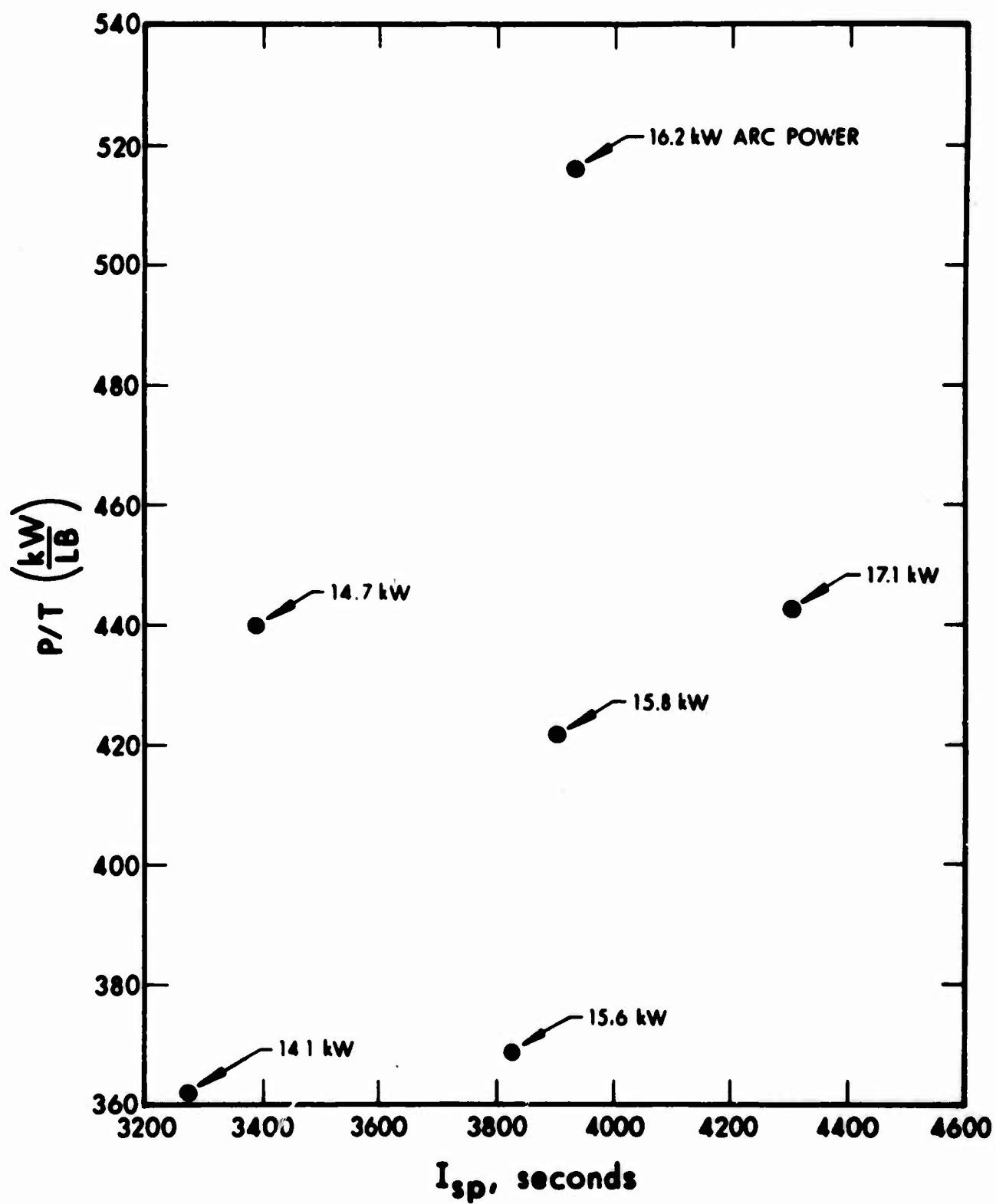
Figure 33 P/T versus I_{sp} for Run 731

7362535
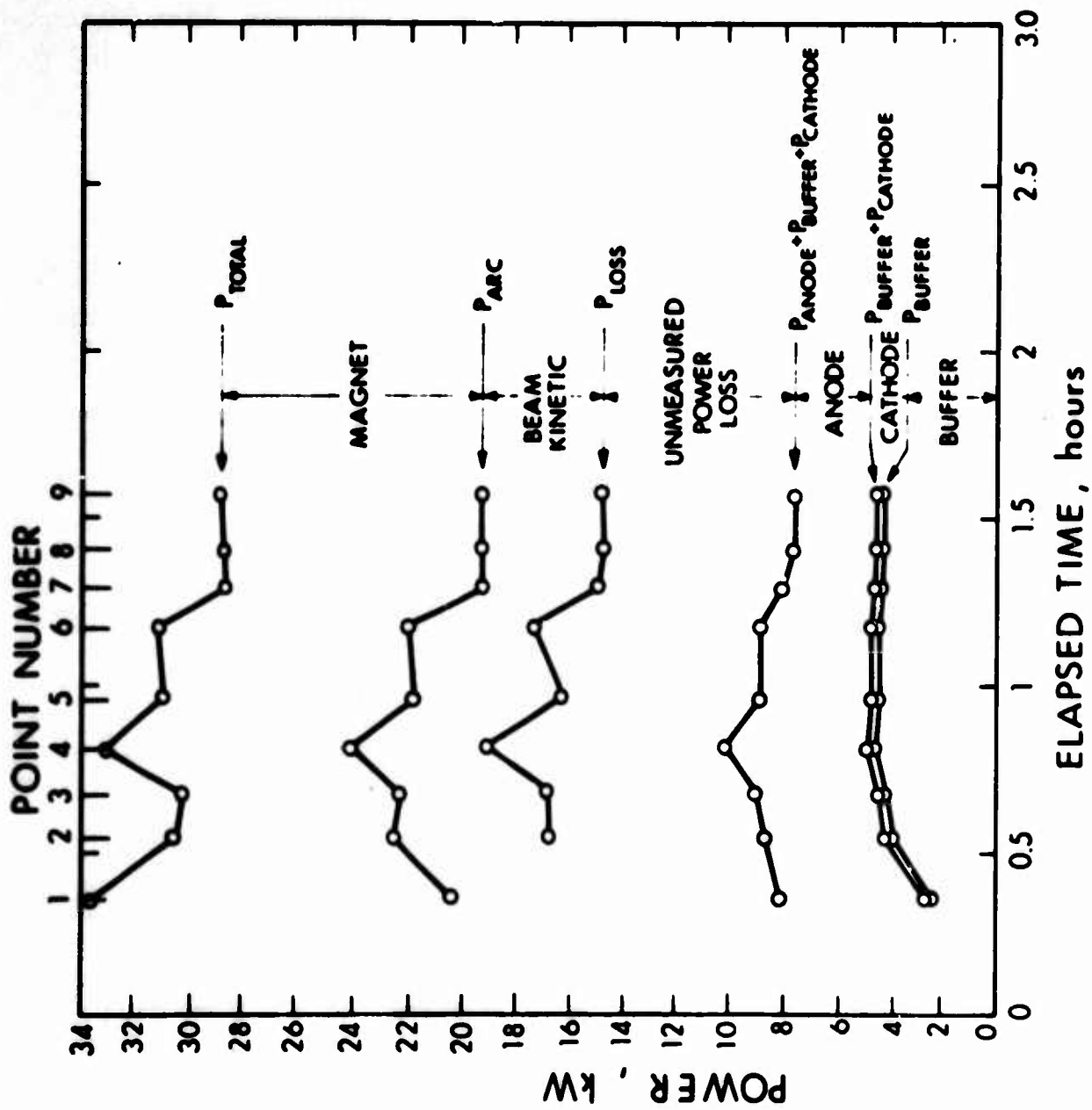
Figure 34   Histogram of Power Distribution for Run 725

73625293
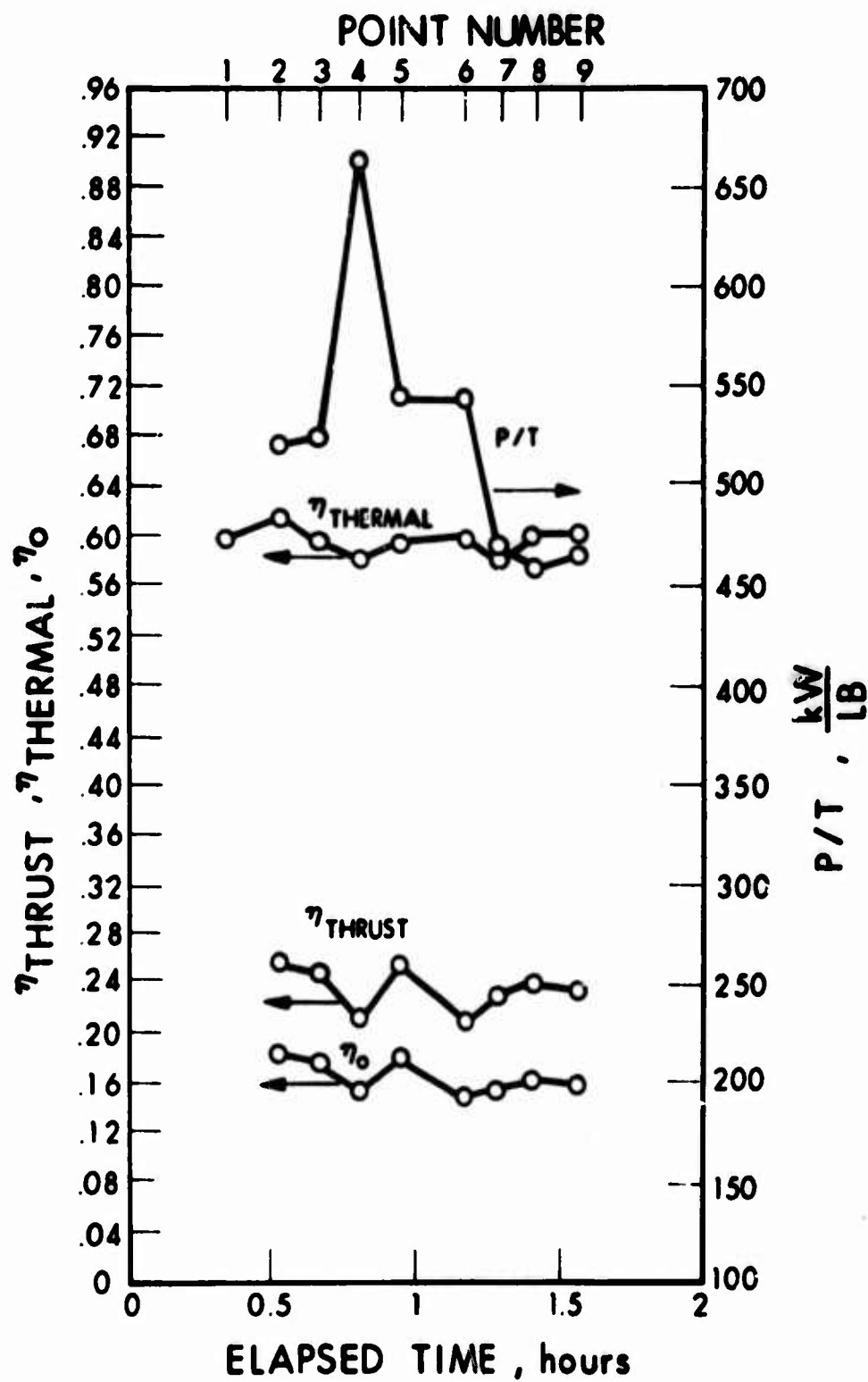
Figure 35   Histogram of Efficiencies and P/T for Run 725

73625312
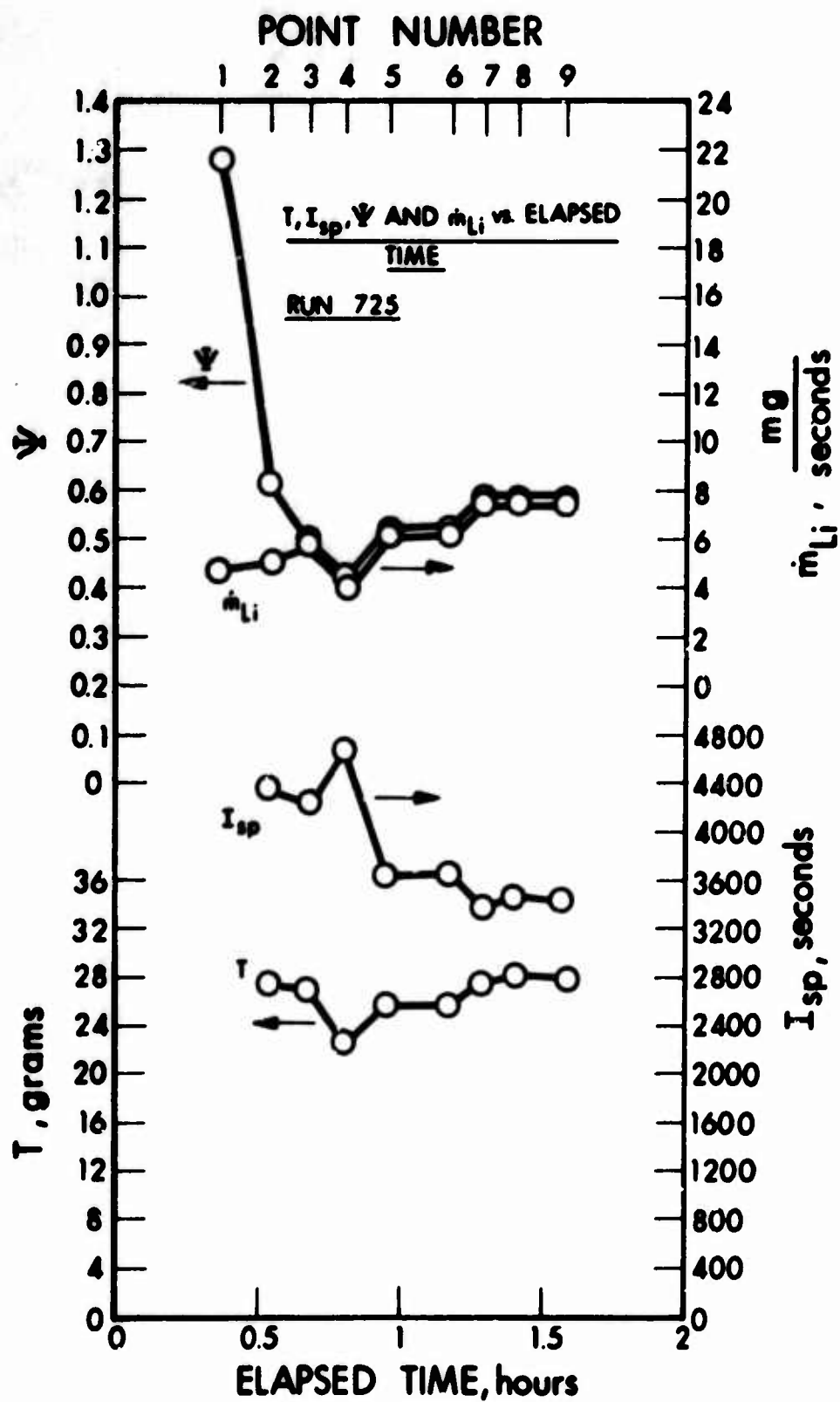
Figure 36   Histogram of T, I_{sp}, $\dot{m}$ and Ψ for Run 725

73625298
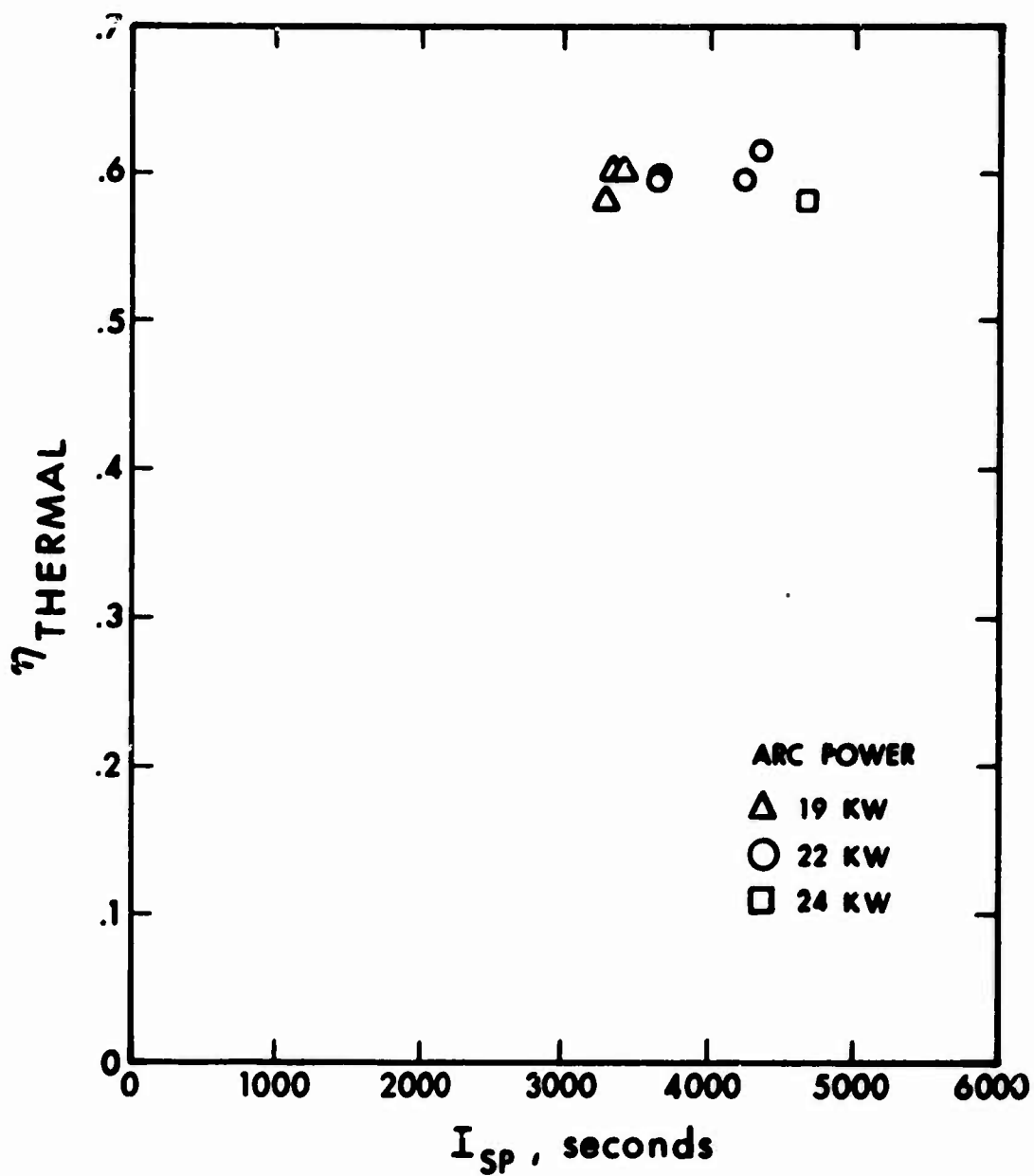
Figure 37   Thermal Efficiency versus I_{sp} for Run 725

73625387
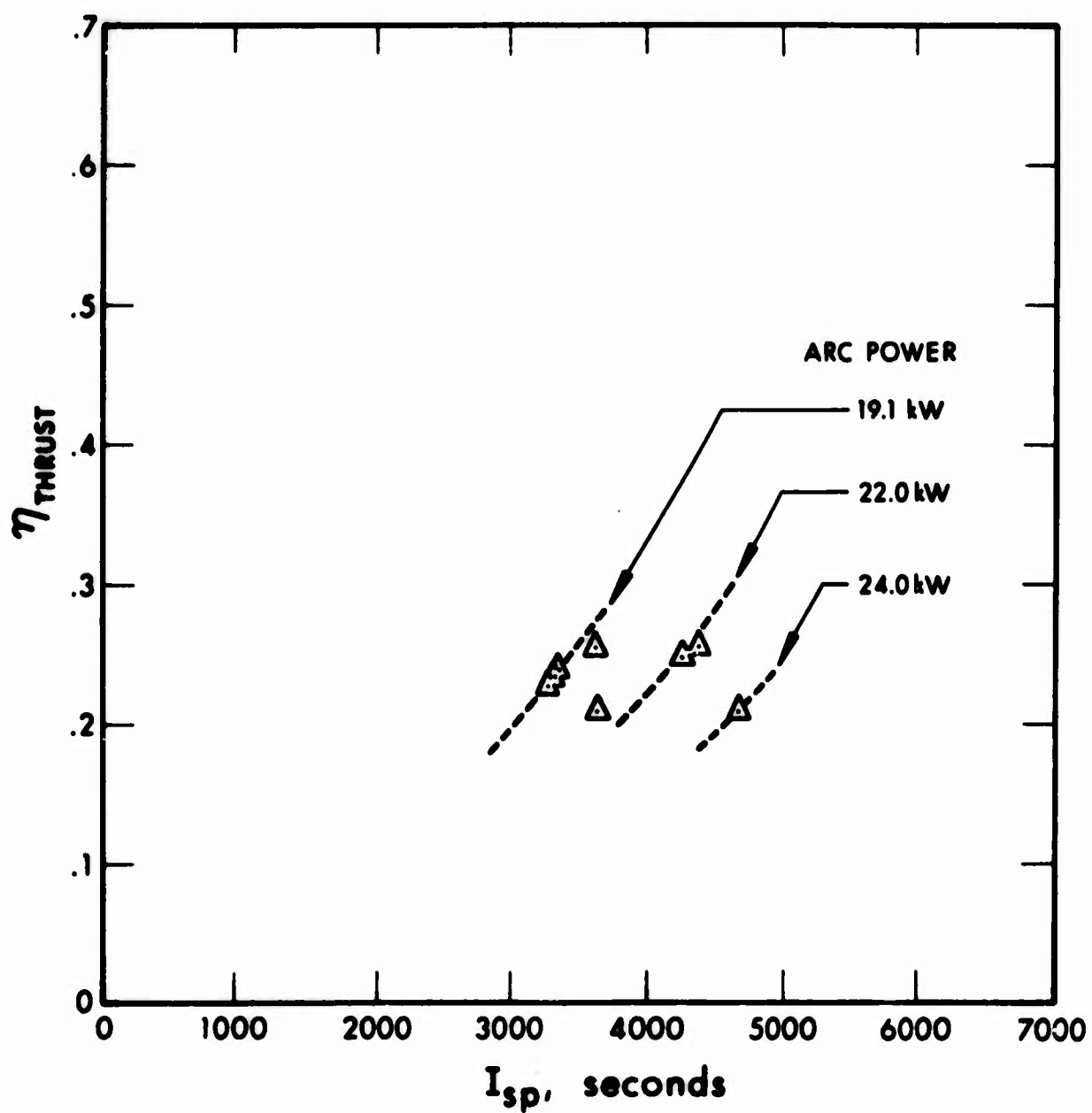
Figure 38   Thrust Efficiency versus I_{sp} for Run 725

625280
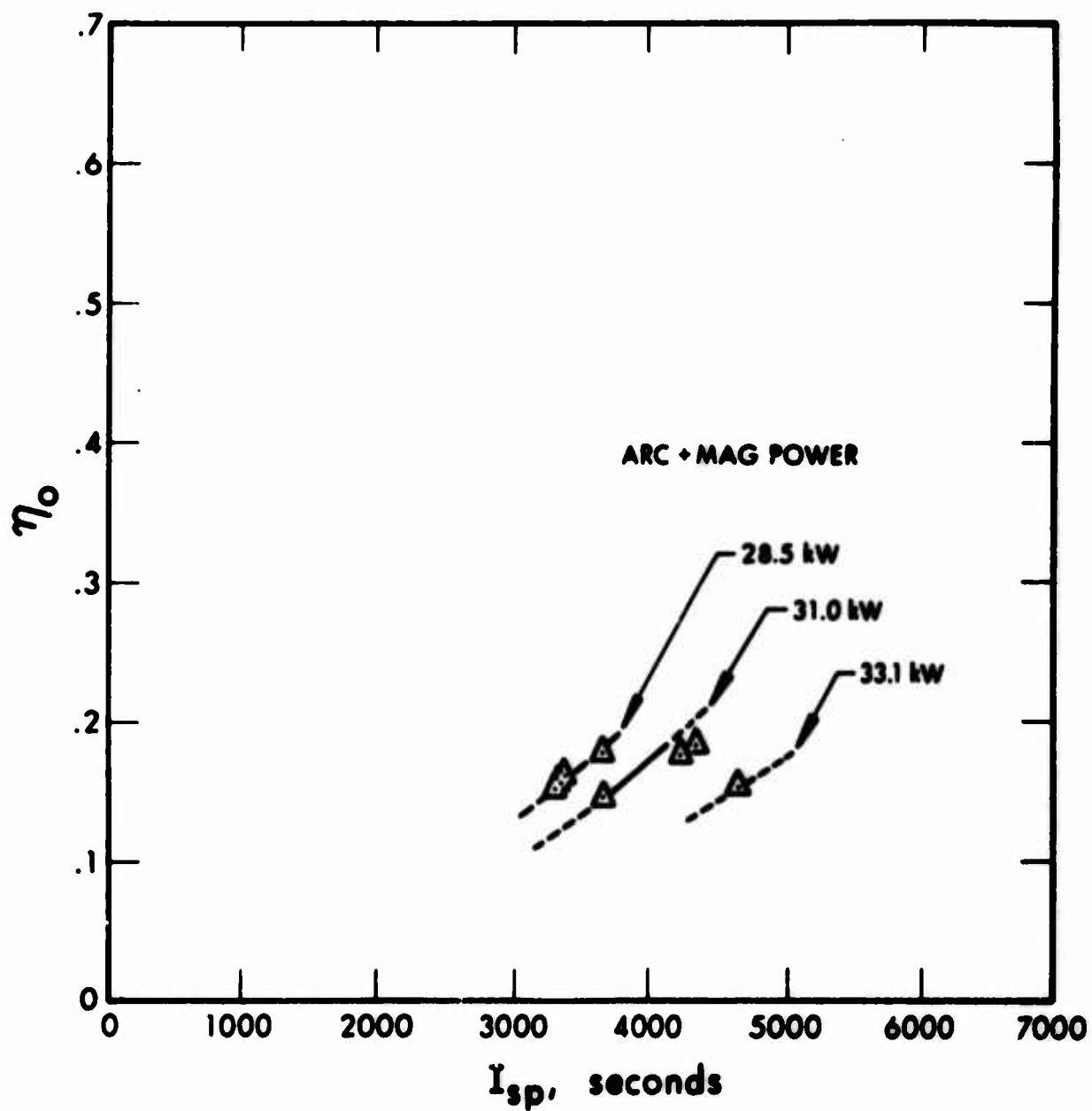
Figure 39   Overall Efficiency versus I_{sp} for Run 725
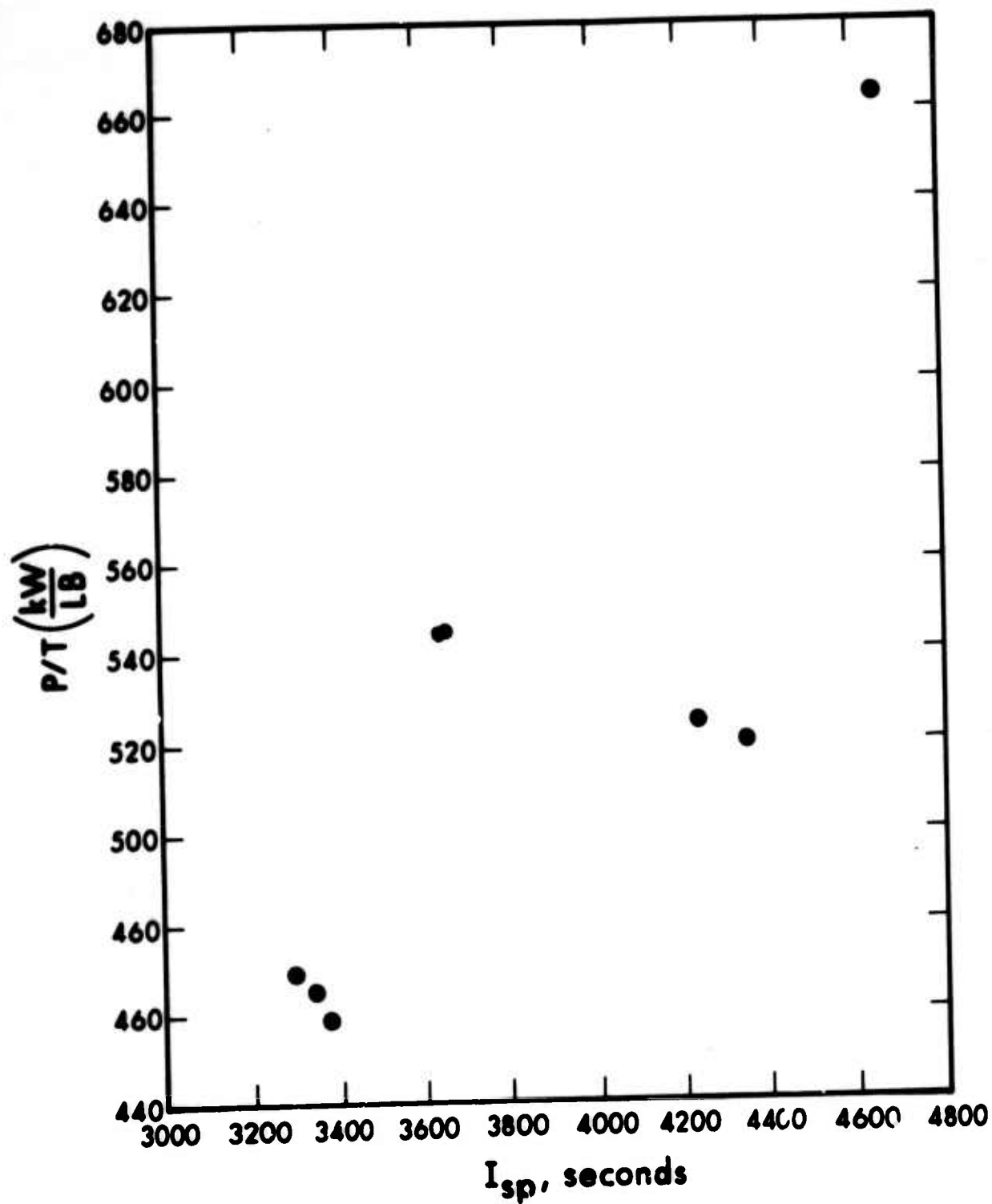
Figure 40 P/T versus I_{sp} for Run 725

73625389
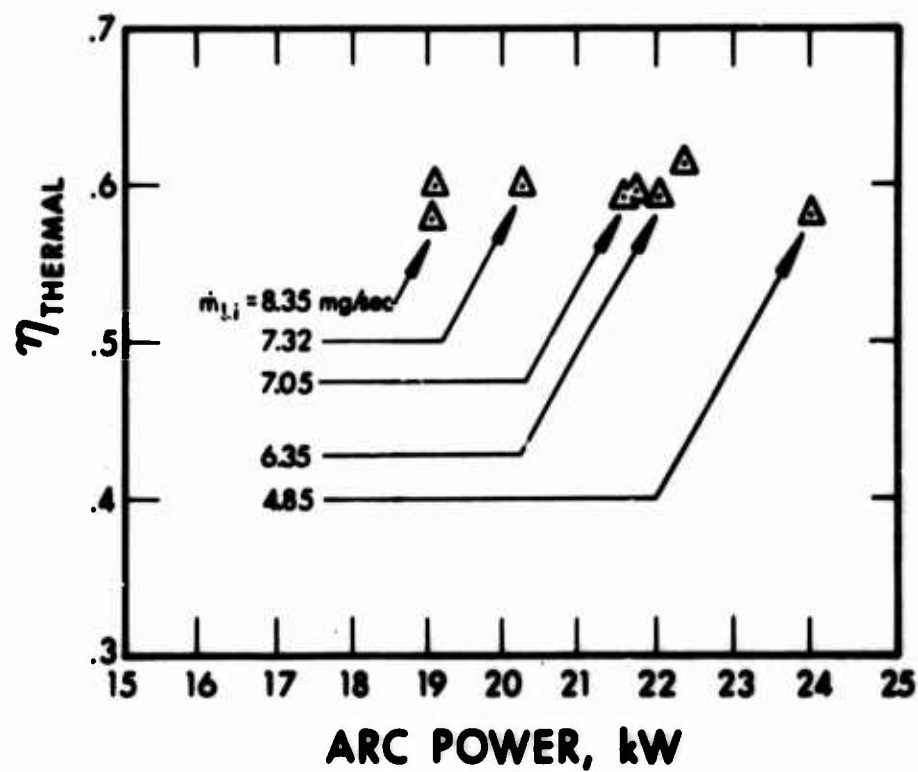
Figure 41   Thermal Efficiency versus Arc Power for Run 725
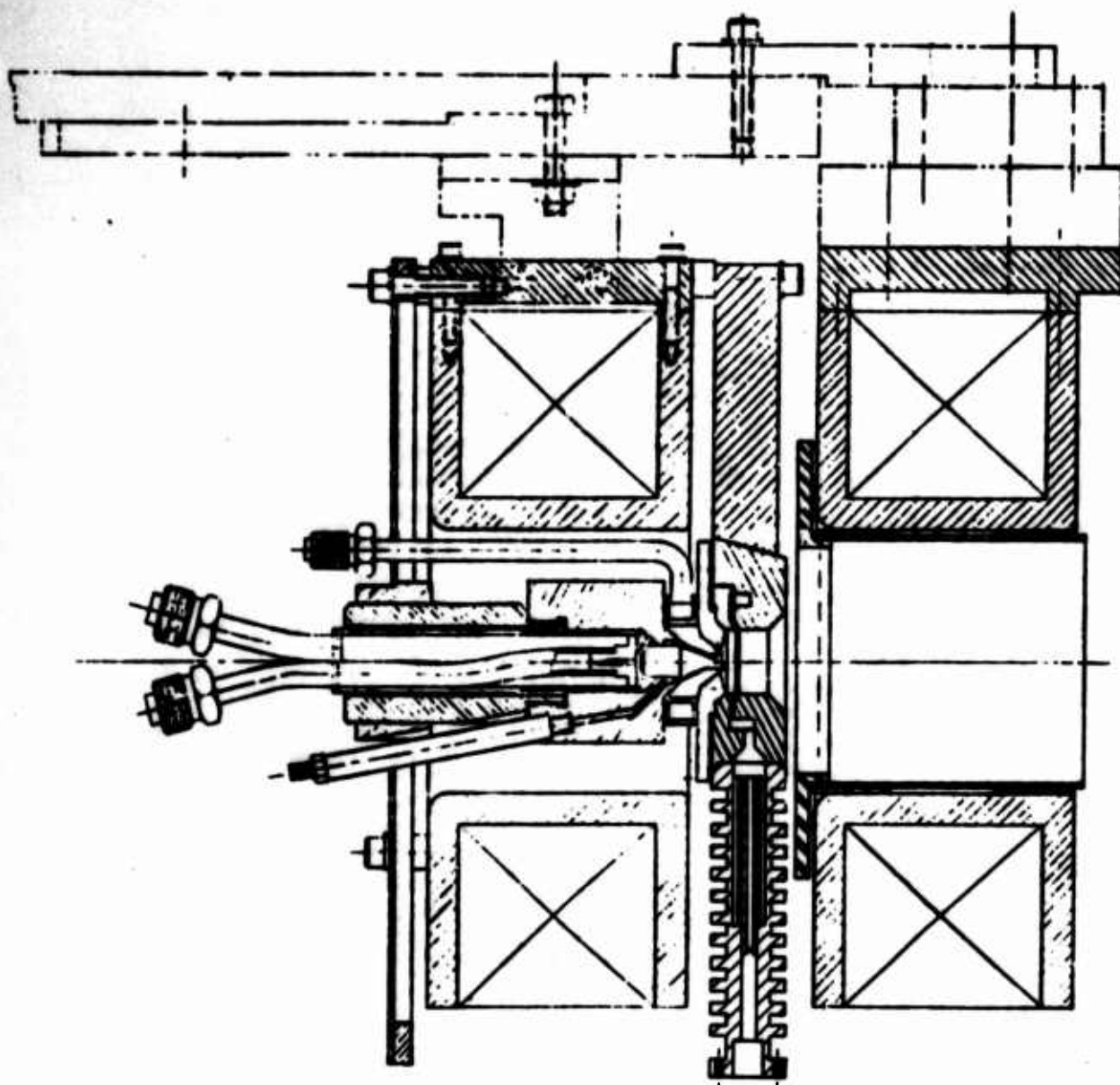
Figure 42   Thrustor Model IAJ-AF-CG-2A with GAF II Feed
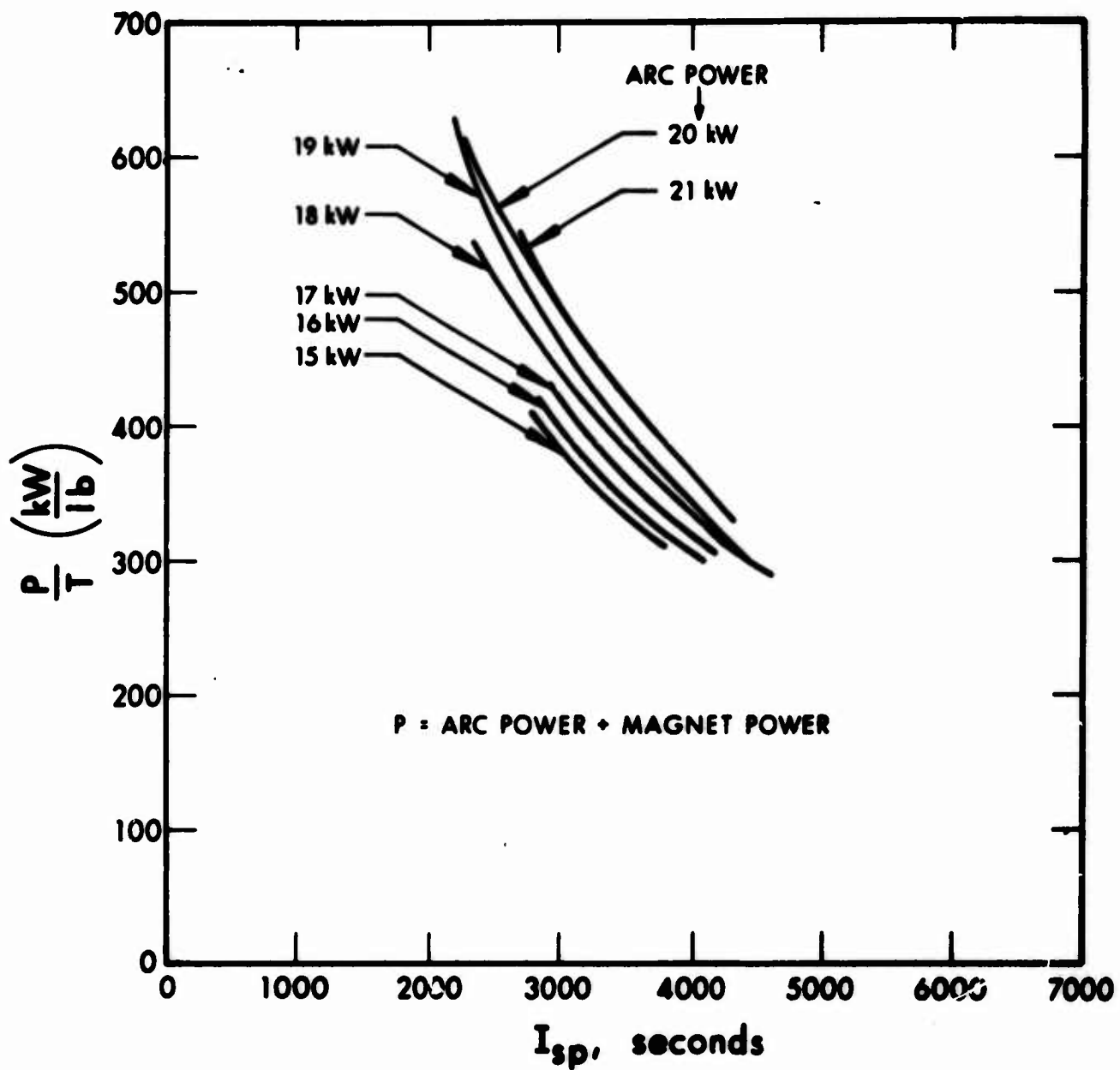
Figure 43   P/T versus I_{sp} for Run 727

73625279
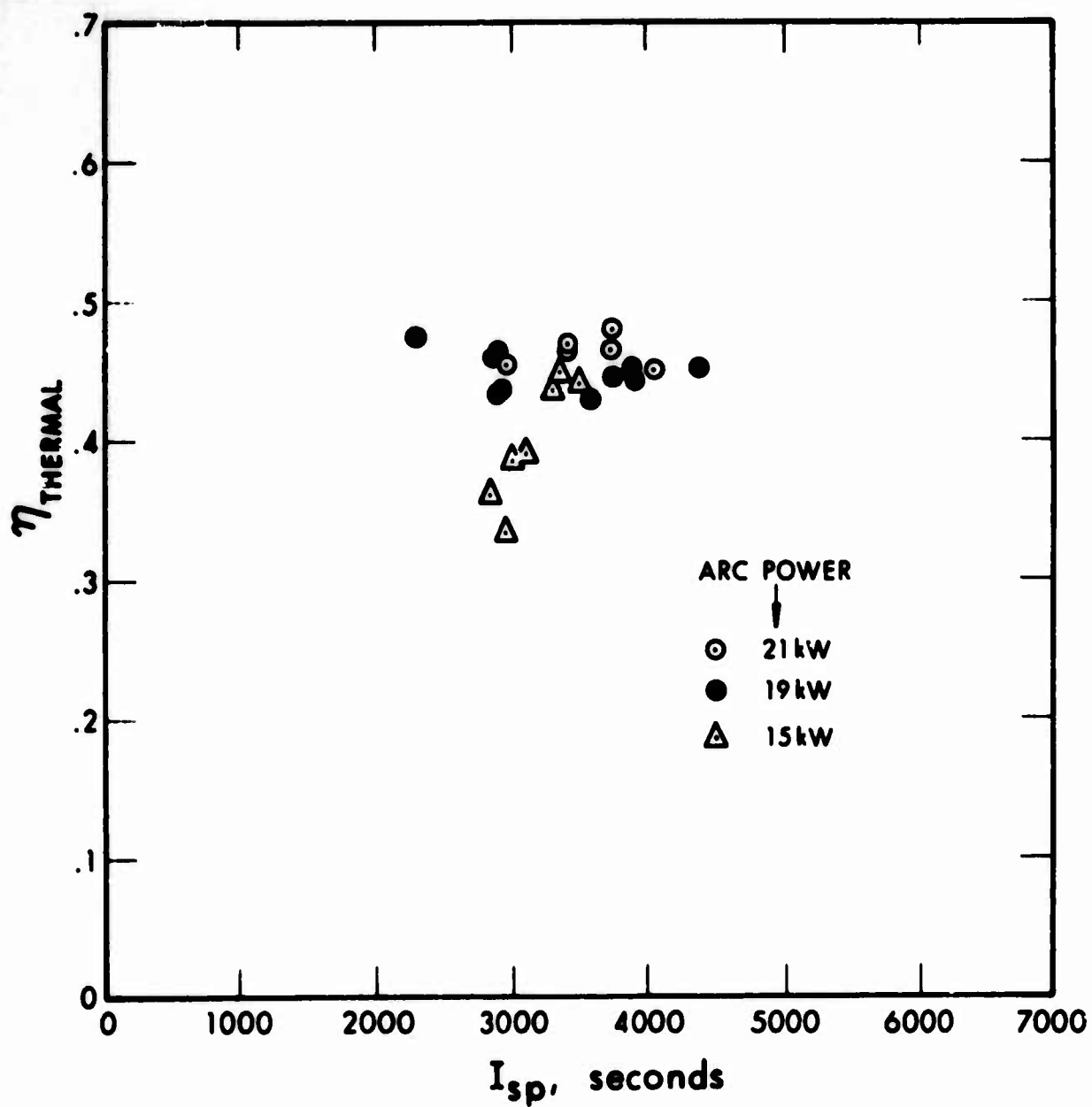
Figure 44   Thermal Efficiency versus I_{sp} for Run 727

73625282
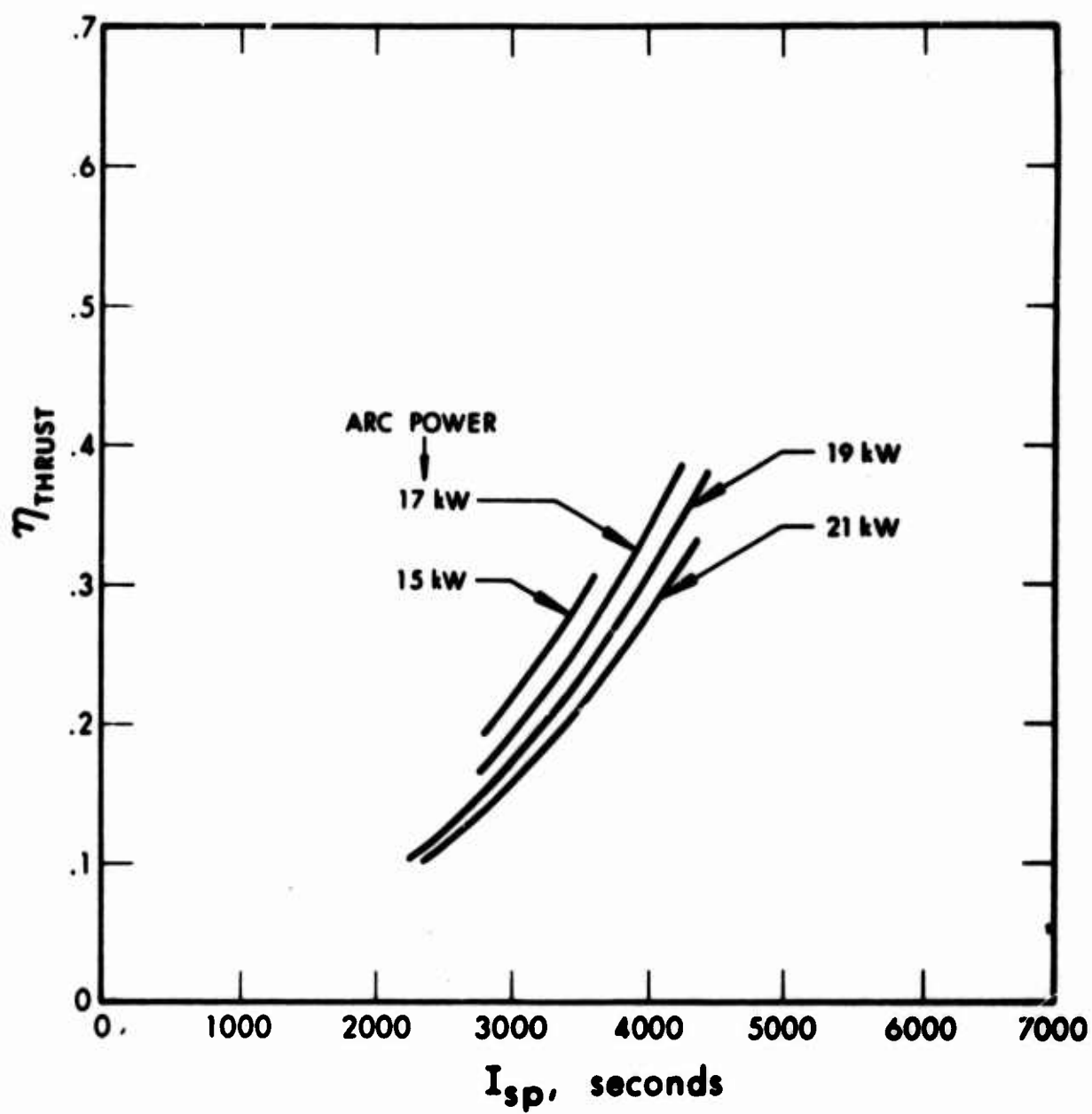
Figure 45   Thrust Efficiency versus I_{sp} for Run 727
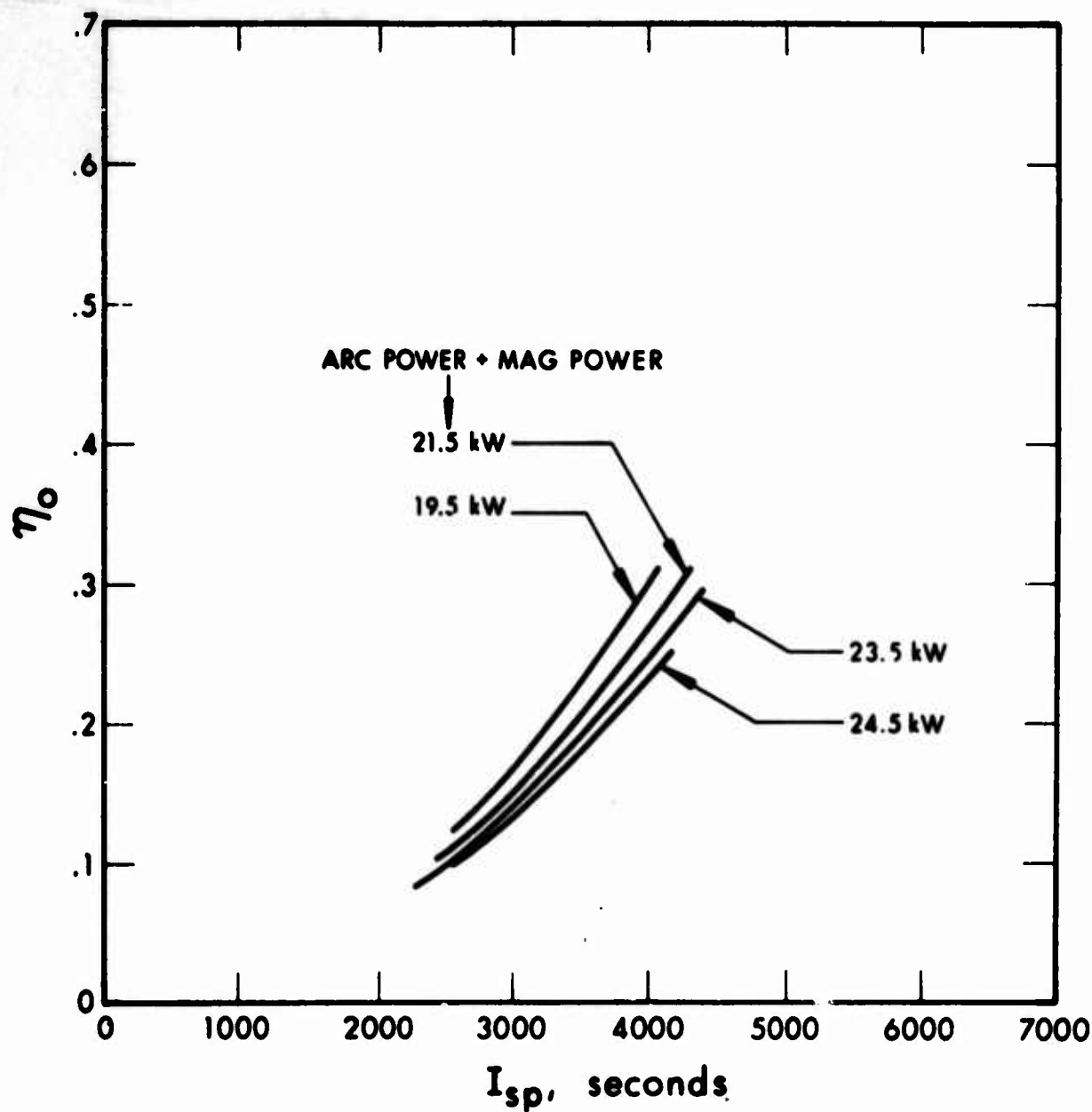
Figure 46 Overall Efficiency versus I_{sp} for Run 727

73625286
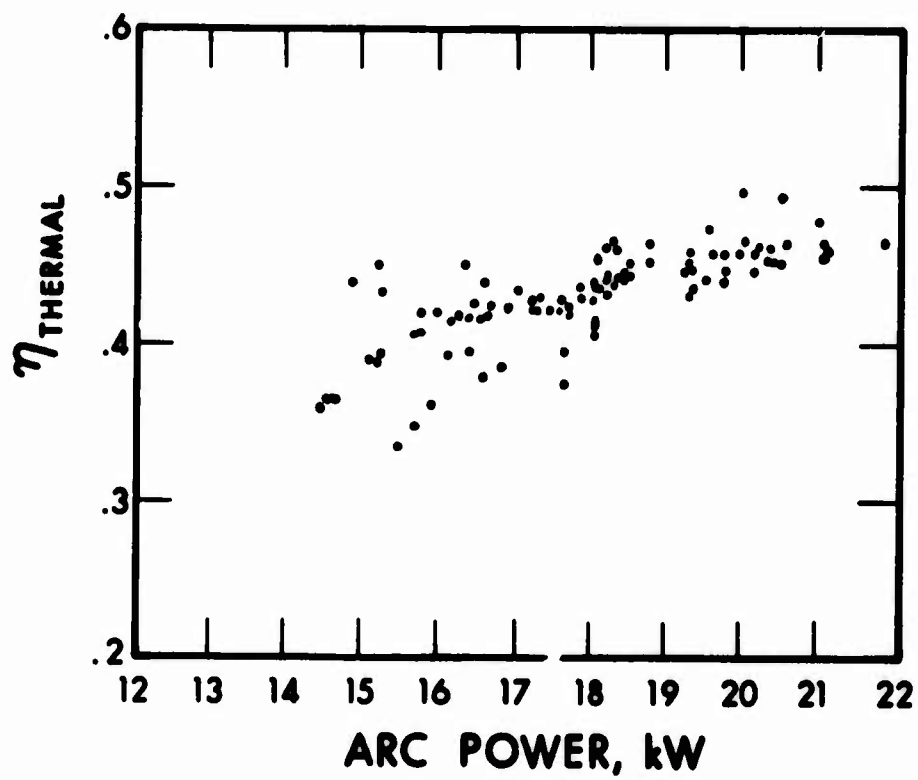
Figure 47   Thermal Efficiency versus Arc Power for Run 727

73625283
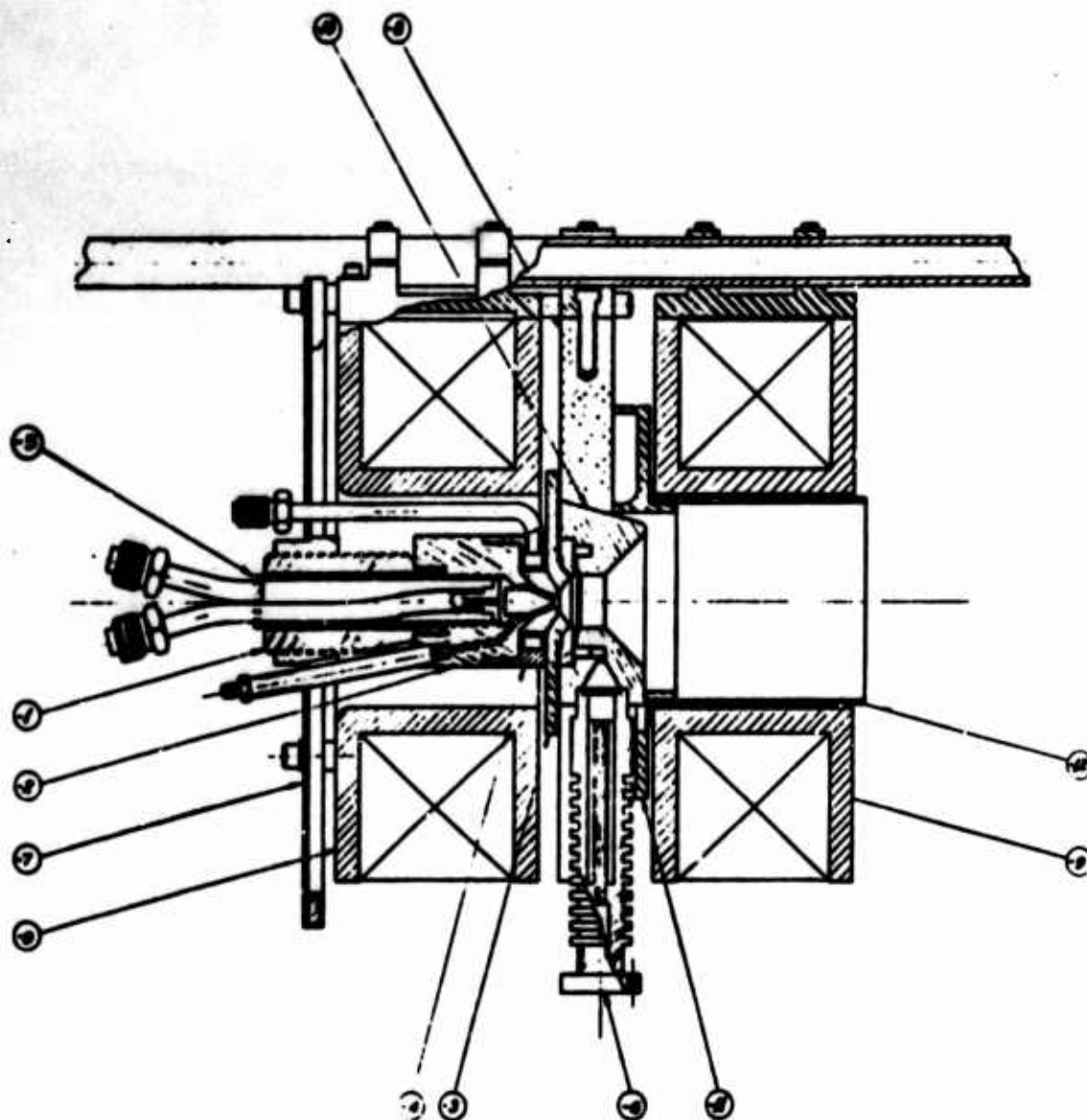
1	12	-502	HOT LINER	MOLY-TUNGSTEN
1	11	-500	MAGNET INSULATOR	BORON NITRIDE
1	10	-503	ANODE	TUNGSTEN
8	9	-504	ELECTROMAGNET	COPPER-EPOXY
1	8	-505	RADIATOR	GRAPHITE
1	7	-520	SPRING PLATE	316 STAINLESS
1	6	-503	VAPORIZER	MOLYBDENUM
1	5	-500	CATHODE ASSEMBLY	TUNGSTEN-COPPER
1	4	-500	BUFFER ASSEMBLY	. . . .
1	3	-501	BUFFER INSULATOR	BORON NITRIDE
1	2	-502	CATHODE . . .	. . . .
1	1	070-500	REAR . . .	. . . .

Figure 48   Thrustor Model LAJ-AF-CG-2B with GAF IV Feed

5090-IR-3   82
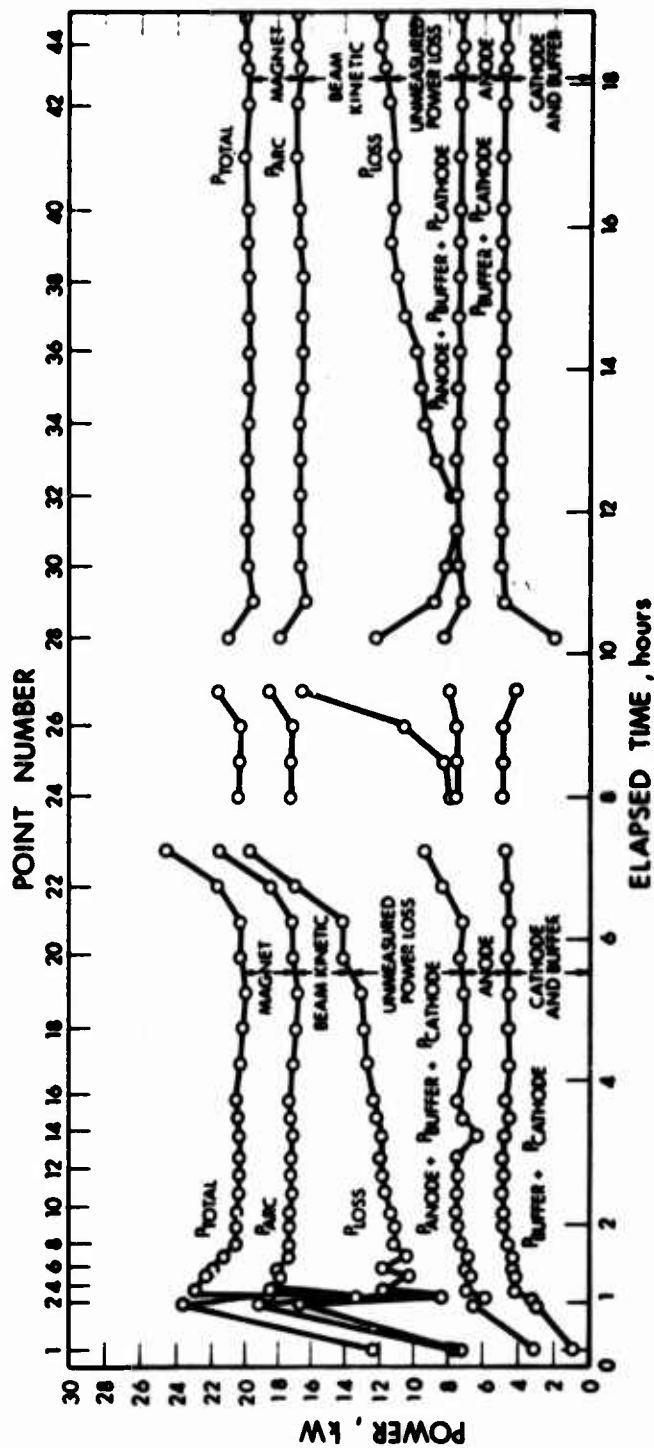
Figure 49 Histogram of Power Distribution for Run 732 (Part 1)
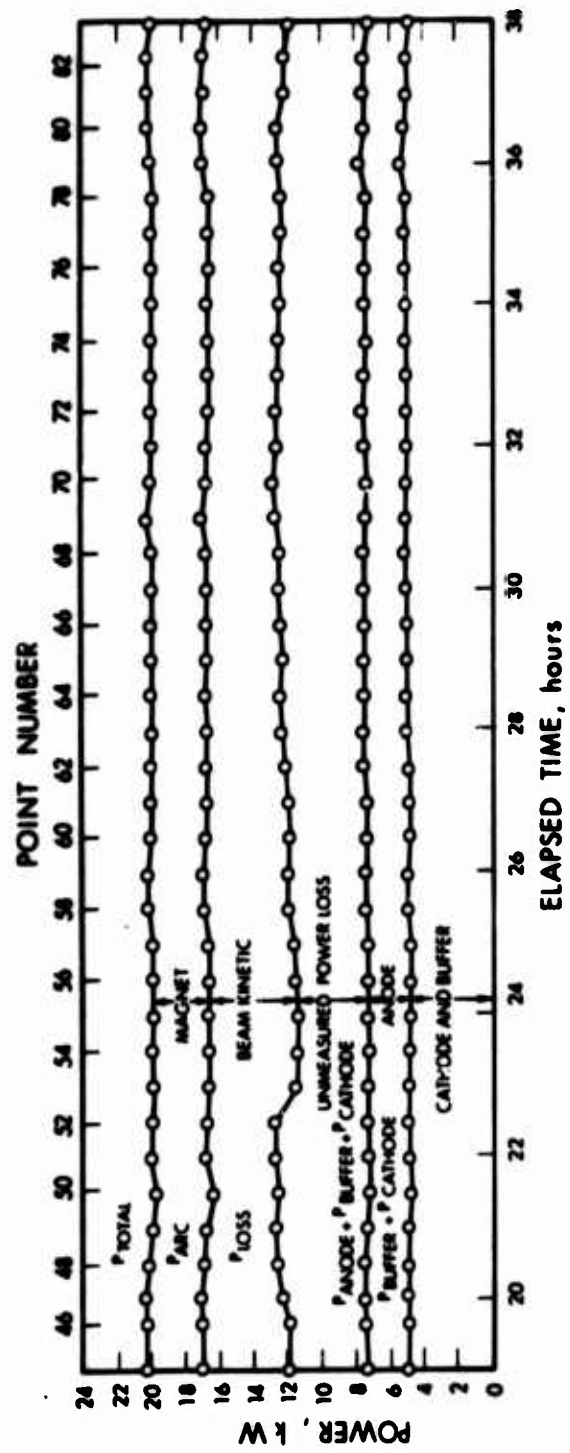
Figure 50 Histogram of Power Distribution for Run 732 (Part 2)
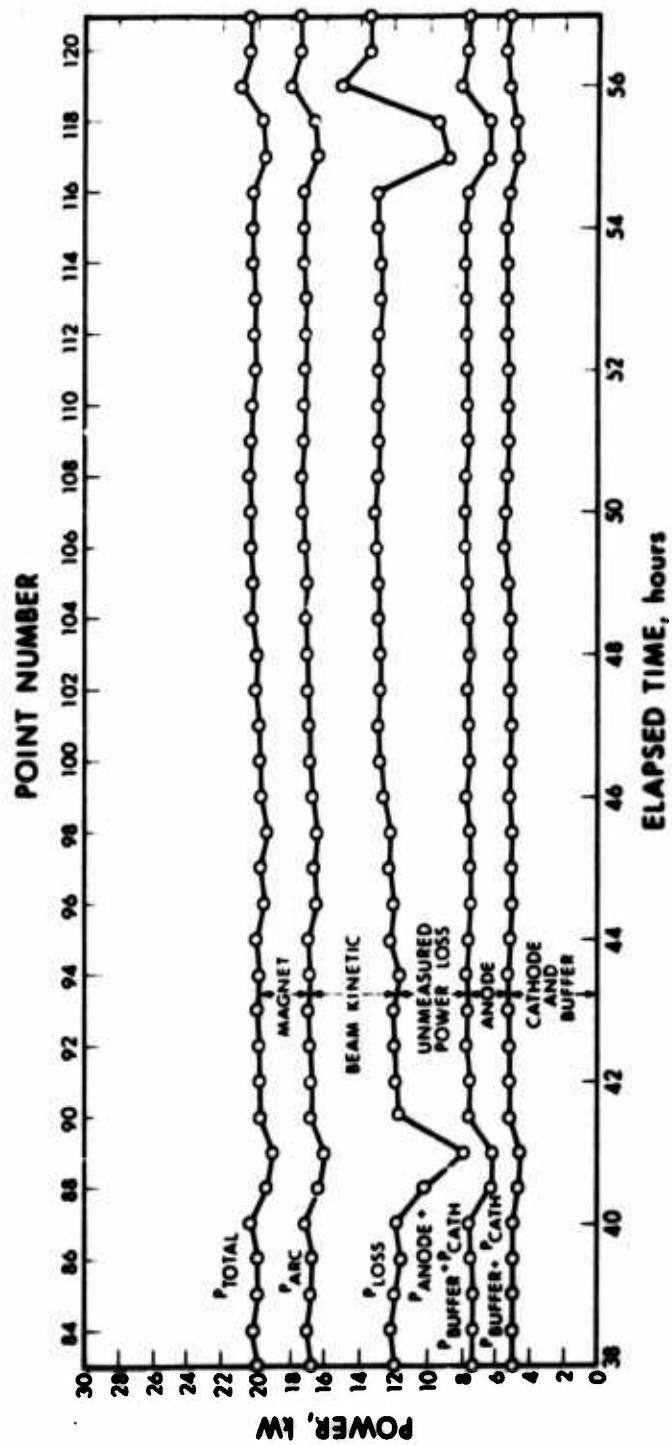
Figure 51 Histogram of Power Distribution for Run 732 (Part 3)
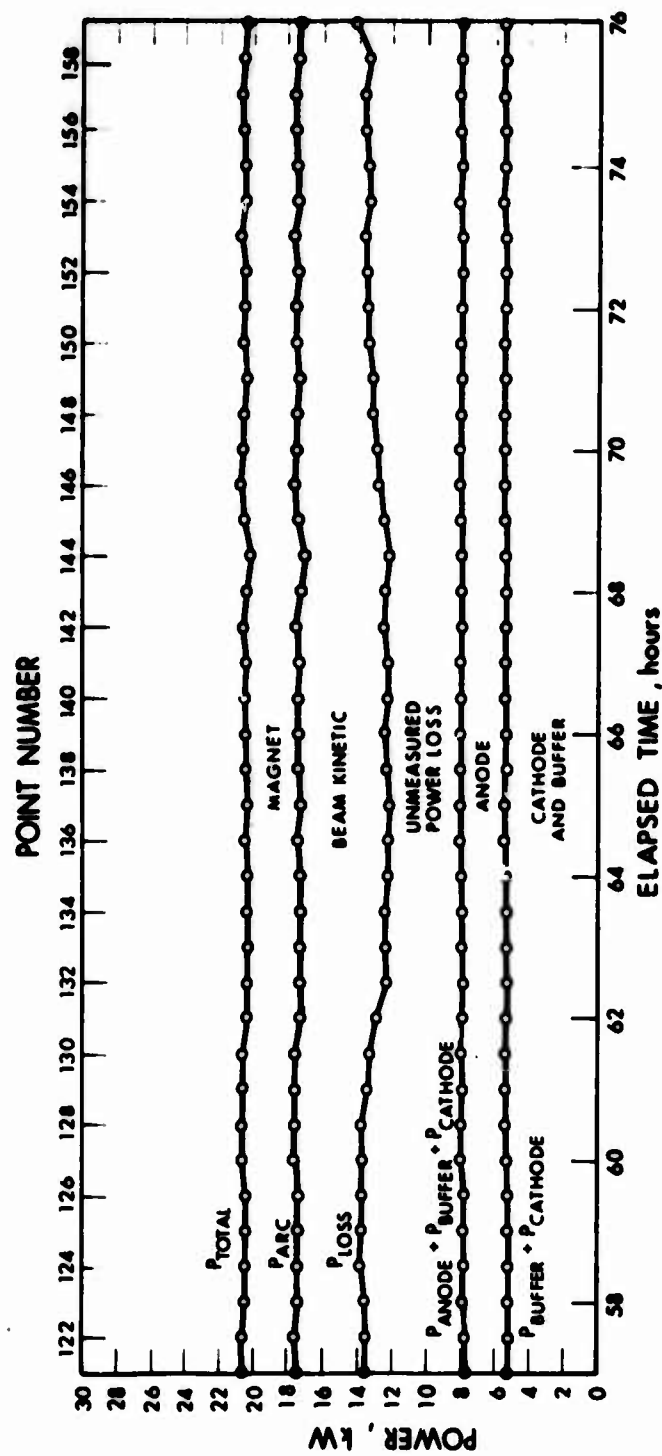
Figure 52   Histogram of Power Distribution for Run 732 (Part 4)
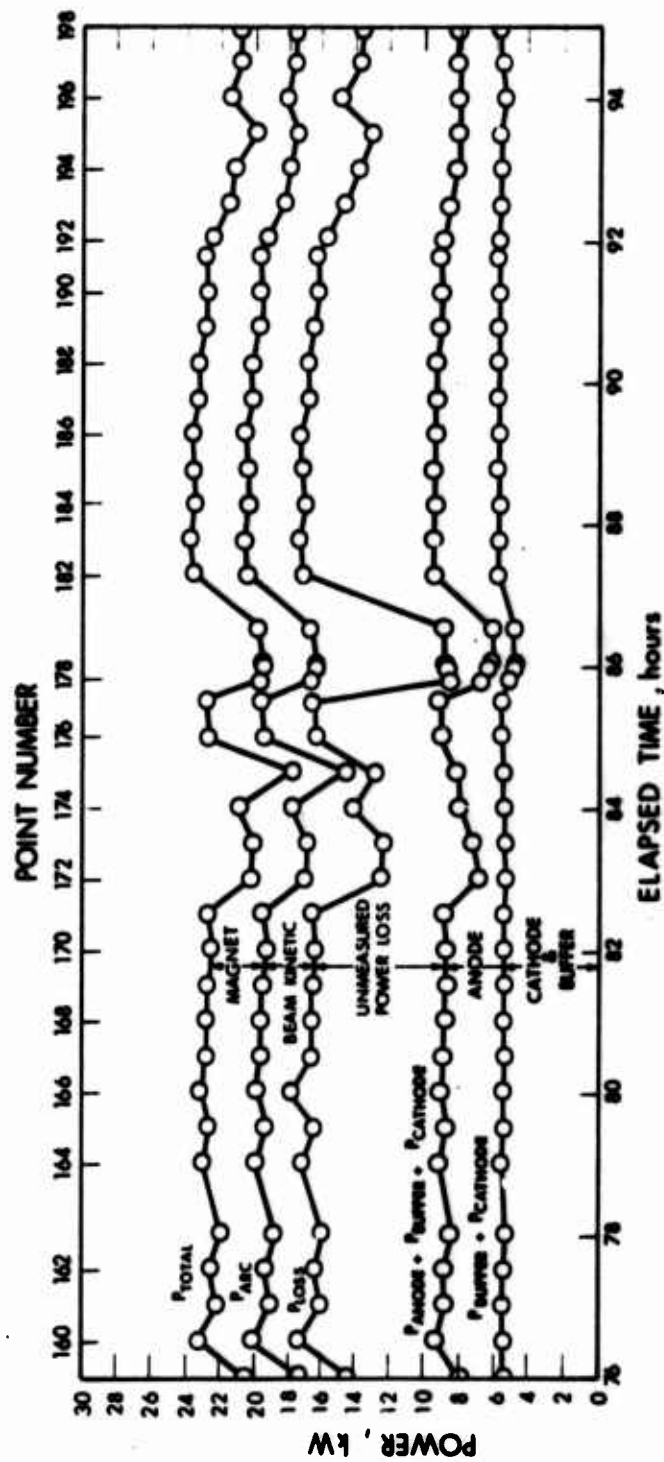
Figure 53 Histogram of Power Distribution for Run 732 (Part 5)

POINT NUMBER

POWER, kW

ELAPSED TIME, hours

P_{TOTAL}

P_{ARC}

P_{LOSS}

MAGNET

BEAM KINETIC

UNMEASURED POWER LOSS

ANODE

CATHODE & BUFFER

$P_{ANODE} + P_{BUFFER} + P_{CATHODE}$

$P_{BUFFER} + P_{CATHODE}$
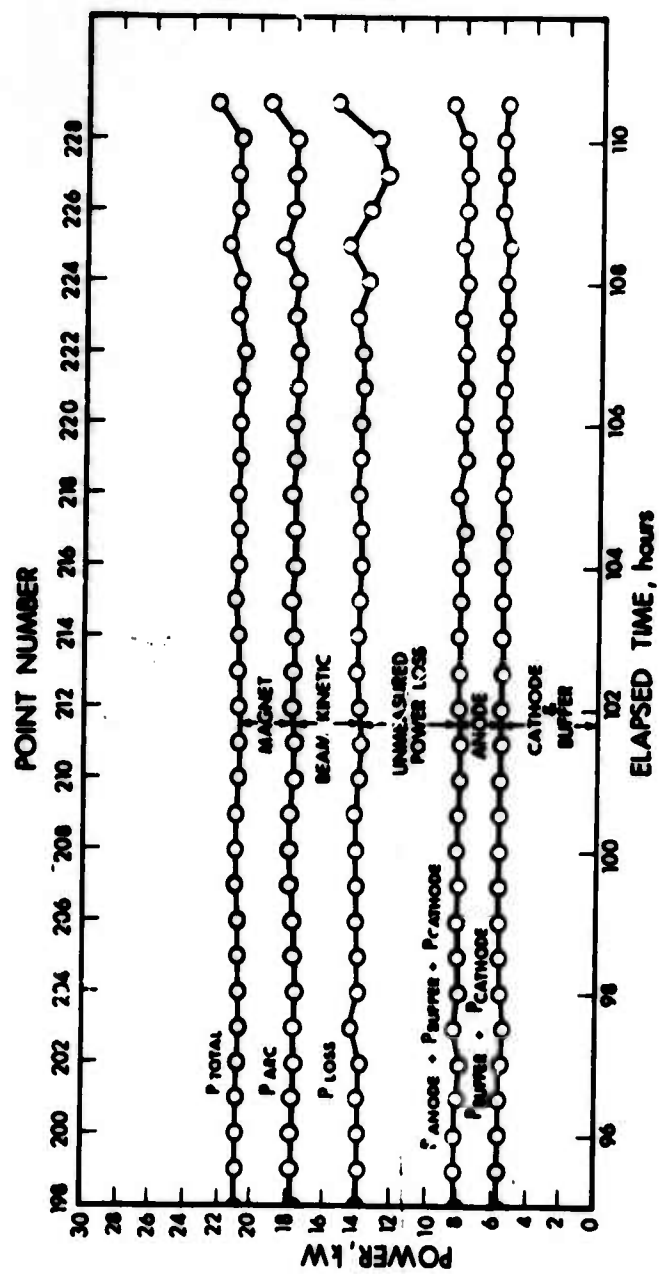
Figure 54 Histogram of Power Distribution for Run 732 (Part 6)
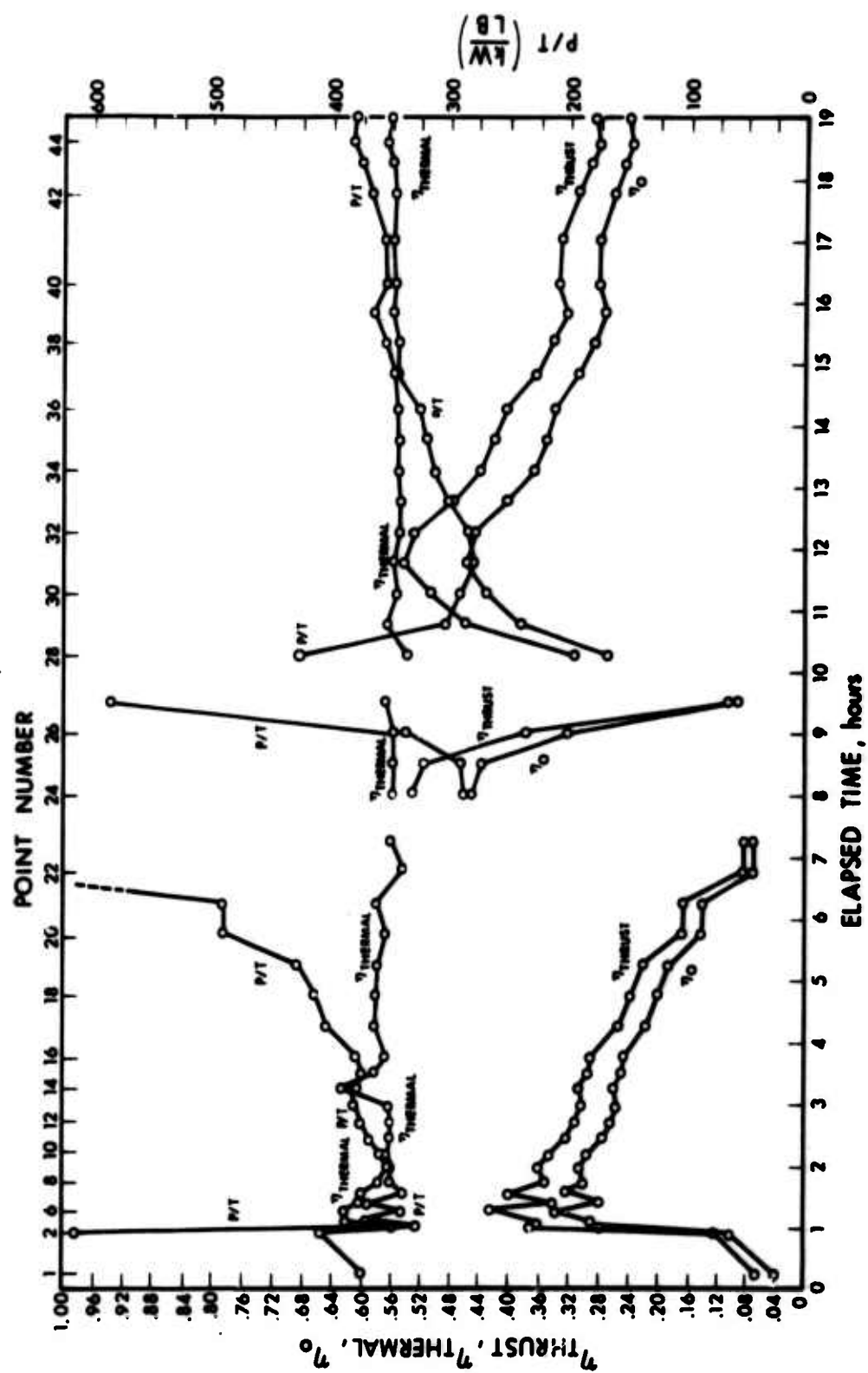
Figure 55 Histogram of Efficiencies and P/T for Run 732 (Part 1)
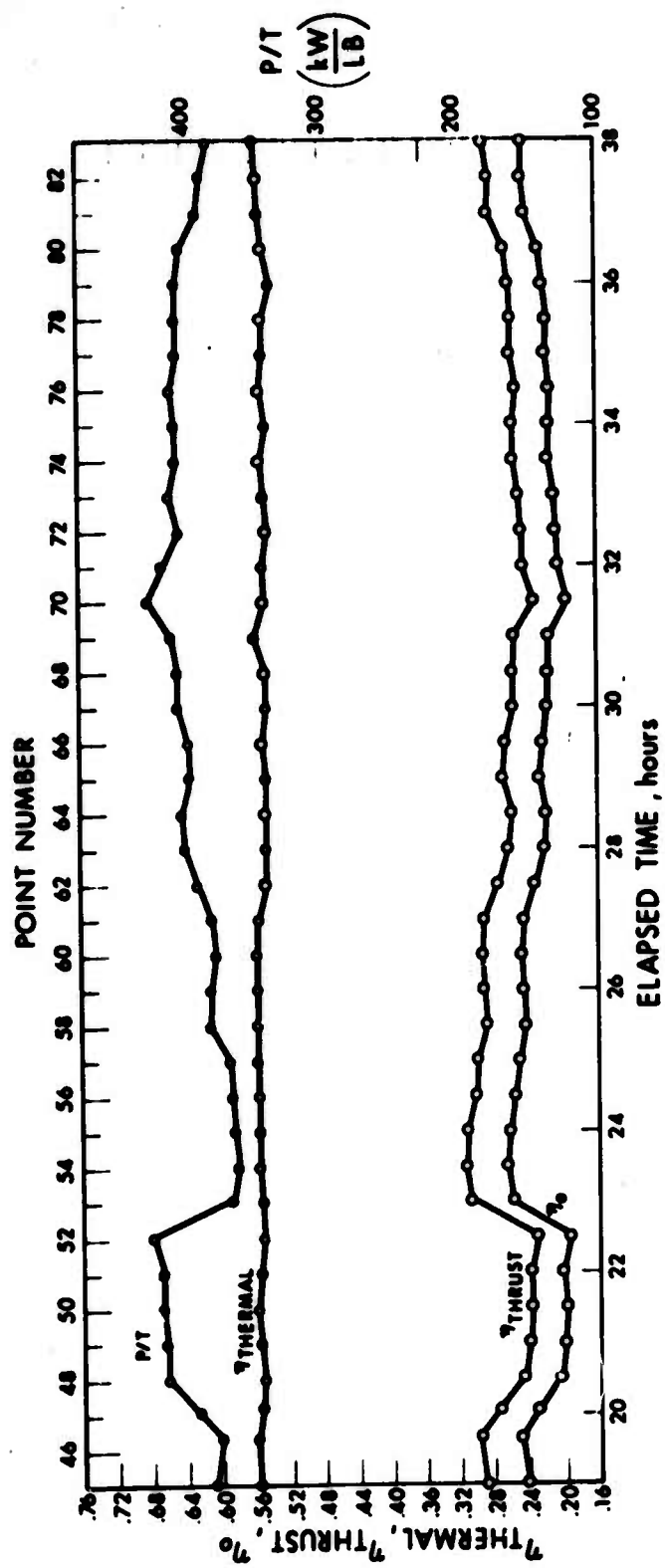
Figure 56 Histogram of Efficiencies and P/T for Run 732 (Part 2)
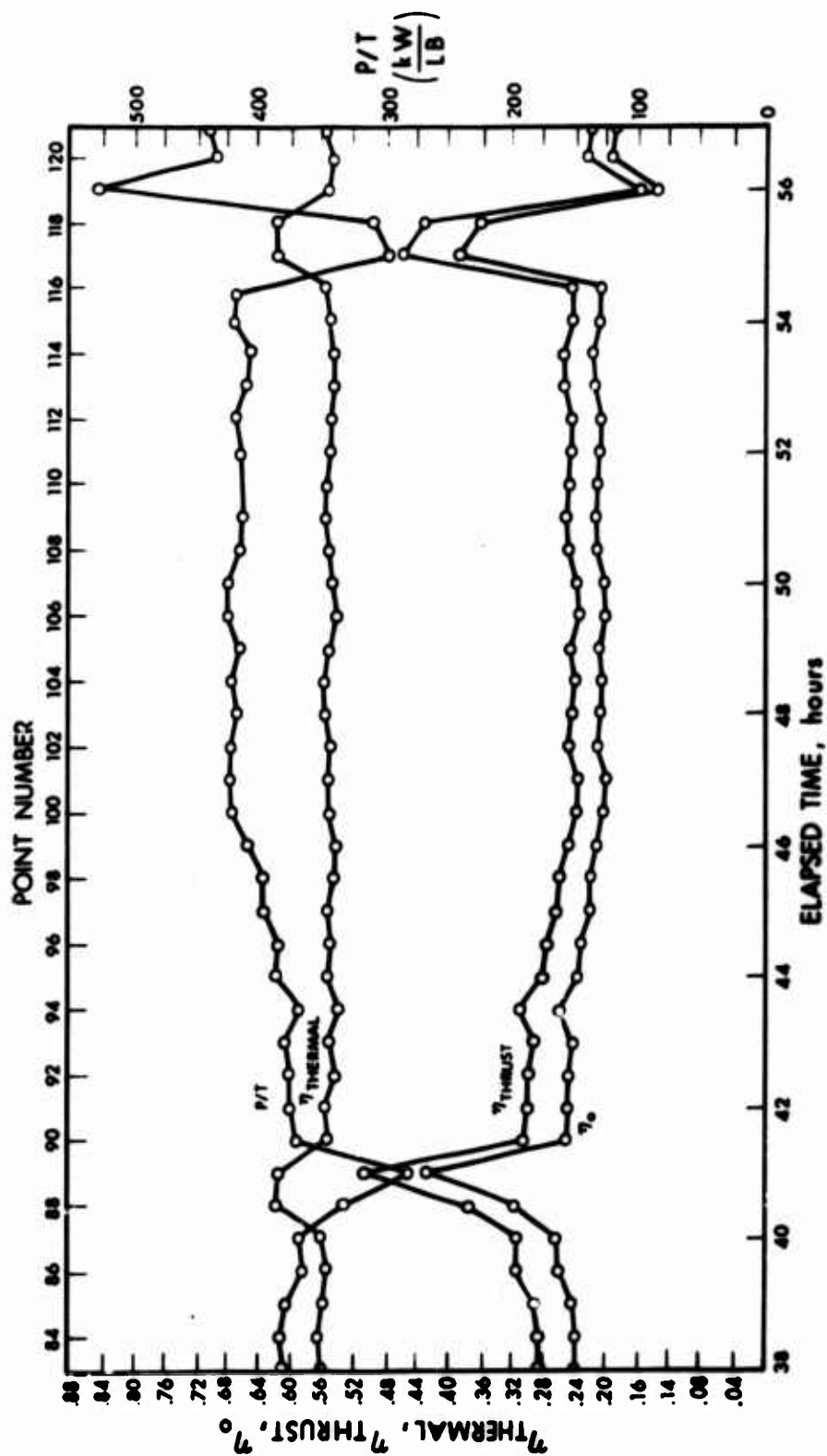
Figure 57 Histogram of Efficiencies and P/T for Run 732 (Part 3)

P/T
$\left(\dfrac{kW}{LB}\right)$

POINT NUMBER

ELAPSED TIME, hours

$\eta_{THERMAL}$, η_{THRUST}, η_o

P/T
$\eta_{THERMAL}$
η_{THRUST}
η_o
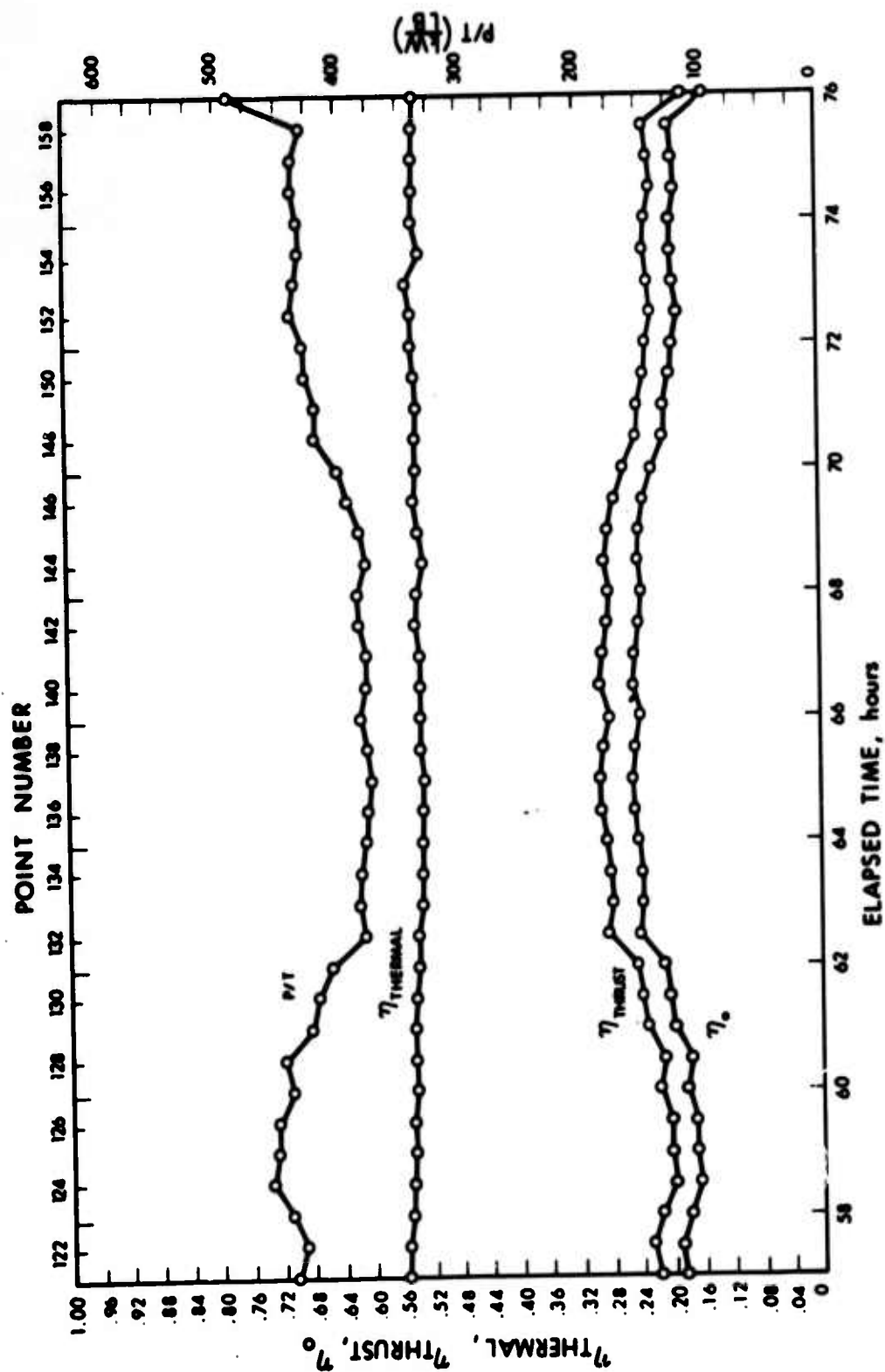
Figure 58 Histogram of Efficiencies and P/T for Run 732 (Part 4)

5090-IR-3

92
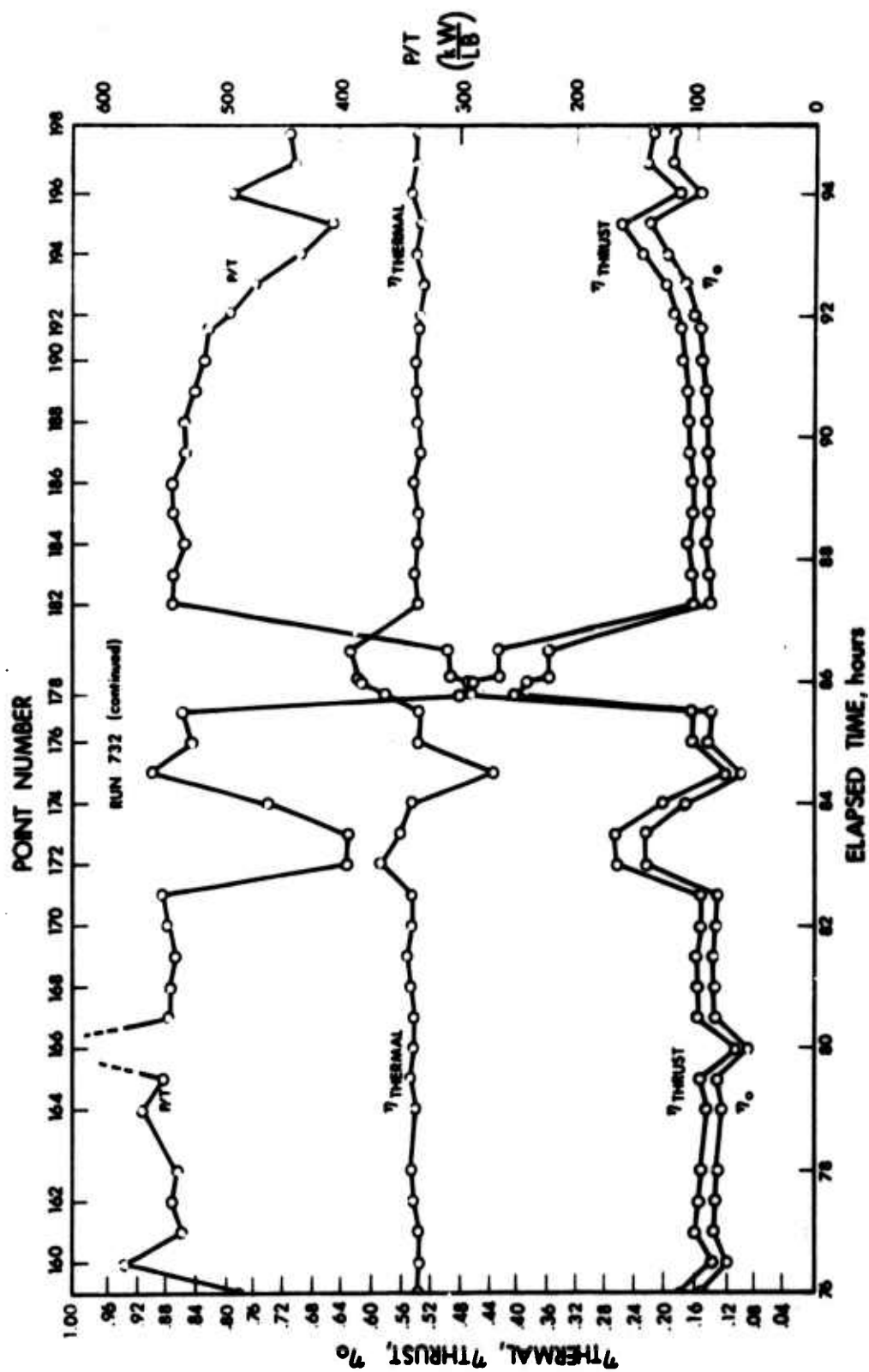
Figure 59 Histogram of Efficiencies and P/T for Run 732 (Part 5)
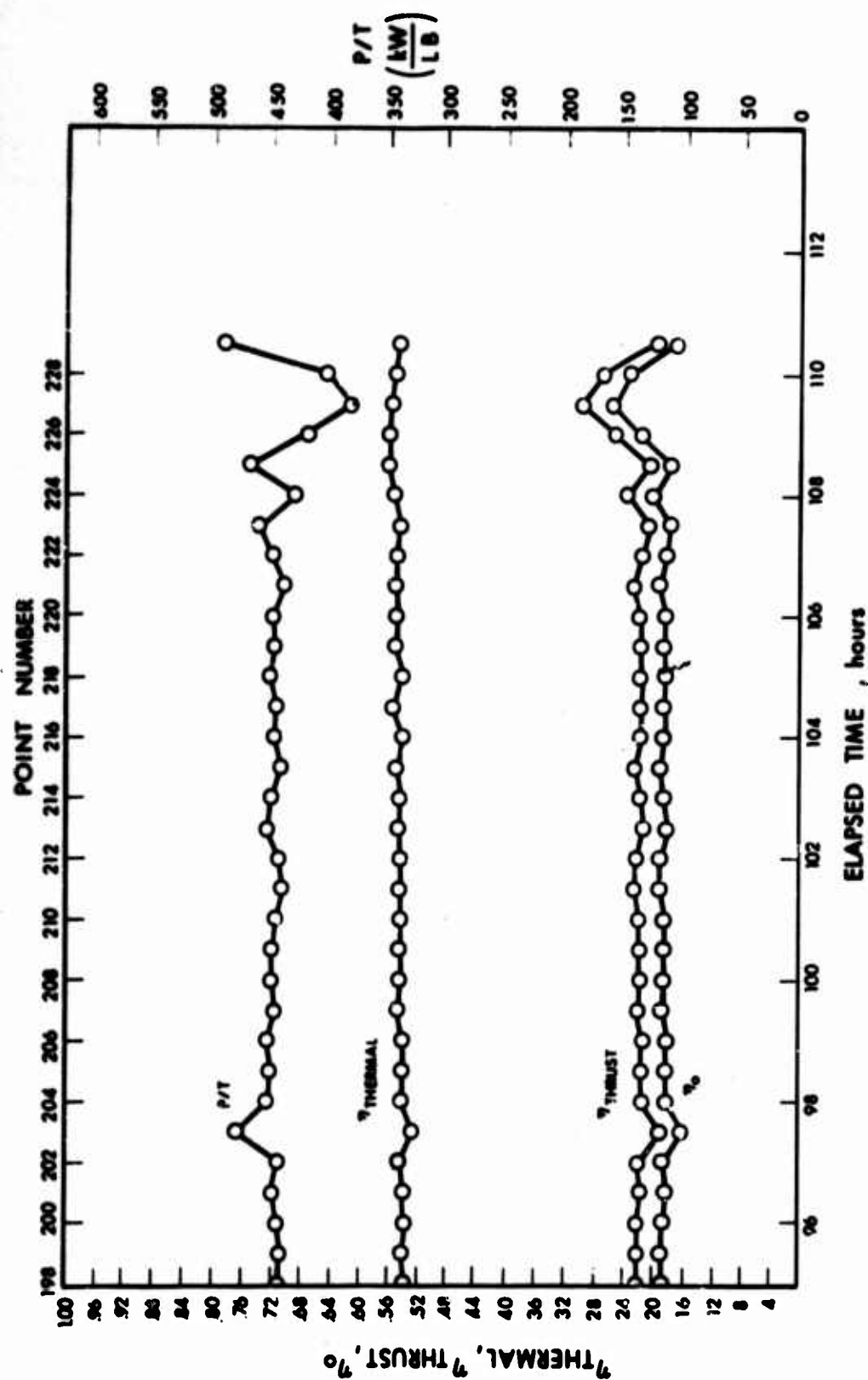
Figure 60 Histogram of Efficiencies and P/T for Run 732 (Part 6)
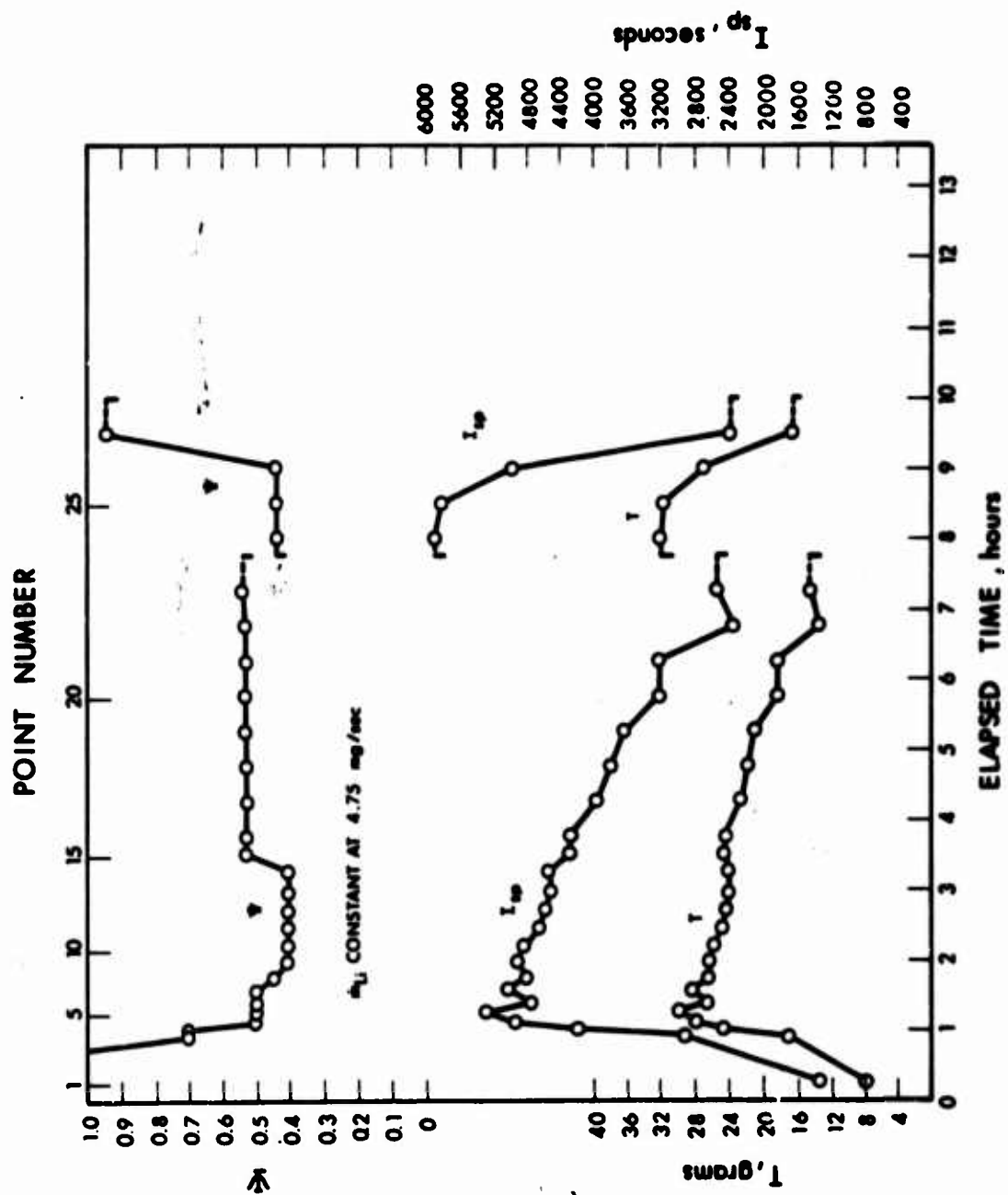
Figure 61 Histogram of T, I$_{sp}$ and Ψ for Run 732 (Part 1)
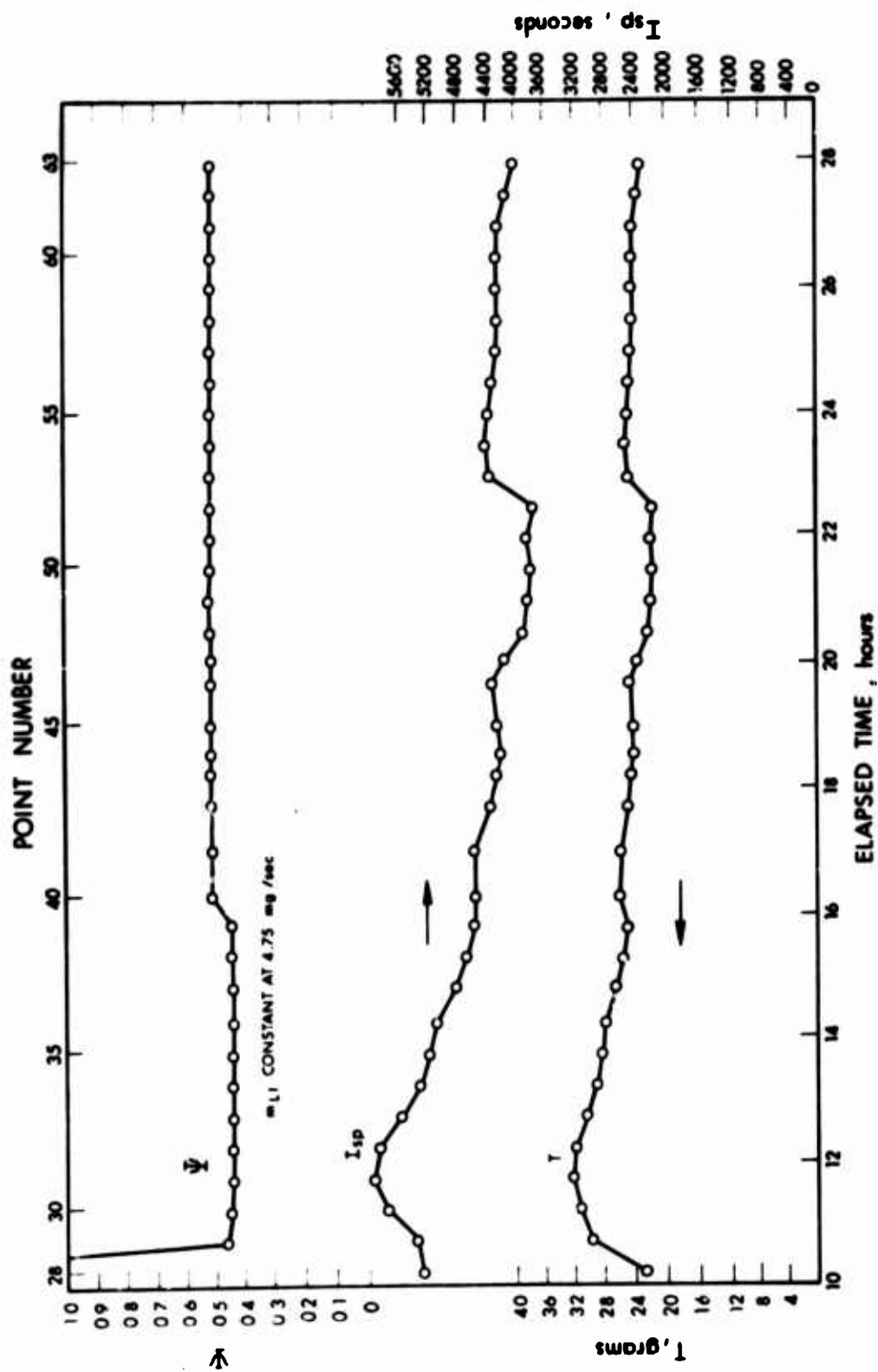
Figure 62 Histogram of T, I_{sp} and Y for Run 732 (Part 2)

36
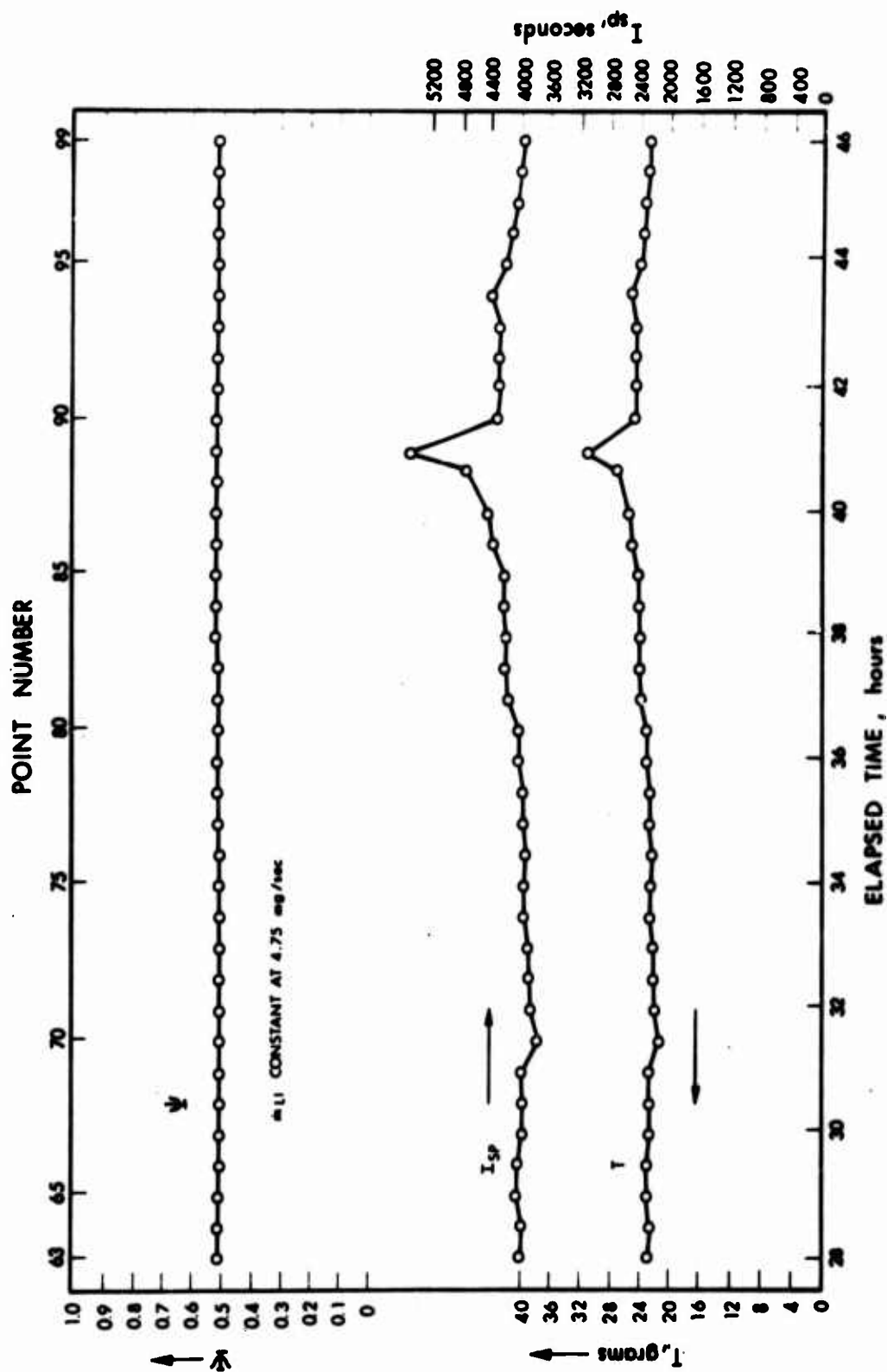
Figure 63 Histogram of T, I_{sp} and Y for Run 732 (Part 3)
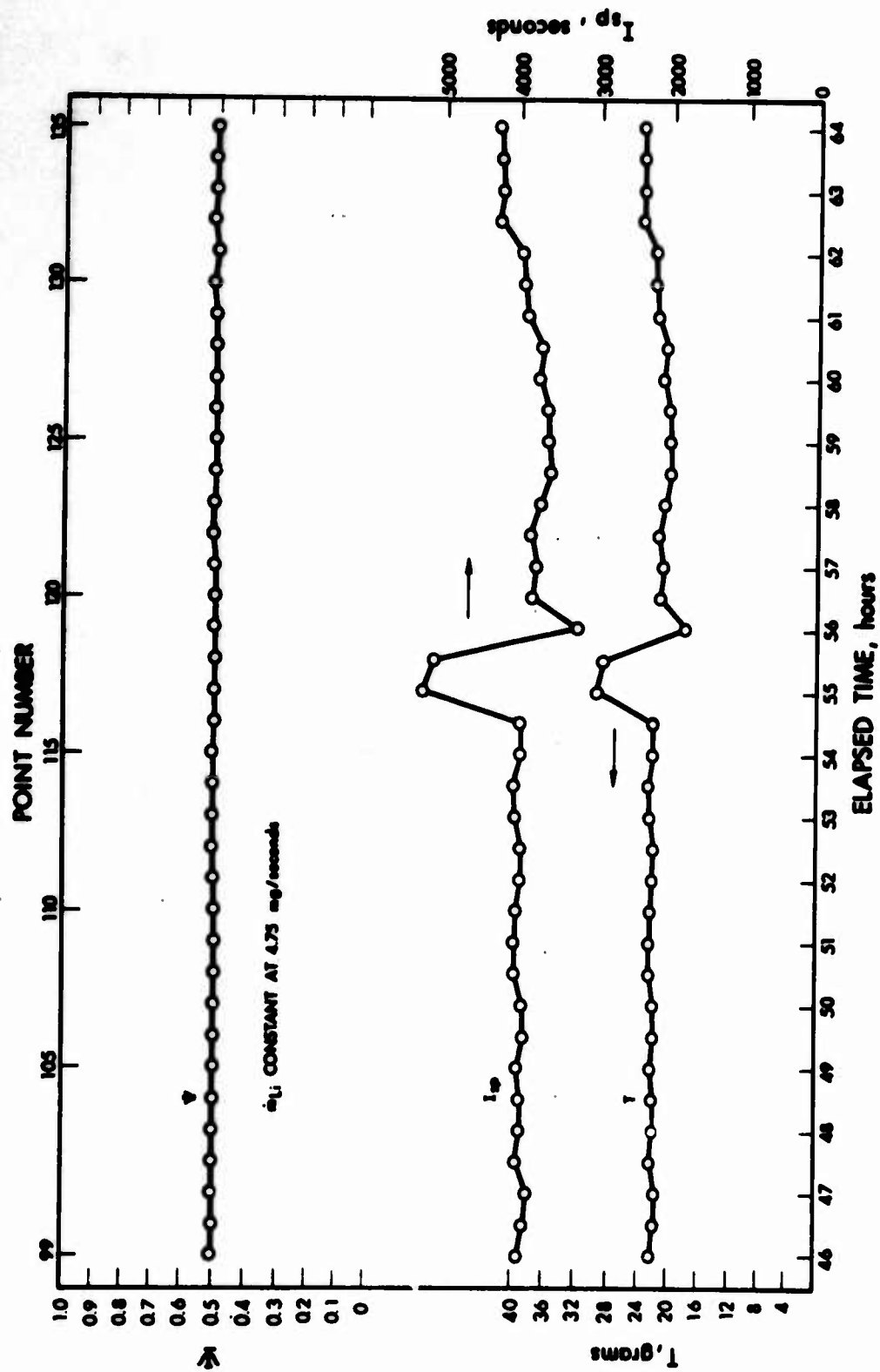
Figure 64   Histogram of T, I_{sp} and Y for Run 732 (Part 4)

98
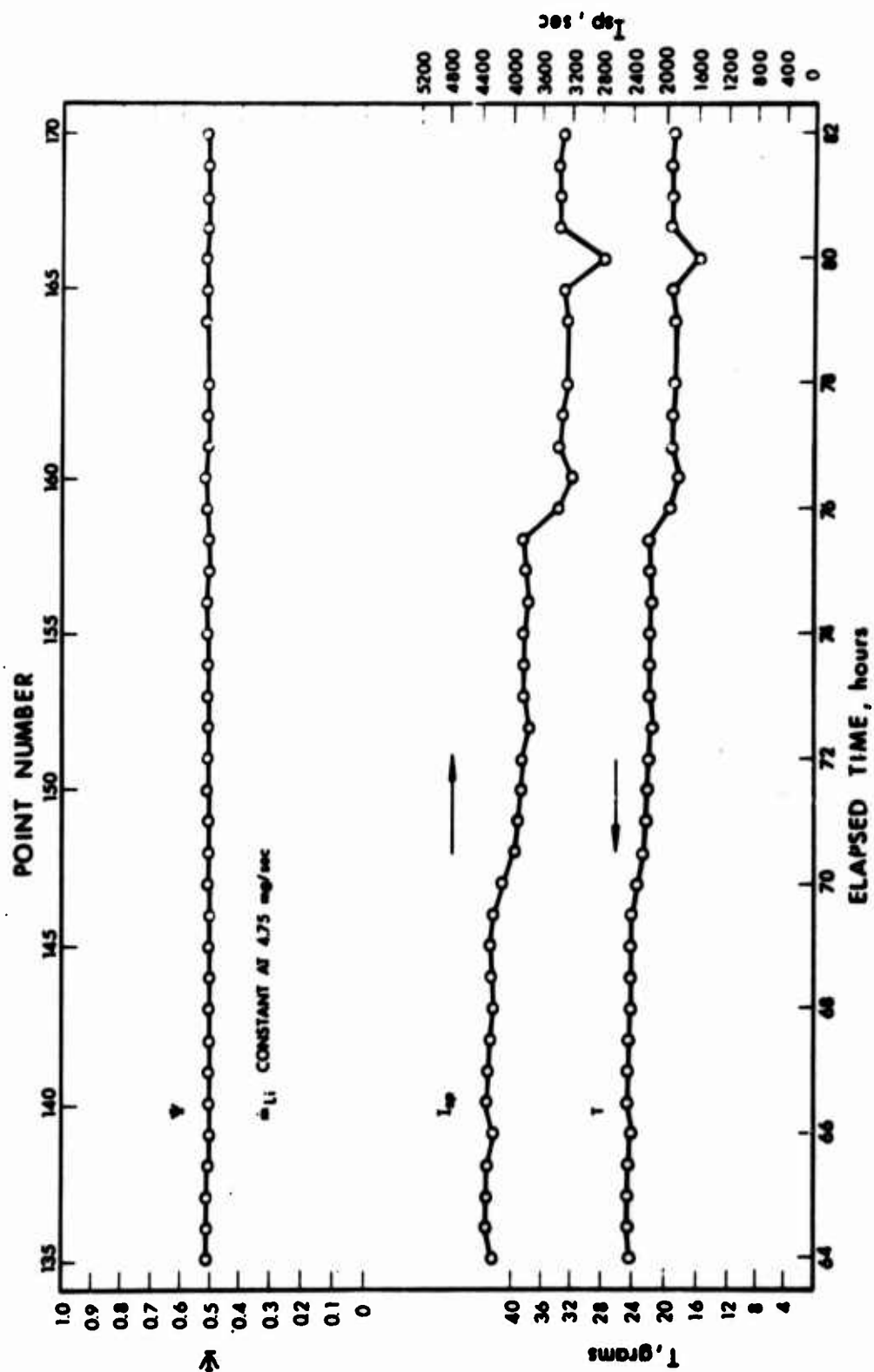
Figure 65 Histogram of T, I_{sp} and $\dot{V}$ for Run 732 (Part 5)
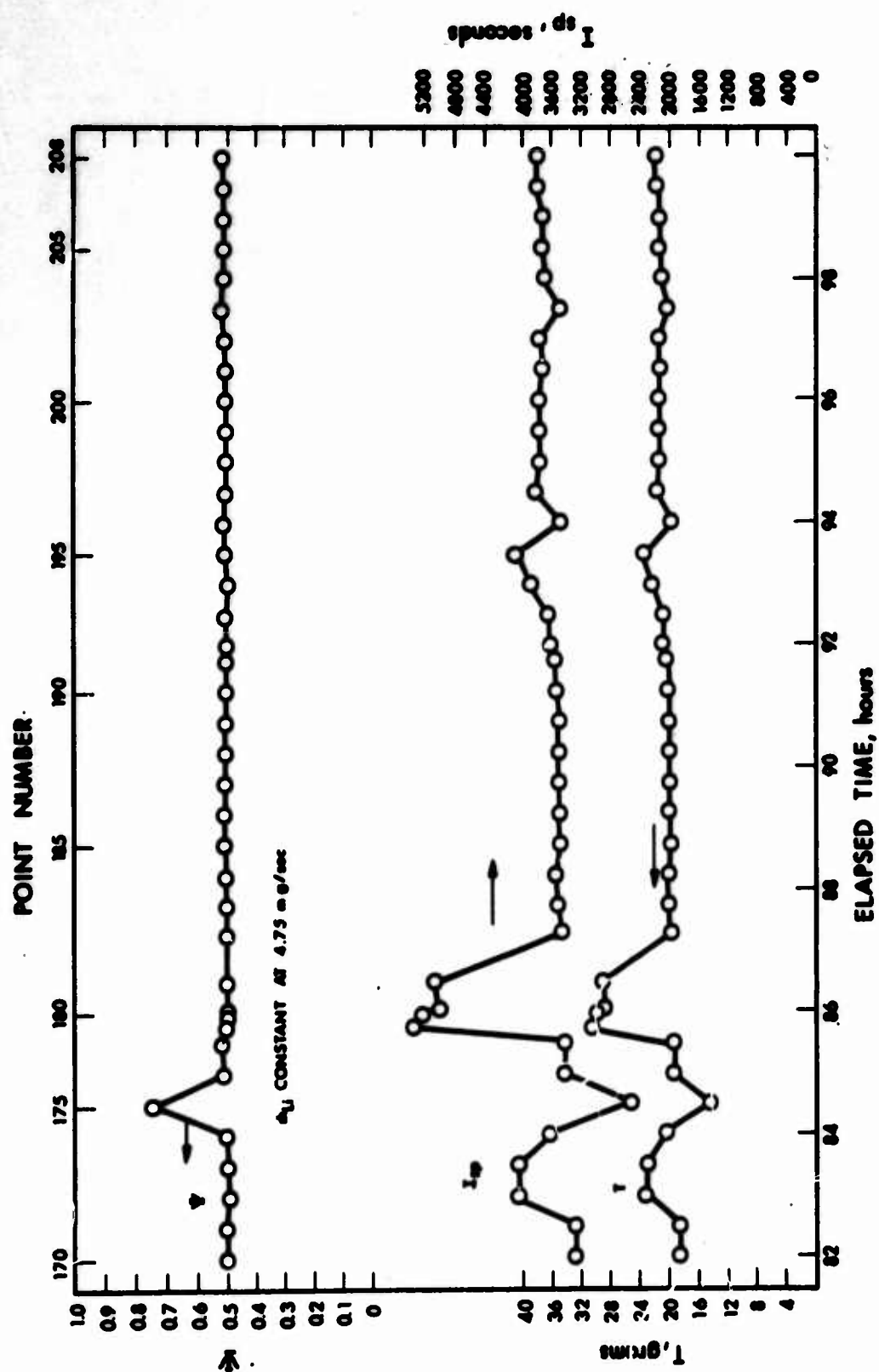
Figure 66 Histogram of T, I_{sp}, and Y for Run 732 (Part 6)

Figure 67 Histogram of T, I$_{sp}$ and Y for Run 732 (Part 7)
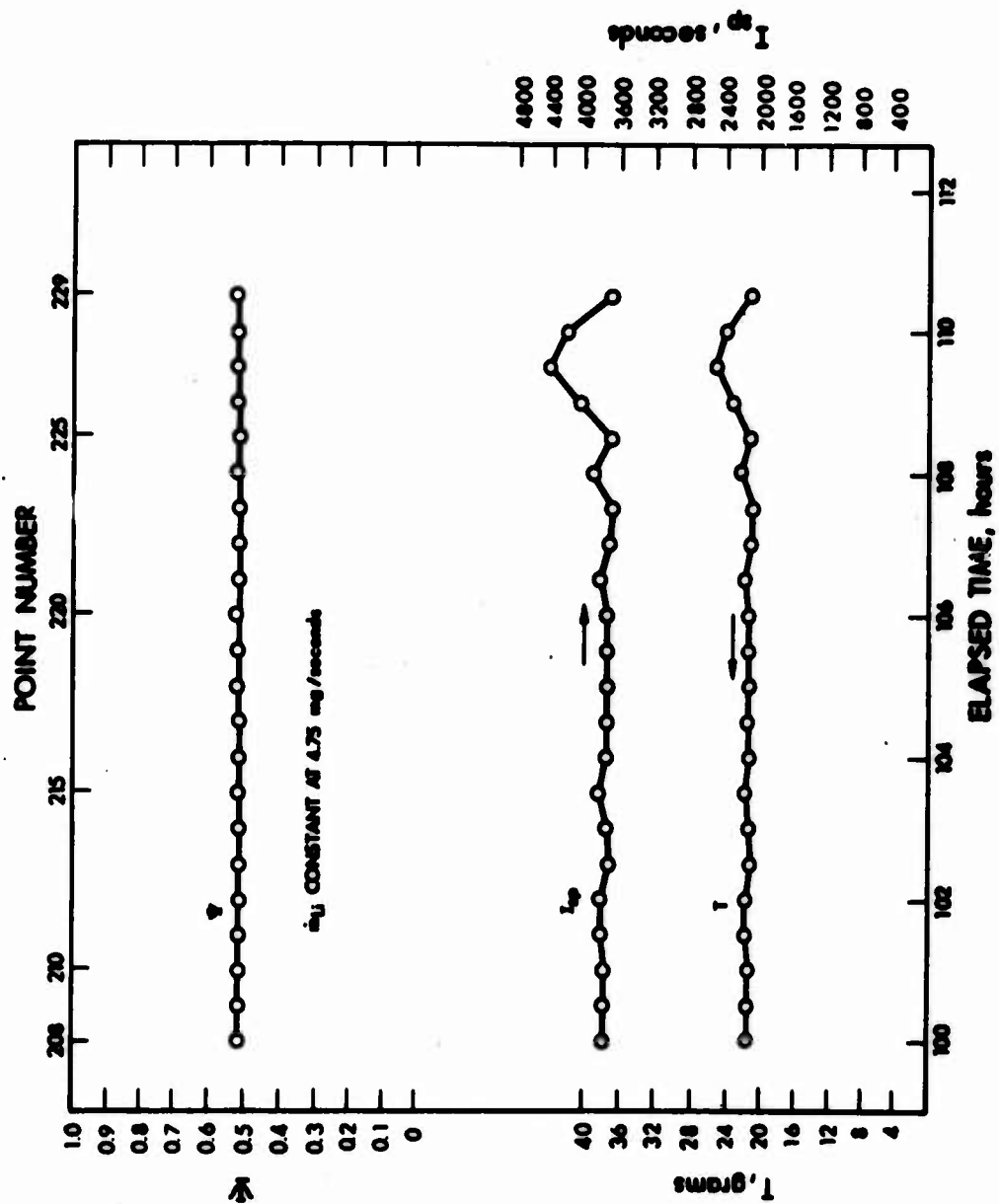
Figure 68 Electrode Components After 100-Hour Test (uncleaned)

Figure 69   Buffer After 100-Hour Test (cleaned)
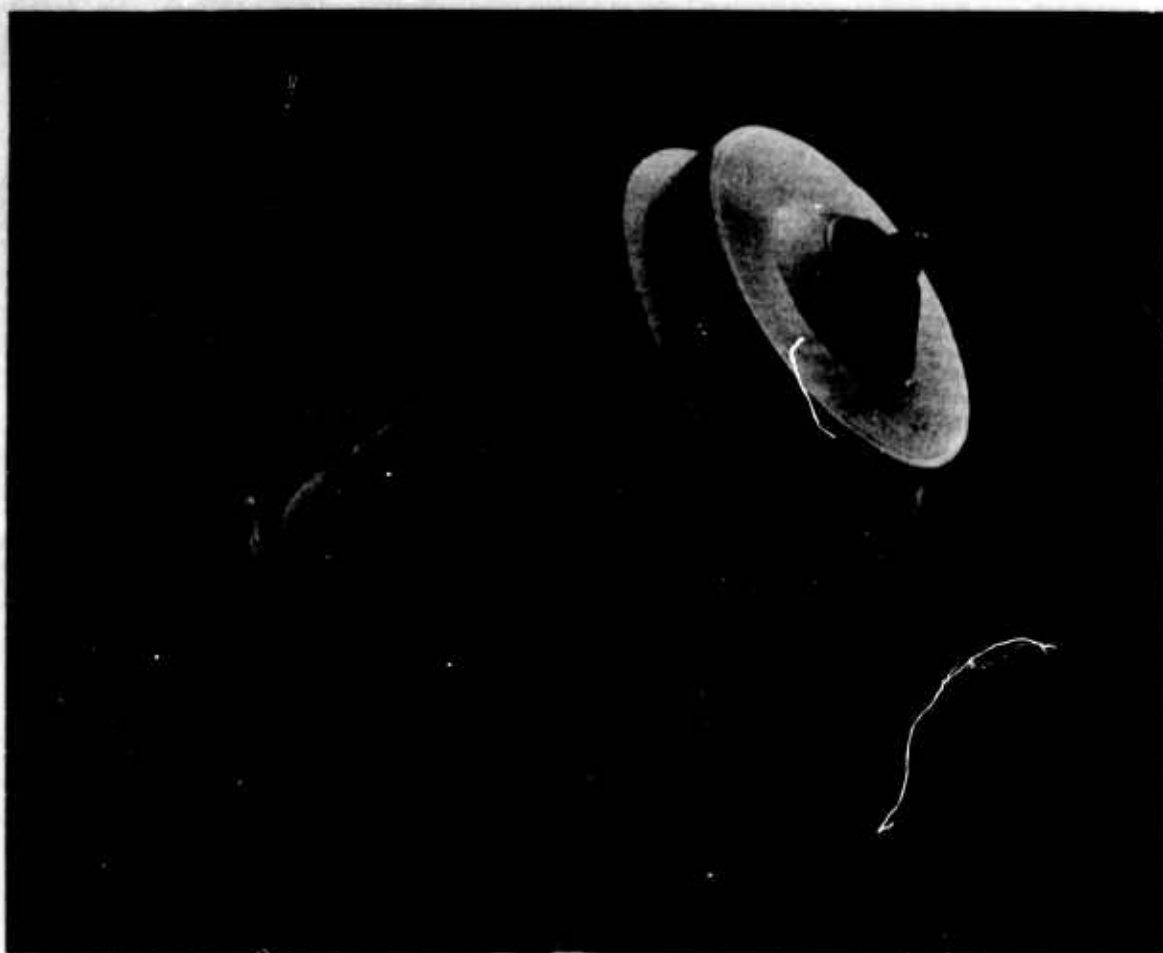
Figure 70 Cathode Tip and Insulator Assembly After 100-Hour Test
(uncleaned)

SP 16756

Figure 71   Anode After 100-Hour Test (cleaned)

SP 16750
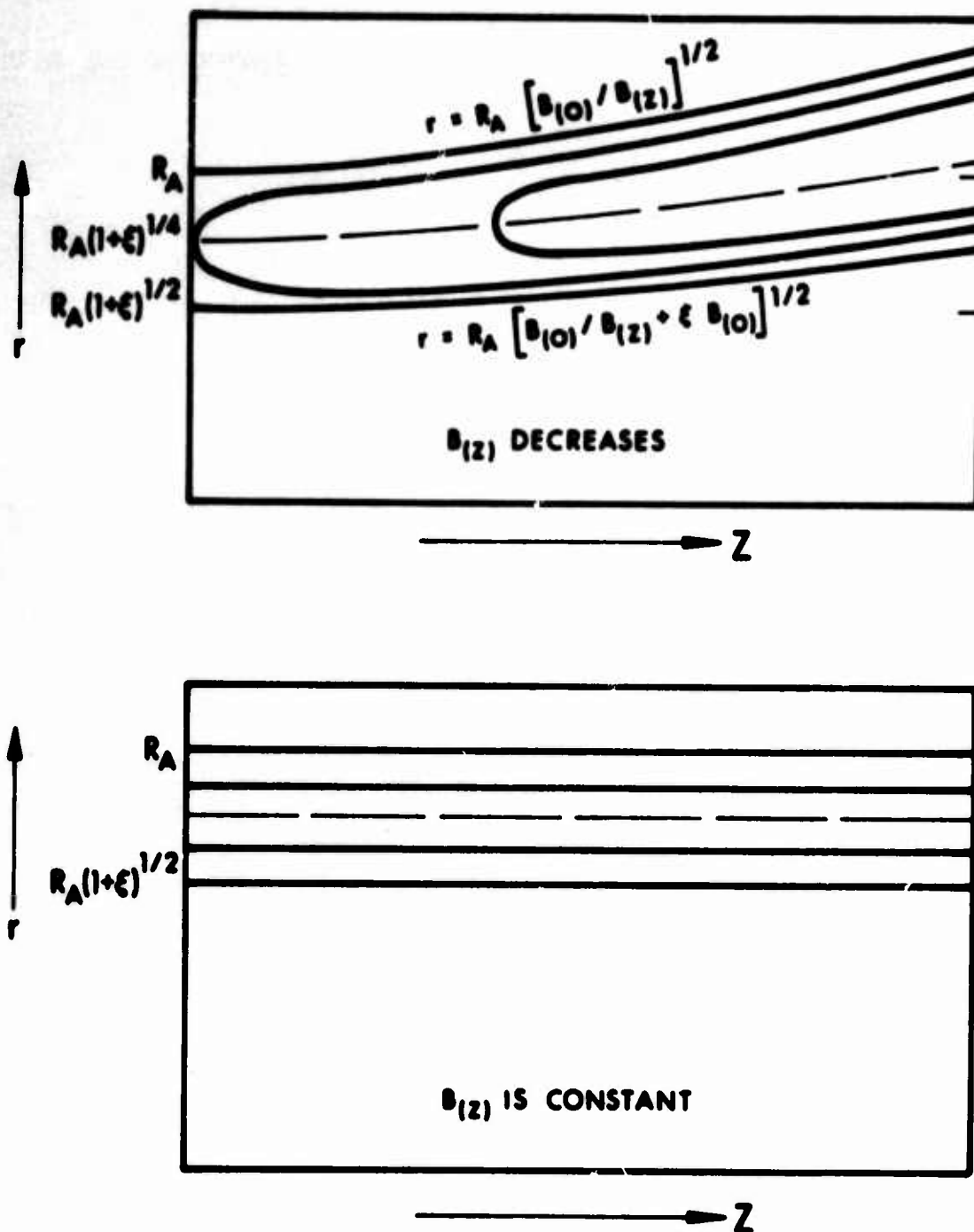
Figure 72 Contour Lines of Constant H_e

73624778
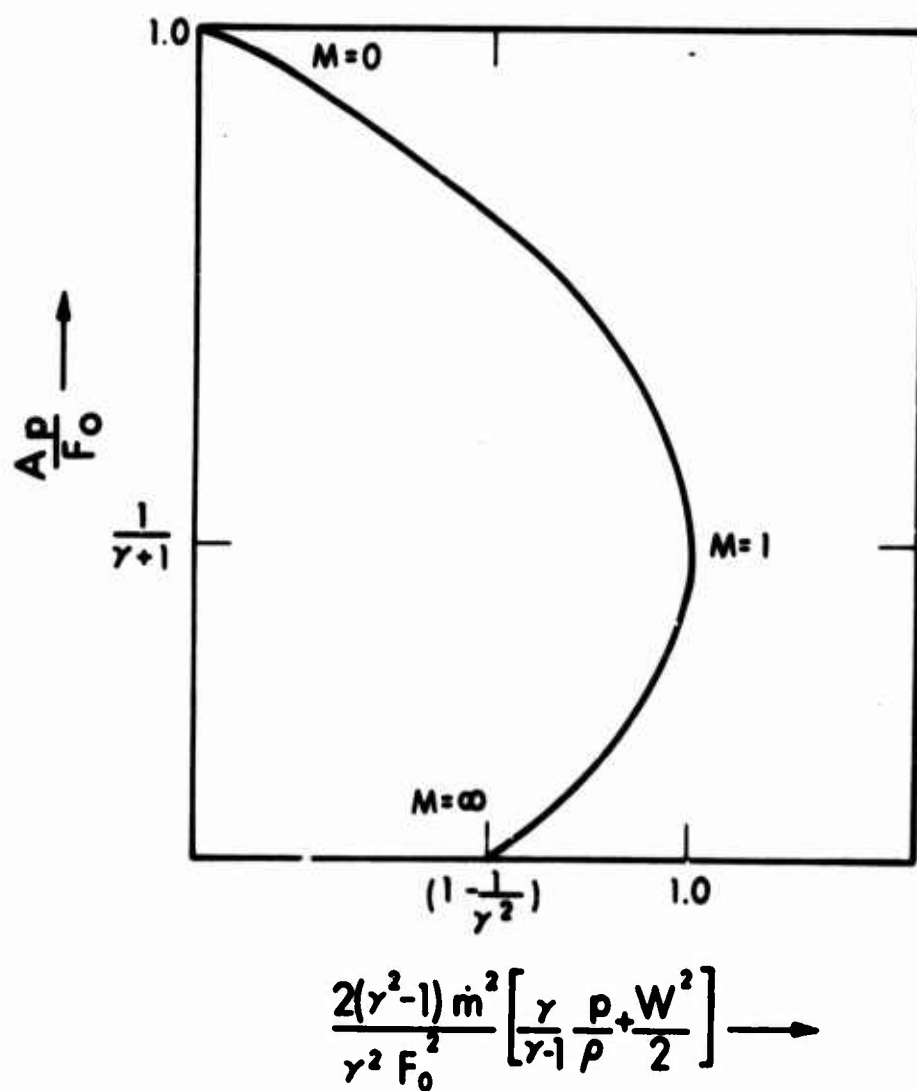
Figure 73   Pressure versus Enthalpy

73624779

REFERENCES

1. R. A. Moore et al, "High Specific Impulse Thermal Arc Jet Thrustor Technology," EOS Report 5090-IR-1, December 1964

2. R. A. Moore et al, "High Specific Impulse Thermal Arc Jet Thrustor Technology — Part I. Performance of Hall Arc Jets with Lithium Propellant," Technical Report AFAPL-TR-65-48, Part I, June 1965

3. G. L. Cann et al, "High Specific Impulse Thermal Arc Jet Thrustor Technology," EOS Report 5090-IR-2, September 1965

4. G. L. Cann et al, "High Specific Impulse Thermal Arc Jet Thrustor Technology — Part II. Performance of Hall Arc Jets with Lithium Propellant," Technical Report AFAPL-TR-65-48, Part II, January 1967

5. P. F. Jacobs, L. R. Gallagher, and R. W. Prichard, "Diagnostic Measurements in an Alkali Plasma Hall Accelerator," AIAA Paper 67-46, January 1967

6. P. F. Jacobs and G. L. Cann, "Diagnostics of an Alkali Plasma Hall Current Accelerator," EOS Report 7053-SA-1, September 1966

7. A. V. Potapov and G. V. Babkin, "T-s Diagram for Lithium Vapour at Temperatures Between 1000° and $10{,}000^{\circ}$K and Pressures 1 and 10^{6} Bar," Russian J. Phys. Chem., Vol. 38 No. 12, December 1964

8. W. D. Weatherford, Jr., et al, "Properties of Inorganic Energy-Conversion and Heat-Transfer Fluids for Space Applications," WADD Technical Report 61-96, November 1961

APPENDIX

TEST DATA

TABLE A-I

SUMMARY OF TESTS CONDUCTED

Run Number	Date	Elapsed Time (hrs/min)	Time on Lithium	Configuration	Propellant	Chamber	Feed System
			Performance and Life Tests				
725	8-23-66	1:46	1:13	LAJ-AF-CG-2A	Li/H$_2$	6x6, 6x8	GAF-II-1
726	8-25-66	--	--	"	"	"	"
727	9-28-66	30:05	29:58	"	"	"	"
			Calibration Tests				
728A	10-19-66	6:26	6:00	LAJ-AF-CG-2A	Li/H$_2$	3x6	GAF-II-2
728B	10-20-66	11:15	11:00	"	"	"	"
728C	10-21-66	5:57	5:29	"	"	"	"
728D	11-2-66	5:35	5:00	"	"	"	"
728E	11-9-66	4:20	4:00	"	"	"	"
728F	11-11-66	5:20	5:00	"	"	"	"
728G	11-15-66	3:20	3:00	"	"	"	"
			Ammonia Tests				
729	12-16-66	:20	0	NH$_3$AJ-AF-CF-2A	NH$_3$	6x6, 6x8	Ammonia Feed
730	12-23-66	:54	0	"	"	"	"
			Performance and Life Tests				
731	12-28-66	4:57	3:34	LAJ-AF-CG-2A	Li/H$_2$	6x6, 6x8	GAF-IV-1
732	1-4-67	111:26	110:13	LAJ-AF-CG-2B	"	"	"

TABLE A-II

TEST DATA

Point No.	T gm	$\dot{m}$ mg/sec	I_{sp} sec	P_t 10^{-4} torr	I_A amp	V_A volt	P_A W	P_{mag} W	P_{c+b} W	P_{an} W	T_{Hi}	η_t	η_b
Run 725													
1	--	7.32	--	500	250	81.0	20.25	13.23	2.62	5.48	0.600	--	--
2	27.4	6.30	4349	1.4	302	74.0	22.35	9.07	4.26	4.35	0.615	0.255	0.182
3	26.9	6.35	4236	0.6	302	73.0	22.05	9.07	4.56	4.36	0.596	0.248	0.175
4	22.6	4.85	4659	0.8	298	80.5	23.99	9.07	4.91	5.16	0.581	0.210	0.152
5	25.7	7.05	3645	0.4	304	71.0	21.58	9.27	4.70	4.07	0.594	0.254	0.178
6	25.8	7.05	3659	0.4	293	73.0	21.75	9.23	4.75	4.01	0.598	0.208	0.146
7	27.5	8.35	3293	0.8	298	64.0	19.07	9.39	4.54	3.47	0.580	0.228	0.152
8	28.2	8.35	3377	0.8	298	64.0	19.07	9.46	4.50	3.15	0.600	0.239	0.160
9	27.9	8.35	3341	0.76	298	64.0	19.07	9.55	4.51	3.12	0.600	0.234	0.156
Run 727													
1	31.79	5.59	5687	1.4	295	75.0	22.13	18.88	3.85	5.31	0.586	0.392	0.212
2	31.27	7.03	4448	1.4	300	70.0	21.00	18.88	4.03	5.07	0.567	0.318	0.167
3	25.81	5.42	4762	1.2	309	61.0	18.54	8.80	4.09	5.32	0.493	0.318	0.216
4	25.86	5.59	4626	1.6	350	54.0	18.90	4.74	4.24	4.04	0.563	0.304	0.243
5	25.62	7.03	3644	1.4	350	50.0	17.50	4.77	5.25	4.08	0.467	0.256	0.201
6	25.23	6.95	3630	1.5	375	52.0	19.50	3.92	5.59	4.31	0.493	0.226	0.188

TABLE A-II

TEST DATA (contd)

Point No.	τ g/cm	ṁ mg/sec	I_{sp} sec	P_t 10^{-4} torr	I_A amp	V_A volt	P_A kw	P_{mag} kw	P_{c+b} kw	P_{an} kw	η_{TH}	η_F	η_o
Run 727 (contd)													
7	26.89	7.65	3515	1.4	400	50.0	20.00	4.00	5.54	4.48	0.499	0.227	0.189
8	28.68	←	3749	1.2	420	50.0	21.00	3.80	5.83	5.11	0.480	0.246	0.208
9	26.06		3407	1.0	421	50.0	21.05	3.80	6.00	5.14	0.471	0.202	0.171
10	22.86		2949	1.4	422	50.0	21.10	3.92	6.38	5.11	0.456	0.151	0.128
11	22.18		2899	1.4	422	50.0	21.10	3.92	6.35	5.03	0.461	0.146	0.124
12	21.05		2752	1.4	425	48.0	20.40	4.08	6.12	4.88	0.461	0.136	0.114
13	20.90		2732	1.3	430	46.0	20.60	4.30	6.14	4.92	0.464	0.133	0.110
14	21.28	→	2782	1.4	430	47.0	20.21	4.30	6.07	4.82	0.461	0.141	0.116
15	21.05	7.65	2752	1.4	425	47.0	19.98	3.99	6.00	4.68	0.465	0.139	0.116
16	22.56	7.61	2965	1.3	425	46.1	19.59	3.87	5.97	4.62	0.459	0.164	0.137
17	21.81	↔	2866	1.3	425	45.5	19.34	3.86	5.90	4.54	0.460	0.155	0.129
18	17.31		2275	1.3	425	46.0	19.55	3.81	5.86	4.42	0.474	0.097	0.081
19	19.19	7.61	2522	1.3	421	43.0	18.10	3.53	5.71	4.15	0.455	0.128	0.097
20	21.80	7.55	2887	1.3	423	44.4	18.78	4.01	5.71	4.34	0.465	0.161	0.133
21	22.07	7.63	2893	1.3	422	43.5	18.36	4.01	5.71	4.21	0.460	0.167	0.137
22	21.56	7.61	2833	1.3	423	43.0	18.19	4.01	5.71	4.11	0.460	0.161	0.132
23	22.43	7.61	2947	1.2	425	43.0	18.28	4.07	5.54	4.24	0.465	0.173	0.142
24	23.06	7.61	3030	1.2	425	43.0	18.28	4.13	5.67	4.13	0.464	0.183	0.149

TABLE A-II

TEST DATA (contd)

Point No.	T km	ṁ mg/sec	I_{sp} sec	P_t 10^{-4} torr	I_A amp	V_A volt	P_A kw	P_{mag} kw	P_{c+b} kw	P_{em} kw	η_{TH}	η_u	η_t
Run 727 (contd)													
25	25.94	7.61	3409	1.2	420	52.0	21.84	4.20	6.64	5.07	0.464	0.194	0.163
26	24.93		3276	1.2	425	48.0	20.40	4.20	6.62	4.56	0.452	0.192	0.159
27	22.16		2912	1.2	430	45.0	19.35	4.40	6.64	4.30	0.435	0.160	0.131
28	20.79	7.61	2732	1.2	430	41.0	17.63	4.36	7.19	3.85	0.374	0.155	0.124
29	21.27	7.56	2813	1.2	430	42.0	18.06	4.29	6.95	3.79	0.405	0.159	0.128
30	22.14	7.56	2929	1.2	430	46.0	19.78	4.36	7.16	3.78	0.447	0.157	0.129
31	22.89		3028	1.2	430	42.0	18.06	4.32	7.13	3.54	0.409	0.184	0.149
32	24.02		3177	1.2	430	42.0	18.06	4.17	6.95	3.66	0.413	0.203	0.165
33	24.77		3276	1.2	430	41.0	17.63	4.29	7.01	3.65	0.395	0.221	0.177
34	24.41		3229	1.2	425	39.0	16.58	3.97	7.03	3.28	0.378	0.228	0.184
35	24.02		3177	1.2	430	37.0	15.91	4.03	7.06	3.10	0.362	0.230	0.184
36	22.39		2962	1.2	430	36.0	15.48	3.94	7.28	3.03	0.334	0.205	0.164
37	24.64		3259	1.2	430	37.0	15.41	3.91	7.01	3.18	0.360	0.242	0.194
38	27.55		3644	1.2	420	40.0	16.80	3.56	7.10	3.22	0.386	0.287	0.237
39	26.91		3560	1.1	425	37.0	15.23	3.64	7.06	3.18	0.349	0.292	0.237
40	26.67		3528	1.0	420	39.0	16.38	3.44	6.77	3.14	0.395	0.276	0.228
41	29.55		3909	1.1	420	46.0	19.32	3.14	6.97	3.60	0.453	0.287	0.247
42	30.31	7.56	4009	1.1	415	49.0	20.34	4.14	6.84	4.30	0.452	0.287	0.238

TABLE A-II

TEST DATA (contd)

Point No.	T gram	ṁ mg/sec	I_{sp} sec	P_t 10^{-4} torr	I_A amp	V_A volt	P_A W	P_{mag} W	P_{c+b} W	P_{em} W	η_{TH}	η_P	η_o
Run 727 (contd)													
43	30.55	7.56	4041	1.1	419	49.0	20.53	4.30	6.77	4.50	0.451	0.289	0.239
44	30.67		4057	1.1	419	49.0	20.53	4.32	6.85	4.42	0.451	0.291	0.240
45	30.55		4041	1.2	420	48.0	20.16	4.32	6.88	4.34	0.444	0.294	0.242
46	30.92		4090	0.9	420	48.0	20.16	4.38	6.85	4.10	0.457	0.301	0.247
47	28.80	7.56	3810	1.1	420	47.0	19.74	4.00	6.85	4.20	0.440	0.267	0.222
48	28.05	7.54	3720	1.1	420	46.5	19.53	4.00	6.82	4.07	0.442	0.257	0.213
49	28.17		3736	1.2	420	46.0	19.32	4.03	6.70	4.00	0.446	0.261	0.216
50	27.92		3703	1.15	420	43.4	18.23	4.03	6.67	3.75	0.429	0.272	0.223
51	28.17		3736	1.1	421	43.3	18.23	4.03	6.74	3.69	0.428	0.277	0.227
52	28.80	7.54	3920	1.1	421	42.8	18.02	4.03	6.70	3.63	0.427	0.301	0.246
53	28.29	7.51	3767	1.1	422	41.7	17.60	4.03	6.62	3.56	0.422	0.291	0.237
54	28.67	7.54	3802	1.1	422	41.4	17.47	4.03	6.60	3.52	0.421	0.299	0.243
55	28.79		3818	1.1	423	40.7	17.22	4.03	6.48	3.49	0.421	0.306	0.248
56	28.91		3834	1.1	423	40.1	16.96	4.03	6.40	3.45	0.419	0.314	0.253
57	28.54		3785	1.1	423	39.9	16.88	4.03	6.19	3.51	0.425	0.307	0.248
58	28.66		3801	1.1	423	39.4	16.67	3.99	6.20	3.41	0.424	0.314	0.253
59	28.91		3834	1.1	424	38.6	16.37	3.99	6.15	3.39	0.417	0.325	0.261
60	28.04	7.54	3719	1.0	424	38.1	16.15	3.99	6.14	3.32	0.414	0.310	0.249

TABLE A-II

TEST DATA (contd)

Point No.	T km	$\dot{t}$ m/sec	t_{sp} sec	P_t 10^{-4} torr	I_A amp	V_A volt	P_A kw	P_{mag} kw	P_{crb} kw	P_{am} kw	η_{TH}	η_P	η_0
Run 727 (contd)													
61	27.54	7.54	3653	1.1	425	36.9	15.68	3.97	6.10	3.25	0.404	0.308	0.246
62	32.67	←	4333	1.1	421	46.5	19.58	4.07	6.78	3.86	0.457	0.347	0.287
63	32.92		4366	1.1	421	44.0	18.52	4.03	6.38	3.77	0.452	0.373	0.306
64	31.92		4233	1.1	422	43.7	13.44	4.08	6.46	3.76	0.446	0.352	0.288
65	31.80		4218	1.1	422	43.5	18.36	4.08	6.56	3.65	0.444	0.351	0.287
66	30.67		4068	1.1	422	42.3	17.35	4.00	6.48	3.57	0.437	0.336	0.274
67	31.42		4167	1.1	422	42.7	18.02	3.97	6.62	3.53	0.437	0.349	0.286
68	31.27		4147	1.0	428	40.4	17.29	4.45	6.37	3.49	0.430	0.360	0.286
69	30.40		4032	1.0	427	40.3	17.21	3.93	6.48	3.37	0.428	0.342	0.278
70	31.64		4196	1.0	429	40.3	17.29	4.14	6.38	3.38	0.436	0.368	0.297
71	31.39	→	4163	1.1	428	39.7	16.99	3.99	6.35	3.27	0.434	0.369	0.299
72	31.63	7.54	4195	1.1	432	38.4	16.59	4.30	6.34	3.34	0.417	0.384	0.305
73	29.76	7.53	3952	1.1	430	37.5	16.13	4.23	6.51	3.29	0.393	0.350	0.278
74	30.37	7.55	4023	1.0	433	37.9	16.41	4.36	6.16	3.44	0.415	0.357	0.282
75	30.12	7.55	3989	1.1	433	38.0	16.45	4.03	6.00	3.44	0.426	0.351	0.282
76	29.75	7.55	3940	1.1	432	36.5	15.77	3.97	5.63	3.51	0.421	0.357	0.285
77	30.74	7.50	4099	1.1	432	37.9	16.37	3.96	5.49	3.52	0.450	0.370	0.298
78	31.13	7.55	4123	1.1	428	48.0	20.54	3.97	6.27	4.06	0.497	0.300	0.251

TABLE A-II

TEST DATA (contd)

Point No.	T gm	i m/sec	I_{sp} sec	P_t 10^{-4} torr	I_A amp	V_A volt	P_A w	P_{mag} w	P_{c+b} w	P_{am} w	η_{TH}	η_T	η_o
Run 727 (contd)													
79	30.01	7.53	3985	1.1	429	46.5	19.95	4.08	6.43	4.40	0.457	0.288	0.239
80	28.51	7.53	3786	1.1	429	46.0	19.73	4.08	6.26	4.39	0.460	0.263	0.218
81	27.01	7.55	3577	1.1	429	45.0	19.31	4.07	6.67	4.34	0.430	0.240	0.198
82	25.88	7.55	3428	1.1	429	45.0	19.31	4.04	6.18	4.27	0.459	0.221	0.182
83	25.76	7.53	3421	1.1	429	43.8	18.79	4.03	6.10	4.20	0.452	0.225	0.185
84	25.37	7.49	3387	1.1	430	43.2	18.58	4.04	6.24	4.14	0.441	0.222	0.183
85	25.25		3371	1.0	430	42.0	18.06	4.06	6.15	3.98	0.439	0.226	0.185
86	25.00		3338	0.9	430	41.0	17.63	4.08	6.21	3.90	0.427	0.227	0.185
87	22.24		2969	1.0	432	40.0	17.28	4.17	6.31	3.71	0.420	0.183	0.148
88	21.48		2868	1.0	435	38.0	16.53	4.17	6.24	3.46	0.413	0.179	0.143
89	21.60		2884	1.0	435	36.8	16.01	4.14	5.88	3.41	0.420	0.187	0.148
90	21.73		2901	1.0	435	36.2	15.75	4.14	6.01	3.35	0.406	0.192	0.152
91	22.35		2984	1.0	435	35.0	15.23	4.14	6.10	3.21	0.389	0.210	0.165
92	23.23		3101	1.0	435	35.2	15.31	4.06	5.99	3.31	0.393	0.226	0.179
93	23.22		3100	1.0	438	34.5	15.11	4.10	6.10	3.11	0.391	0.228	0.180
94	21.34		2849	1.0	438	33.2	14.54	4.10	6.12	3.11	0.365	0.201	0.157
95	21.22		2833	1.0	438	33.5	14.67	4.14	6.21	3.12	0.364	0.197	0.154
96	21.22	7.49	2833	1.1	438	33.0	14.45	4.14	6.15	3.08	0.361	0.200	0.155

TABLE A-II

TEST DATA (contd)

Point No.	T rpm	ṁ mg/sec	I_{sp} sec	P_t 10^{-4} torr	I_A amp	V_A volt	P_A W	P_{mag} W	P_{c+b} W	P_{em} W	η_{tr}	η_y	η_o
Run 727 (contd)													
97	28.25	7.49	3772	1.1	430	42.0	18.06	4.13	6.07	4.04	0.440	0.283	0.230
98	31.25		4172	0.9	430	42.5	18.28	4.17	6.18	4.06	0.440	0.342	0.279
99	33.00		4406	1.0	430	42.0	18.06	4.13	6.23	4.02	0.433	0.386	0.315
100	33.37	7.49	4455	0.9	430	42.5	18.28	4.19	6.21	3.98	0.443	0.391	0.318
101	31.02	7.57	4098	1.0	429	42.5	18.23	3.89	6.23	3.97	0.441	0.335	0.276
102	29.25	7.49	3905	1.0	430	43.2	18.58	3.90	6.21	4.09	0.446	0.295	0.244
103	29.25	7.49	3905	1.0	430	42.5	18.28	3.92	6.24	3.97	0.442	0.300	0.247
104	28.74	7.45	3858	1.0	429	42.9	18.40	3.92	6.32	4.05	0.437	0.289	0.238
105	28.50	7.49	3805	1.0	430	43.0	18.49	3.97	6.40	4.09	0.433	0.282	0.232
106	27.87		3721	1.0	430	43.0	18.49	3.97	6.35	3.87	0.448	0.269	0.222
107	27.25		3638	1.0	430	42.9	18.45	4.01	6.32	4.00	0.441	0.258	0.212
108	26.25		3505	1.0	430	42.2	18.15	4.03	6.34	3.94	0.434	0.244	0.199
109	25.99		3470	1.0	431	41.5	17.89	4.14	6.37	3.83	0.430	0.242	0.197
110	27.36		3653	1.0	432	41.0	17.71	4.17	6.57	3.72	0.419	0.271	0.219
111	28.11		3753	1.0	432	41.0	17.71	4.23	6.51	3.73	0.422	0.286	0.231
112	26.98		3602	1.0	435	41.0	17.84	4.29	6.44	3.80	0.427	0.261	0.211
113	25.36	7.49	3386	1.0	403	40.4	16.28	4.13	6.08	3.39	0.419	0.253	0.202
114	25.23	7.48	3373	0.9	403	41.1	16.56	4.17	6.08	3.22	0.439	0.246	0.197

8

TABLE A-II

TEST DATA (contd)

Point No.	T gram	ṁ mg/sec	I_{sp} sec	P_t 10^{-4} torr	I_A amp	V_A volt	P_A kW	P_{mag} kW	P_{c+b} kW	P_{an} kW	η_{TH}	η_p	η_o
Run 727 (contd)													
115	24.57	7.48	3285	0.85	376	40.7	15.30	4.17	5.75	2.93	0.433	0.253	0.199
116	25.07	7.48	3352	0.80	376	40.5	15.23	4.19	5.66	2.74	0.449	0.265	0.208
117	26.20	7.48	3503	0.85	377	39.5	14.89	4.23	5.64	2.69	0.441	0.296	0.231
Run 729 (NH_3)													
1	3.82	14.2	269	5.6	148	72.0	10.66	6.93	3.06	4.19	0.320	0.005	0.003
2	13.57	8.3	1635	4.0	200	118.0	23.60	6.85	4.45	--	--	0.045	0.035
Run 730 (NH_3)													
1	9.27	14.4	644	2.0	244	79.0	19.28	12.56	3.94	8.74	0.343	0.015	0.009
2	7.70	11.2	687	2.2	250	73.5	18.38	4.28	3.88	8.12	0.348	0.014	0.011
3	7.75	9.1	852	2.4	350	67.0	23.45	1.84	6.25	10.2	0.299	0.014	0.013
4	12.11	8.9	1360	2.8	400	62.0	24.80	1.82	7.62	12.0	0.210	0.032	0.030
5	12.70	8.3	1530	2.2	450	68.0	30.60	1.77	7.86	15.4	0.242	0.030	0.029
Run 731													
1A	24.5	5.69	4306	3.8	300	57.0	17.10	6.81	4.50	3.42	0.537	0.296	0.211
1B	22.2	6.55	3389	4.6	300	49.0	14.70	6.34	6.26	3.19	0.357	0.246	0.168
2	25.0	6.53	3828	4.3	300	52.0	15.60	4.75	6.69	3.06	0.375	0.294	0.226

TABLE A-II

TEST DATA (contd)

Point No.	T RPM	ṁ mg/sec	I_{sp} sec	P_t 10^{-4} torr	I_A amp	V_A volt	P_A W	P_{mag} W	P_{c+b} W	P_{em} W	η_{TH}	η_F	η_o
Run 731 (contd)													
3	21.4	6.53	3277	4.4	300	47.0	14.10	3.00	6.97	2.64	0.319	0.239	0.197
4	22.1	5.66	3905	4.5	300	52.5	15.80	4.75	6.92	3.35	0.350	0.262	0.201
5	18.4	4.68	3932	4.5	300	54.0	16.20	4.75	6.72	3.58	0.364	0.214	0.166
Run 732													
1	8.1	6.00	1350	--	100	79.0	7.90	4.59	1.00		0.602	0.066	0.042
2	17.5	5.94	2946	--	254	76.0	19.30	4.53	3.08		0.658	0.128	0.104
3	25.0	5.94	4208	3.0	253	53.5	13.54	4.51	3.39		0.558	0.373	0.279
4	28.2	5.66	4982	2.0	300	62.0	18.60	4.53	4.40		0.621	0.362	0.291
5	30.0	5.65	5309	1.9	300	60.0	18.00	4.53	4.29		0.623	0.425	0.339
6	27.0	5.65	4778	2.0	300	60.5	18.15	3.98	4.54		0.603	0.341	0.230
7	28.7	5.65	5079	1.0	300	58.5	17.55	3.98	4.45		0.602	0.399	0.325
8	26.7	5.51	4845	3.2	300	58.5	17.55	3.15	4.76		0.577	0.354	0.300
9	26.6	5.36	4962	2.2	300	58.5	17.55	3.12	4.96		0.565	0.361	0.306
10	26.1	5.35	4878	2.2	300	58.5	17.55	3.12	4.98		0.564	0.348	0.296
11	25.1	5.35	4691	1.9	300	58.1	17.43	3.12	5.00		0.562	0.324	0.275
12	24.6	5.35	4598	1.7	300	58.0	17.40	3.12	5.03		0.562	0.312	0.265
13	24.3	5.35	4542	1.7	300	58.0	17.40	3.12	5.05		0.564	0.304	0.258

TEST DATA (contd)

Point No.	T km	ṁ m/sec	I_{sp} sec	P_t 10^{-4} torr	I_A amp	V_A volt	P_A kw	P_{mag} kw	P_{c+b} kw	P_{sm} kw	η_{TH}	η_F	η_o
Run 732 (contd)													
14	24.4	5.35	4560	1.3	300	57.8	17.34	3.15	5.03		0.627	0.308	0.261
15	24.8	5.75	4313	2.8	300	58.0	17.40	3.15	4.72		0.583	0.295	0.250
16	24.7	5.75	4295	2.9	300	58.5	17.55	3.18	4.87		0.569	0.290	0.246
17	22.9	5.73	3996	2.8	300	57.5	17.25	3.18	4.74		0.582	0.255	0.215
18	22.1	5.75	3843	2.8	300	57.0	17.10	3.18	4.73		0.580	0.238	0.201
19	21.2	5.75	3686	2.8	300	56.5	16.95	3.15	4.71		0.579	0.221	0.187
20	18.7	5.76	3246	3.3	300	57.5	17.25	3.15	4.77		0.568	0.169	0.143
21	18.7	5.75	3252	3.0	300	57.5	17.25	3.13	4.71		0.580	0.169	0.143
22	13.7	5.75	2382	3.7	298	62.5	18.63	3.13	4.84		0.545	0.084	0.072
23	14.8	5.75	2573	4.2	295	73.5	21.68	3.13	4.93		0.560	0.084	0.074
24	32.4	5.45	5944	1.2	300	58.0	17.40	3.15	5.14		0.558	0.531	0.450
25	31.9	5.45	5852	1.0	300	58.0	17.40	3.10	5.14		0.556	0.515	0.436
26	27.3	5.45	5009	0.9	300	57.5	17.25	3.15	5.10		0.556	0.380	0.322
27	16.9	7.00	2414	--	296	63.0	18.65	3.15	4.25		0.567	0.105	0.090
28	22.4	4.25	5271	--	250	72.0	18.00	3.15	2.00		0.538	0.315	0.268
29	29.4	5.49	5355	2.2	300	55.0	16.50	3.15	4.85		0.566	0.458	0.385
30	31.1	5.43	5727	1.4	300	56.0	16.80	3.15	5.09		0.552	0.509	0.429

TEST DATA (contd)

Point No.	T Km	ẇ mg/sec	I_{sp} sec	P_t 10^{-4} torr	I_A amp	V_A volt	P_A kw	P_{mag} kw	P_{c+b} kw	P_{em} kw	η_{TH}	η_t	η_o
Run 732 (contd)													
31	32.1	5.42	5923	2.8	300	56.0	16.80	3.15	5.05		0.557	0.543	0.457
32	31.7	←	5848	2.4	300	56.0	16.80	3.15	5.12		0.549	0.530	0.446
33	30.1		5553	2.4	300	56.0	16.80	3.18	5.11		0.548	0.478	0.402
34	28.8		5313	2.3	300	56.0	16.80	3.18	5.07		0.551	0.437	0.368
35	28.1		5184	2.3	300	55.5	16.65	3.18	5.05		0.549	0.420	0.353
36	27.6	→	5092	2.4	300	55.5	16.65	3.20	4.98		0.553	0.405	0.340
37	26.2	5.42	4833	2.9	300	55.5	16.65	3.23	4.98		0.550	0.365	0.306
38	25.4	5.43	4677	2.4	300	55.5	16.65	3.23	5.00		0.551	0.342	0.287
39	24.3	5.43	4567	2.2	300	56.0	16.80	3.23	5.03		0.556	0.324	0.272
40	25.8	5.66	4558	2.9	300	56.0	16.80	3.25	4.94		0.559	0.336	0.281
41	25.7	5.64	4556	2.8	300	56.5	16.95	3.21	4.98		0.560	0.332	0.279
42	24.6	5.65	4353	2.8	300	55.5	16.65	3.21	4.98		0.555	0.309	0.259
43	24.1	5.65	4265	2.8	300	55.9	16.77	3.20	4.95		0.559	0.293	0.246
44	23.8	5.66	4204	2.8	300	56.5	16.95	←	4.88		0.567	0.283	0.238
45	24.0	5.65	4247	3.0	300	56.5	16.95		4.95		0.561	0.288	0.242
46	24.4	5.66	4310	3.2	301	56.5	16.95		4.97		0.561	0.297	0.250
47	23.5	5.65	4159	3.4	300	57.0	17.10		5.03		0.556	0.274	0.231
48	22.0	5.65	3893	3.0	300	56.2	16.86	→	5.03		0.553	0.244	0.205

TEST DATA (contd)

Point No.	T RPM	$\dot{m}$ mg/sec	I_{sp} sec	p_t 10^{-4} torr	I_A amp	V_A volt	P_A W	P_{mag} W	P_{c+b} W	P_{em} W	η_{TH}	η_F	η_o
Run 732 (contd)													
49	21.7	5.66	3833	3.4	298	56.2	16.75	3.16	4.95		0.557	0.238	0.201
50	21.4	5.66	3780	3.1	300	55.0	16.50	3.20	4.77		0.560	0.235	0.197
51	21.7	5.65	3841	2.8	300	56.0	16.80	3.13	4.97		0.556	0.238	0.200
52	21.2	↑	3752	2.6	300	55.5	16.65	3.20	4.95		0.551	0.229	0.192
53	24.5		4336	2.4	300	55.5	16.65	←	4.90		0.553	0.306	0.257
54	24.3		4389	2.6	300	55.5	16.65		4.85		0.557	0.314	0.263
55	24.6	5.65	4353	2.6	300	55.5	16.65		4.88		0.556	0.309	0.259
56	24.3		4300	2.3	300	55.5	16.65		4.86		0.557	0.301	0.253
57	24.1		4265	2.4	300	55.5	16.65	3.20	4.86		0.558	0.296	0.249
58	23.9		4230	2.3	300	56.5	16.95		4.97		0.558	0.286	0.241
59	24.0		4247	2.2	300	56.5	16.95		4.97		0.558	0.289	0.243
60	24.0		4247	2.2	300	56.0	16.80		4.92		0.558	0.291	0.245
61	23.9		4230	2.2	300	56.0	16.30	→	4.92		0.557	0.289	0.243
62	23.2		4106	2.4	300	56.0	16.30		5.10		0.547	0.272	0.229
63	22.7		4017	2.4	300	56.0	16.80		5.10		0.547	0.260	0.219
64	22.5	5.65	3982	2.3	300	56.0	16.80	3.18	5.15		0.548	0.256	0.215
65	22.9	5.64	4060	2.4	300	56.0	16.80	3.18	5.10		0.548	0.266	0.223
66	22.8	5.64	4042	2.3	300	56.0	16.80	3.18	5.11		0.552	0.263	0.221

TABLE A-II

TEST DATA (contd)

Point No.	T Km?	ú m/sec	I_{sp} sec	P_t 10^{-4} torr	I_A ma	V_A volt	P_A W	P_{mag} W	P_{c+b} W	$P_{a\,m}$ W	η_n	η_b	η_o
Run 732 (contd)													
67	22.4	5.64	3971	2.2	300	56.0	16.80	3.18	5.14		0.546	0.254	0.214
68	22.4		3971	2.4	300	56.0	16.80		5.14		0.548	0.254	0.214
69	22.5		3989	2.4	300	57.0	17.10		5.07		0.559	0.252	0.212
70	21.2		3758	2.2	300	56.0	16.80		5.09		0.549	0.228	0.191
71	21.8		3865	2.2	300	56.0	16.80	3.18	5.09		0.549	0.241	0.202
72	21.9		3882	2.4	300	56.0	16.80	3.15	5.16		0.544	0.243	0.205
73	22.0		3900	2.3	300	56.0	16.80		5.14		0.547	0.245	0.206
74	22.3		3953	2.0	300	56.0	16.80		5.16		0.551	0.252	0.212
75	22.3		3953	2.3	300	56.0	16.80		5.18		0.544	0.252	0.212
76	22.1	5.64	3918	2.2	300	56.0	16.80		5.07		0.552	0.247	0.208
77	22.4	5.65	3964	2.3	300	56.0	16.80		5.14		0.547	0.254	0.214
78	22.4	5.66	3957	2.3	300	56.0	16.80		5.09		0.550	0.253	0.213
79	22.7	5.65	4017	2.2	300	57.0	17.10	3.15	5.38		0.538	0.256	0.216
80	22.9	5.65	4053	2.3	300	57.0	17.10	3.18	5.17		0.549	0.260	0.220
81	23.7	5.65	4194	2.3	300	57.0	17.10	3.20	5.13		0.552	0.279	0.235
82	23.8	5.65	4212	2.2	300	57.0	17.10	3.18	5.17		0.552	0.281	0.237
83	23.8	5.67	4197	2.3	300	56.0	16.80	3.18	4.97		0.556	0.285	0.240
84	24.0	5.68	4225	2.4	300	57.0	17.10	3.18	5.02		0.563	0.285	0.240

Point No.	T °K	ṁ m/sec	I_{sp} sec	P_t 10^{-4} torr	I_A amp	V_A volt	P_A W	P_{mag} W	P_{c+b} W	P_{em} W	η_{TR}	η_F	η_o
Run 732 (contd)													
85	24.0	5.68	4225	(1.0)	300	56.0	16.80	3.18	4.97		0.556	0.290	0.244
86	24.9	5.68	4383	--	300	56.0	16.80	3.18	5.04		0.552	0.312	0.262
87	25.2	5.68	4436	2.4	302	57.0	17.21	3.20	5.08		0.558	0.312	0.263
88	26.9	5.66	4752	(1.1)	300	54.5	16.35	3.18	4.68		0.617	0.375	0.314
89	31.0	5.67	5467	0.9	300	53.5	16.05	←	4.57		0.615	0.507	0.423
90	24.5	5.67	4320	2.1	300	56.0	16.80		5.20		0.548	0.302	0.254
91	24.3	5.66	4293	2.0	300	56.2	16.86		5.20		0.552	0.297	0.250
92	24.3	5.65	4300	2.2	300	56.3	16.89	3.18	5.30		0.541	0.297	0.250
93	24.1	5.65	4265	2.1	302	56.3	17.00		5.28		0.547	0.290	0.244
94	24.3	5.65	4389	2.1	303	55.7	16.88		5.26		0.536	0.309	0.260
95	23.7	5.66	4187	2.1	303	56.0	16.97	→	5.19		0.549	0.281	0.236
96	23.2	5.66	4098	2.1	303	54.5	16.51	3.18	5.08		0.545	0.276	0.232
97	22.8	5.66	4028	2.1	304	55.0	16.72	3.20	5.08		0.548	0.264	0.221
98	22.5	5.66	3975	2.1	302	54.5	16.46	3.15	5.08		0.541	0.261	0.219
99	22.2	5.65	3929	2.0	302	55.5	16.76	3.15	5.26		0.537	0.250	0.210
100	21.7	5.65	3840	2.0	303	55.7	16.88	3.15	5.13		0.548	0.237	0.200
101	21.6	5.65	3823	1.9	303	55.7	16.88	3.18	5.17		0.547	0.235	0.198
102	22.3	5.65	3946	2.0	303	56.2	17.03	3.15	5.24		0.546	0.248	0.209

TABLE A-II

TEST DATA (cont'd)

Point No.	T °K	ṁ mg/sec	I_{sp} sec	P_t 10^{-4} torr	I_A ma	V_A volt	P_A W	P_{mag} W	P_{crb} W	P_{em} W	η_T	η_b	η_o
Run 732 (cont'd)													
103	22.1	5.65	3911	1.8	303	56.0	16.97	3.18	5.15		0.552	0.244	0.206
104	22.1		3911	2.2	303	56.8	17.21	3.18	5.22		0.554	0.241	0.203
105	22.3		3946	1.8	303	56.5	17.12	3.19	5.26		0.548	0.247	0.208
106	21.9		3876	1.8	303	57.0	17.27	3.19	5.51		0.539	0.236	0.199
107	22.0		3893	2.0	303	57.0	17.27	3.19	5.39		0.544	0.238	0.201
108	22.6		4000	1.9	304	57.1	17.36	3.20	5.37		0.548	0.250	0.211
109	22.6		4000	1.9	303	57.0	17.27	3.20	5.24		0.553	0.251	0.212
110	22.5		3982	1.9	303	57.0	17.27	3.21	5.28		0.551	0.249	0.210
111	22.2		3929	1.9	300	57.0	17.10	3.15	5.28		0.548	0.245	0.207
112	22.1		3911	1.9	300	57.0	17.10	←	5.31		0.548	0.243	0.205
113	22.6		4000	1.9	300	57.0	17.10		5.35		0.541	0.254	0.214
114	22.8	5.65	4035	2.0	300	57.5	17.25		5.37		0.544	0.256	0.216
115	22.2	5.65	3929	2.0	300	57.5	17.25		5.35		0.546	0.243	0.205
116	22.2	5.64	3936	2.0	301	57.2	17.22		5.26		0.551	0.244	0.206
117	29.8	5.66	5265	0.3	302	54.5	16.46		4.60		0.618	0.458	0.384
118	29.0	5.66	5123	0.5	302	55.0	16.61		4.78		0.616	0.429	0.361
119	18.2	5.65	3221	2.6	300	60.0	18.00		5.20		0.549	0.156	0.133
120	21.5	5.65	3805	2.0	300	58.0	17.40	3.15	5.38		0.548	0.226	0.191

TABLE A-II

TEST DATA (contd)

Point No.	T RPM	u m/sec	I_{sp} sec	P_t 10^{-4} torr	I_A amp	V_A volt	P_A kW	P_{mag} kW	P_{c+b} kW	P_{an} kW	T_H	η_r	η_o
Run 732 (contd)													
121	21.2	5.65	3752	2.2	300	58.0	17.40	3.15	5.20		0.556	0.219	0.186
122	21.7	5.66	3833	2.2	300	58.5	17.55	3.15	5.22		0.557	0.227	0.193
123	21.0	5.66	3710	2.4	300	58.0	17.40	3.15	5.20		0.550	0.215	0.182
124	20.2	5.65	3575	2.4	300	58.0	17.40	3.13	5.20		0.551	0.199	0.159
125	20.4	5.64	3617	2.4	300	58.0	17.40	3.13	5.24		0.548	0.204	0.172
126	20.5	5.65	3628	2.2	300	58.0	17.40	3.13	5.26		0.549	0.205	0.173
127	21.2	5.65	3752	2.2	300	58.5	17.55	3.15	5.35		0.545	0.217	0.184
128	20.9	5.65	3699	2.4	300	58.5	17.55	3.13	5.35		0.546	0.211	0.179
129	22.0	5.65	3893	2.3	300	58.5	17.55	3.15	5.33		0.547	0.234	0.199
130	22.3	5.68	3926	2.3	300	58.5	17.55	3.13	5.40		0.544	0.239	0.203
131	22.5	5.67	3968	2.4	300	57.5	17.25	3.13	5.33		0.540	0.248	0.210
132	24.2	5.68	4260	2.5	300	57.5	17.25	3.15	5.31		0.541	0.287	0.243
133	23.9	5.66	4222	2.4	300	57.5	17.25	3.13	5.38		0.536	0.281	0.238
134	24.0	5.66	4240	2.4	300	57.5	17.25	3.15	5.38		0.534	0.283	0.239
135	24.2	5.66	4275	2.4	300	57.5	17.25	3.15	5.40		0.534	0.288	0.243
136	24.6	5.66	4346	2.4	300	58.0	17.40	3.15	5.46		0.534	0.295	0.250
137	24.6	5.66	4346	2.4	300	57.5	17.25	3.15	5.46		0.532	0.297	0.252
138	24.5	5.65	4336	2.4	302	57.5	17.37	3.15	5.42		0.537	0.293	0.248

17

TABLE A-II

TEST DATA (contd)

Point No.	T °R	ů m/sec	I_{sp} sec	P_t 10⁻⁴ torr	I_A amp	V_A volt	ρ_A M	P_{mag} M	P_{c-b} M	P_{an} M	η_m	η_u	η_b
Run 732 (contd)													
139	24.1	5.65	4265	2.3	302	57.5	17.37	3.15	5.42		0.537	0.284	0.240
140	24.6	⟶	4353	2.2	302	57.6	17.40	3.18	5.44		0.557	0.295	0.250
141	24.4		4318	2.2	302	57.3	17.30	3.18	5.40		0.537	0.292	0.247
142	24.3		4300	2.3	302	58.0	17.52	3.18	5.42		0.542	0.286	0.242
143	24.0		4247	2.2	302	57.2	17.27	3.18	5.38		0.539	0.283	0.239
144	24.1		4265	2.2	302	56.5	17.06	3.15	5.38		0.531	0.289	0.244
145	24.2		4283	2.3	301	58.0	17.46	3.15	5.44		0.538	0.285	0.241
146	24.0	5.65	4247	2.2	304	58.0	17.63	3.23	5.47		0.542	0.277	0.235
147	23.3	5.66	4116	2.3	302	58.0	17.52	3.15	5.47		0.538	0.263	0.223
148	22.4	5.65	3964	2.4	302	58.0	17.52	3.15	5.47		0.540	0.243	0.206
149	22.2	5.66	3922	2.3	302	57.5	17.37	3.15	5.43		0.538	0.241	0.204
150	21.9	5.65	3876	2.2	300	58.5	17.55	3.13	5.47		0.540	0.232	0.197
151	21.8	⟶	3858	2.2	300	58.5	17.55	3.11	5.43		0.544	0.230	0.195
152	21.3		3769	2.4	301	58.0	17.46	3.15	5.36		0.544	0.221	0.187
153	21.7		3840	2.2	300	59.0	17.70	3.15	5.39		0.550	0.226	0.192
154	21.7	5.65	3840	2.3	300	58.0	17.40	3.13	5.56		0.532	0.230	0.195
155	21.7	5.66	3833	2.3	301	58.0	17.46	3.13	5.45		0.540	0.229	0.194
156	21.4	5.66	3780	2.3	300	58.5	17.55	3.13	5.45		0.540	0.221	0.188

TABLE A-II

TEST DATA (contd)

Point No.	T gm	ṁ mg/sec	I_{sp} sec	P_t 10^{-4} torr	I_A amp	V_A volt	P_A W	P_{mag} W	P_{c+b} W	P_{en} W	η_{TH}	η_F	η_o
Run 732 (contd)													
157	21.6	5.66	3816	2.2	302	58.5	17.67	3.13	5.54		0.540	0.224	0.190
158	21.8	5.65	3851	2.2	304	57.5	17.48	3.15	5.48		0.539	0.230	0.195
159	19.1	5.66	3374	2.4	300	58.0	17.40	3.13	5.47		0.538	0.178	0.151
160	18.0	5.65	3155	3.4	296	68.0	20.13	3.13	5.52		0.535	0.137	0.118
161	18.9	5.65	3345	3.1	299	64.0	19.14	3.13	5.50		0.536	0.159	0.136
162	18.8	5.65	3327	3.2	299	65.0	19.44	3.15	5.49		0.543	0.154	0.133
163	18.5	5.65	3244	3.2	300	63.0	18.90	3.15	5.29		0.546	0.152	0.131
164	18.4	5.66	3250	3.2	298	67.0	19.97	3.16	5.53		0.540	0.144	0.124
165	18.7	5.66	3303	3.2	300	65.0	19.50	3.18	5.47		0.548	0.152	0.131
166	15.6	5.66	2756	3.0	298	67.0	19.97	3.18	5.55		0.544	0.103	0.089
167	19.0	5.65	3362	3.2	299	66.0	19.73	3.18	5.53		0.542	0.155	0.134
168	19.0		3362	3.2	299	66.0	19.73	3.18	5.49		0.543	0.155	0.134
169	19.1		3380	3.2	300	65.5	19.65	3.13	5.47		0.551	0.158	0.136
170	18.7		3309	3.0	299	65.0	19.44	3.13	5.51		0.546	0.153	0.132
171	18.7		3309	3.2	298	66.0	19.67	3.13	5.55		0.545	0.131	0.130
172	23.1		4063	0.7	303	56.5	17.12	3.15	5.40		0.589	0.265	0.224
173	23.1		4088	1.0	300	56.5	16.95	3.15	5.49		0.562	0.267	0.225
174	20.6	5.65	3646	2.2	300	59.5	17.85	3.13	5.53		0.546	0.202	0.172

TEST DATA (contd)

Point No.	T gram	ṁ mg/sec	I_{sp} sec	P_t 10^{-4} torr	I_A amp	V_A volt	P_A w	P_{mag} w	P_{c+b} w	P_{em} w	η_{TR}	η_P	η_o
Run 732 (contd)													
175	14.3	5.65	2530	2.5	203	72.0	14.62	3.15	5.49		0.434	0.119	0.098
176	19.5		3451	3.2	293	67.0	19.63	3.13	5.67		0.537	0.164	0.142
177	19.4		3433	3.2	293	67.5	19.78	3.15	5.69		0.536	0.162	0.139
178	30.7		5433	0.3	300	55.5	16.65	3.13	5.20		0.583	0.481	0.405
179	30.0		5309	0.23	300	55.0	16.50	3.15	4.96		0.614	0.463	0.389
180	23.8		5097	0.23	300	55.0	16.50	3.13	4.94		0.620	0.427	0.359
181	29.1	5.65	5150	0.3	300	56.0	16.80	3.14	4.96		0.628	0.428	0.361
182	19.7	5.66	3480	3.2	302	68.0	20.54	3.14	5.86		0.538	0.160	0.139
183	20.0	5.67	3527	3.4	302	69.0	20.34	3.14	5.91		0.541	0.162	0.141
184	20.1	5.67	3557	3.3	302	68.0	20.54	3.15	5.86		0.538	0.167	0.145
185	19.8	5.67	3504	3.4	301	68.5	20.62	3.14	5.93		0.537	0.161	0.140
186	19.9	5.66	3515	3.3	301	69.0	20.77	3.14	5.91		0.543	0.161	0.140
187	19.9		3515	3.3	301	67.5	20.32	3.14	5.89		0.534	0.165	0.143
188	20.0		3533	3.3	302	67.5	20.39	3.14	5.91		0.538	0.166	0.144
189	19.9		3515	3.2	302	66.0	19.93	3.15	5.84		0.539	0.168	0.145
190	20.1		3551	3.2	303	65.5	19.85	3.15	5.84		0.539	0.173	0.149
191	20.3		3586	3.2	304	65.5	19.91	3.15	5.89		0.536	0.175	0.152
192	20.6	5.66	3639	3.1	304	64.0	19.46	3.15	5.84		0.534	0.185	0.159

TABLE A-II

TEST DATA (contd)

Point No.	T gram	$\dot{m}$ mg/sec	I_{sp} sec	P_t 10^{-4} torr	I_A amp	V_A volt	P_A kW	P_{mag} kW	P_{c+b} kW	P_{an} kW	η_{TH}	η_F	η_o
Run 732 (contd)													
193	20.7	5.69	3657	3.0	304	62.0	18.65	3.15	5.77		0.528	0.197	0.168
194	22.1	5.66	3904	2.4	307	59.0	18.11	←	5.75		0.540	0.229	0.195
195	23.2	5.66	4098	1.8	302	58.5	17.67		5.82		0.533	0.256	0.219
196	19.6	5.65	3469	2.8	300	61.0	18.30		5.53		0.546	0.178	0.152
197	21.6	←	3623	1.7	302	59.0	17.82		5.80		0.539	0.222	0.189
198	21.3		3769	1.7	303	58.5	17.73	→	5.82		0.538	0.217	0.185
199	21.3		3769	1.7	303	58.5	17.73	3.15	5.82		0.539	0.217	0.185
200	21.3		3769	1.7	303	58.5	17.73	3.16	5.82		0.538	0.217	0.185
201	21.1		3734	1.6	303	58.5	17.73	3.15	5.82		0.538	0.213	0.181
202	21.2	5.65	3752	1.6	302	58.5	17.67	←	5.66		0.545	0.216	0.183
203	19.7	5.66	3480	1.7	300	59.0	17.70		5.56		0.527	0.186	0.158
204	20.9	←	3692	1.7	302	58.5	17.67		5.74		0.542	0.210	0.178
205	21.0		3710	1.8	303	58.5	17.73		5.83		0.539	0.211	0.179
206	21.0		3710	1.7	302	59.0	17.82	3.15	5.87		0.540	0.210	0.178
207	21.4		3780	1.5	302	59.5	17.97	3.13	5.82		0.547	0.216	0.184
208	21.3		3763	1.6	300	60.0	18.00	3.13	5.84		0.545	0.214	0.182
209	21.3	→	3763	1.6	300	60.0	18.00	3.13	5.86		0.545	0.214	0.182
210	21.2	5.66	3745	1.7	301	59.0	17.76	3.13	5.77		0.543	0.215	0.182

TABLE A-II

TEST DATA (contd)

Point No.	T kg	ṁ mg/sec	I_{sp} sec	P_t 10^{-4} torr	I_A amp	V_A volt	P_A W	P_{mag} W	P_{c+b} W	P_{em} W	T_{TH}	η_T	η_o
Run 732 (contd)													
211	21.5	5.66	3798	1.6	301	59.0	17.76	3.13	5.75		0.545	0.221	0.188
212	21.5	5.66	3798	1.6	301	59.5	17.91		5.82		0.543	0.219	0.186
213	21.0	5.66	3710	1.6	301	59.5	17.91		5.77		0.546	0.209	0.178
214	21.2	5.66	3745	1.6	301	59.5	17.91		5.82		0.544	0.213	0.181
215	21.7	5.67	3827	1.9	301	60.0	18.06		5.80		0.549	0.221	0.188
216	21.2			1.8	302	59.0	17.82		5.82		0.541	0.213	0.182
217	21.2		3738	1.9	302	59.0	17.32		5.77		0.553	0.213	0.182
218	21.2		3738	1.9	300	60.0	18.00		5.89		0.540	0.211	0.180
219	21.2		3738	1.9	300	59.5	17.85	3.13	5.75		0.551	0.213	0.182
220	21.2	5.67	3738	1.9	298	60.0	17.88	3.10	5.86		0.548	0.213	0.181
221	21.6	5.66	3816	1.9	300	59.5	17.85	3.10	5.80		0.550	0.222	0.189
222	21.0	5.66	3710	1.6	300	59.0	17.70	3.11	5.77		0.548	0.211	0.180
223	20.8	5.66	3674	1.3	300	60.0	18.00	3.13	5.69		0.544	0.204	0.174
224	22.1	5.67	3897	1.3	300	59.5	17.85	3.13	5.80		0.553	0.232	0.197
225	21.0	5.67	3703	2.4	302	61.5	18.57	3.16	5.60		0.560	0.201	0.172
226	23.0	5.68	4049	2.0	301	60.0	18.06	3.15	5.95		0.559	0.248	0.211
227	25.1	5.69	4411	2.2	303	59.5	18.03	3.16	5.91		0.556	0.295	0.251
228	23.8	5.68	4190	2.0	303	59.3	17.97	3.16	5.95		0.550	0.266	0.227
229	20.9	5.67	3686	2.8	300	64.5	19.35	3.16	5.77		0.545	0.191	0.164